UNCLASSIFIED

CENTRAL RESEARCH LIBRARY
DOCUMENT COLLECTION

MARTIN MARIETTA ENERGY SYSTEMS LIBRARIES
3 4456 0350104 8

ORNL-2051
Progress

cy. 92

SOLID STATE DIVISION

SEMIANNUAL PROGRESS REPORT

FOR PERIOD ENDING FEBRUARY 29, 1956

CENTRAL RESEARCH LIBRARY
DOCUMENT COLLECTION

LIBRARY LOAN COPY

DO NOT TRANSFER TO ANOTHER PERSON

If you wish someone else to see this document, send in name with document and the library will arrange a loan.

OAK RIDGE NATIONAL LABORATORY
OPERATED BY
UNION CARBIDE NUCLEAR COMPANY
A Division of Union Carbide and Carbon Corporation
UCC
POST OFFICE BOX P · OAK RIDGE, TENNESSEE

UNCLASSIFIED

LEGAL NOTICE

This report was prepared as an account of Government sponsored work. Neither the United States, nor the Commission, nor any person acting on behalf of the Commission:

A. Makes any warranty or representation, express or implied, with respect to the accuracy, completeness, or usefulness of the information contained in this report, or that the use of any information, apparatus, method, or process disclosed in this report may not infringe privately owned rights; or

B. Assumes any liabilities with respect to the use of, or for damages resulting from the use of any information, apparatus, method, or process disclosed in this report.

As used in the above, "person acting on behalf of the Commission" includes any employee or contractor of the Commission to the extent that such employee or contractor prepares, handles or distributes, or provides access to, any information pursuant to his employment or contract with the Commission.

SOLID STATE DIVISION
SEMIANNUAL PROGRESS REPORT
FOR PERIOD ENDING FEBRUARY 29, 1956

PAGE	COLUMN	LINE	ERRATA
2	2	6	*for*: Little change was observed in internal friction. *read*: Little change was observed in internal friction for all the materials except cordierite and forsterite.
30	1	11	*for*: The dependance of the amplitude ... *read*: The amplitude dependence ...
63	2	15	*for*: curve 3′, ... *read*: curve 3″, ...

changed 9/7/56

UNCLASSIFIED

ORNL-2051

Contract No. W-7405-eng-26

SOLID STATE DIVISION

SEMIANNUAL PROGRESS REPORT

For Period Ending February 29, 1956

D. S. Billington, Director
J. H. Crawford, Jr., Assistant Director

DATE ISSUED

JUN 11 1956

OAK RIDGE NATIONAL LABORATORY
Operated by
UNION CARBIDE NUCLEAR COMPANY
A Division of Union Carbide and Carbon Corporation
Post Office Box P
Oak Ridge, Tennessee

MARTIN MARIETTA ENERGY SYSTEMS LIBRARIES

3 4456 0350104 8

UNCLASSIFIED

Reports previously issued in this series are:

ORNL-1025	Period Ending January 31, 1951
ORNL-1095	Period Ending April 30, 1951
ORNL-1128	Period Ending July 31, 1951
ORNL-1214	Period Ending October 31, 1951
ORNL-1261	Period Ending January 31, 1952
ORNL-1301	Period Ending May 10, 1952
ORNL-1359	Period Ending August 10, 1952
ORNL-1429	Period Ending November 10, 1952
ORNL-1506	Period Ending February 10, 1953
ORNL-1606	Period Ending August 31, 1953
ORNL-1677	Period Ending February 28, 1954
ORNL-1762	Period Ending August 30, 1954
ORNL-1851	Period Ending February 28, 1955
ORNL-1852	Period Ending February 28, 1955
ORNL-1944	Period Ending August 30, 1955
ORNL-1945	Period Ending August 30, 1955
ORNL-2052	Period Ending February 29, 1956

ORNL-2051
Progress

INTERNAL DISTRIBUTION

1. C. D. Baumann
2. R. G. Berggren
3. J. O. Betterton, Jr.
4. D. S. Billington
5. D. Binder
6. T. H. Blewitt
7. A. L. Boch
8. C. D. Bopp
9. G. E. Boyd
10. H. Brooks (consultant)
11. W. E. Browning
12. W. E. Brundage
13. D. W. Cardwell
14. R. M. Carroll
15. C. E. Center
16. R. A. Charpie
17. J. W. Cleland
18. G. H. Clewett
19. A. F. Cohen
20. D. D. Cowen
21. J. H. Crawford, Jr.
22. F. L. Culler
23. J. E. Cunningham
24. R. R. Dickison
25. S. E. Dismuke
26. L. B. Emlet (K-25)
27. M. J. Feldman
28. J. H. Frye, Jr.
29. J. L. Gabbard
30. R. J. Gray
31. C. S. Harrill
32. A. Hollaender
33. D. K. Holmes
34. A. S. Householder
35. J. T. Howe
36. R. E. Jamison
37. L. K. Jetter
38. R. W. Johnson
39. R. J. Jones
40. W. H. Jordan
41. G. W. Keilholtz
42. C. P. Keim
43. M. T. Kelley
44. R. H. Kernohan
45. E. M. King
46. G. E. Klein
47. T. A. Lincoln
48. S. C. Lind
49. R. S. Livingston
50. H. G. MacPherson (consultant)
51. C. J. McHargue
52. W. D. Manly
53. A. J. Miller
54. E. C. Miller
55. J. G. Morgan
56. K. Z. Morgan
57. E. J. Murphy
58. J. P. Murray (Y-12)
59. M. L. Nelson
60. R. B. Oliver
61. W. W. Parkinson
62. P. M. Reyling
63. M. T. Robinson
64. E. S. Schwartz
65. H. C. Schweinler
66. F. Seitz (consultant)
67. F. A. Sherrill
68. E. D. Shipley
69. O. Sisman
70. M. J. Skinner
71. G. P. Smith
72. A. H. Snell
73. R. L. Sproull (consultant)
74. E. E. Stansbury
75. D. K. Stevens
76. W. J. Sturm
77. C. D. Susano
78. J. A. Swartout
79. E. H. Taylor
80. J. M. Warde
81. C. C. Webster
82. M. S. Wechsler
83. R. A. Weeks
84. A. M. Weinberg
85. E. P. Wigner (consultant)
86. G. C. Williams
87. W. R. Willis
88. J. C. Wilson
89. C. E. Winters
90. M. C. Wittels

91. Biology Library
92-94. Central Research Library
95. Health Physics Library
96-115. Laboratory Records Department
116. Laboratory Records, ORNL R.C.
117. ORNL, Y-12 Technical Library, Document Reference Section
118. Reactor Experimental Engineering Library

EXTERNAL DISTRIBUTION

119. R. F. Bacher, California Institute of Technology
120. W. W. Shaver, Corning Glass Works, Corning, New York
121. S. H. Liebson, Naval Research Laboratory, Washington, D. C.
122. W. C. Sears, University of Georgia
123. Boeing Airplane Company
124. H. V. Klaus, Phillips Petroleum Company
125. Division of Research and Development, AEC, ORO
126. J. R. Johnson, Minnesota Mining and Manufacturing Co., St. Paul
127. J. B. Trice, Operations Analysis, Headquarters, SAC, Offutt Air Force Base, Nebraska
128. R. N. Little, ANP Project Office, Fort Worth
129. G. L. Stiehl, Convair Division of General Dynamics Corp., San Diego
130-532. Given Distribution as shown in TID-4500 (11th ed.) under Physics category

DISTRIBUTION PAGE TO BE REMOVED IF REPORT IS GIVEN PUBLIC DISTRIBUTION

CONTENTS

PUBLICATIONS AND PAPERS vii

SUMMARY 1

SOLID STATE REACTIONS 5

- Thermal-Neutron Irradiation of Indium Antimonide 5
- Effects of Gamma Radiation on Germanium 6
- Magnetic Susceptibility of n-Type Silicon 9
- Diamagnetism of Pure Germanium and Silicon 10
- Optical Absorption Behavior of Irradiated Silica 11

ENGINEERING PROPERTIES 16

- Infrared Spectra of Plastics and Elastomers After Irradiation 16
  - Polystyrene Irradiated in Vacuum 17
  - Polyethylene in Vacuum 18
  - Polybutadiene in Vacuum 18
  - GR-S in Vacuum 18
  - Natural Rubber in Vacuum 23
  - Polyvinyl Chloride in Vacuum 23
  - Other Polymers in Vacuum 23
  - Oxidation of Polymers Initiated by Irradiation 23
  - Comments on Results 24
- Radiation Effects on the Elastic Constants and the Internal Friction of Ceramics 24
- Radiation Stability of Cordierite 202 30
- Effect of Annealing on Irradiated Zirconia 30
- X-Ray Examination of Irradiated Thoria 30

RADIATION METALLURGY 32

- HRP Radiation Metallurgy 32
- Ductility of Nickel Alloys 33

CHEMICAL EFFECTS OF NUCLEAR REACTIONS 34

- Pyridinium Borate 34
- Yields of Chemical Elements in the Thermal-Neutron Fission of U^{235} 35

SPECIAL PROJECTS 37

- Resistivity Changes in Alpha Brass as a Function of Neutron Irradiation 37
- Effect of Neutron Radiation on the Precipitation-Hardening Reaction 37
- A High-Temperature Furnace for Growing Alloy Crystals 39
- Small-Angle X-Ray Scattering Technique 39
- Effect of Neutron Radiation on an Al-Ag Precipitate Alloy 41
- Paramagnetic Resonances in Unirradiated MgO 43
- Paramagnetic Resonances in Irradiated Fused and Crystalline Quartz 45
- Displacements from a Pile-Neutron Spectrum: Calculation for Germanium 48
- Initial Expansion of LiF Under Neutron Irradiation 50
- Annealing of Quenched-In Lattice Defects in Au-Cd 50
- A Rocking-Curve Adapter for the X-Ray Diffractometer 53
- Structural Studies in Irradiated Nonmetals 54
  - Comparison of Radiation and Thermal Effects in Quartz 54

A Radiation-induced Phase Transition 55
Examples of Radiation-induced Amorphism 57
Fast-Neutron Effects on Single-Crystal X-Ray Reflection 57
Annealing of Neutron-irradiated Diamond Powder 58
Effect of Radiation on Electrical Insulation 58
Radiation Effects in Barriers 59
Thermal Conductivity of Dielectrics at Low Temperatures 60

PUBLICATIONS AND PAPERS

C. D. Bopp and O. Sisman, "How Radiation Changes Polymer Mechanical Properties," *Nucleonics* **13**, No. 10, 51 (1955).

C. D. Bopp and O. Sisman, "How to Calculate Gamma Radiation Induced in Reactor Materials," *Nucleonics* **14**, No. 1, 46 (1956).

R. M. Carroll, ORNL-1938 (Aug. 23, 1955) (Secret).

M. T. Morgan, *Hermetically Sealed High-Temperature Pressure Transmitter and Hermetically Sealed High-Temperature Liquid-Level Probe*, ORNL-1939 (Aug. 29, 1955).

R. G. Berggren and J. C. Wilson, "A Remotely Operated Extensometer," *ASTM Bull.* No. 210, p 35 (Dec. 1955).

J. C. Wilson and D. S. Billington, "Effect of Nuclear Radiation on Structural Materials." Paper presented at Engineers Joint Council Nuclear Engineering and Science Congress, December 12–16, 1955. Preprint No. 91 published by Am. Inst. Chem. Engrs.

M. S. Wechsler, "The Quenching-In of Lattice Defects in Au-Cd." Oral seminar presented at Hammond Metallurgical Laboratory, Yale University, January 4, 1956.

R. H. Kernohan, D. S. Billington, and A. B. Lewis, "Effect of Neutron Irradiation on the Precipitation-Hardening Reaction in Alloys Containing Beryllium," *J. Appl. Phys.* **27**, 40 (1956).

D. K. Stevens, J. W. Cleland, J. H. Crawford, Jr., and H. C. Schweinler, "Magnetic Susceptibility of Germanium," *Phys. Rev.* **100**, 1084 (1955).

J. W. Cleland and J. H. Crawford, Jr., "Fast-Neutron Bombardment of GaSb," *Phys. Rev.* 100, 1614 (1955).

J. H. Crawford, Jr., "Uses of High Energy Radiation in the Study of Solids." Paper delivered before the National Meeting of Am. Assoc. Advance. Sci., Atlanta, December 30, 1955.

R. A. Weeks, "Paramagnetic Resonances in Irradiated Fused and Crystalline Quartz," *Bull. Am. Phys. Soc.* Series II, **1**, 12 (1956).

D. S. Billington and J. H. Crawford, Jr., "The Effect of Neutron Irradiation on Dielectric Materials – A Report of Some Studies at ORNL," *Conference on Effects of Radiation on Dielectric Materials*, Office of Naval Research Symposium Report, ACR-2, p 71 (Nov. 1, 1955).

M. C. Wittels and F. A. Sherrill, "Pile Bombardment Effects in Some Refractory Crystals," *Conference on Effects of Radiation on Dielectric Materials*, Office of Naval Research Symposium Report, ACR-2, p 81 (Nov. 1, 1955).

O. Sisman and C. D. Bopp, "Radiation Stability of Polymers," *Conference on Effects of Radiation on Dielectric Materials*, Office of Naval Research Symposium Report, ACR-2, p 85 (Nov. 1, 1955).

W. J. Sturm, "The Effects of Pile Neutron Irradiation on the Structure of Lithium Fluoride," *Conference on Effects of Radiation on Dielectric Materials*, Office of Naval Research Symposium Report, ACR-2, p 97 (Nov. 1, 1955).

C. C. Webster and A. F. Zulliger, "Remotely Operated Band Saw." Paper presented at the Fourth Annual Symposium on Hot Laboratories and Equipment, Washington, D.C., September 29–30, 1955.

C. C. Webster, "Remotely Operated Controlled Atmosphere Tube Furnace." Paper presented at the Fourth Annual Symposium on Hot Laboratories and Equipment, Washington, D.C., September 29–30, 1955.

L. N. Howell and C. C. Webster, "Remote Slitting Machine." Paper presented at the Fourth Annual Symposium on Hot Laboratories and Equipment, Washington, D.C., September 29–30, 1955.

SOLID STATE DIVISION SEMIANNUAL PROGRESS REPORT

SUMMARY

SOLID STATE REACTIONS

Thermal-Neutron Irradiation of InSb. – Data are presented that indicate the existence of an effect in InSb under slow-neutron irradiation that may be attributed to a Szilard-Chalmers type of reaction. A possible model of carrier-concentration changes that result from interstitial Sn^{116} atoms produced by slow-neutron activation is described. Slow-neutron flux measurements with gold foil do not agree with the slow-neutron flux measurements that are expected from carrier-concentration changes obtained from Hall-coefficient measurements. A further comparison of these two methods of flux determination will, therefore, be required.

Effects of Gamma Radiation on Germanium. – High-purity n- and p-type samples of germanium have been exposed to gamma rays from a 900-curie Co^{60} source. The extrinsic electron concentration of n-type material decreases at a rate only approximately 10^{-3} times that which occurs when the sample is irradiated with fast neutrons. Two electron-trapping levels, which are apparently identical to those produced by fast neutrons, have been observed. Extended exposure converts n-type material to p-type, indicating the presence of an acceptor level at approximately 0.26 ev above the valence band. This energy is somewhat larger than that found in fast-neutron-irradiated material. Interstitial clustering and nonuniform defect distribution are believed to lower the energy levels produced by fast neutrons; hence energetic photons apparently produce randomly distributed defects throughout the volume of the specimen. Exposure of p-type material causes a decrease in extrinsic hole concentration with a removal rate much less than that for n-type germanium. The cross section for atomic displacements obtained from these results is approximately 3×10^{-26} cm^2. This value is in reasonable agreement with the calculated cross section expected for the Compton electrons and photoelectrons produced by Co^{60} gamma-ray absorption in germanium.

Magnetic Susceptibility of n-Type Silicon. – The temperature dependence of the magnetic susceptibility of single-crystal specimens of silicon, two n-type and one p-type, has been determined. The curve for the p-type sample, 35 ohm-cm at room temperature, displays the same temperature dependence as that for pure germanium. The room-temperature value of the susceptibility was measured to be -1.156×10^{-7} cgs units. The value of the square of the reciprocal mass-ratio tensor for motion of conduction electrons (in silicon) in a magnetic field was found to be 14.4 from the susceptibility curve of one n-type sample. The curve for the second n-type sample appears to be anomalous.

Diamagnetism of Pure Germanium and Silicon. – The magnetic data for carbon in the form of diamond and for pure germanium and silicon are reviewed from the standpoint of the proposed theory of Krumhansl and Brooks concerning the origin of the temperature dependence of the susceptibility of the last two elements. Assuming, as a basis for argument, that the Van Vleck temperature-independent magnetic susceptibility for diamond is small (compared with the induced diamagnetic susceptibility), it is shown that the Van Vleck terms for germanium and silicon can be comparable in magnitude to the induced diamagnetic susceptibilities of these elements.

Optical Absorption Behavior of Irradiated Silica. – Transmission photographs of irradiated Corning silica by means of 2150-Å light indicate no inhomogeneities in this material in the far ultraviolet region. A re-evaluation of the oscillator strength of the 2120-Å band gives a value of 0.2, with indications of even a higher value. Irradiated specimens were annealed at 700°C and then irradiated again in order to study the rate of color-center formation. Also, unirradiated samples were annealed at 700 and at 1000°C in order to study the rate constants for a first-order reaction. Apparently, neutron bombardment generated sites available for color-center formation, not all of which were removed by the thermal bleaching process. It is postulated that color-center formation is due to free radicals, with stability achieved by stresses present in the glassy network.

ENGINEERING PROPERTIES

Infrared Spectra of Plastics and Elastomers After Irradiation. – The infrared spectra of polystyrene, polyethylene, polybutadiene, GR-S, natural rubber, deproteinized natural rubber, polyvinyl chloride, and Teflon have been measured before and after irradiation. These irradiations with a Co^{60} source, the Graphite Reactor, and the LITR were carried out in vacuum and in oxygen atmospheres. Dosages of the order of 10^8 to 10^{10} rads were required in most polymers to produce significant changes in their infrared spectra.

A large postirradiation effect was observed in the spectra of polystyrene, GR-S, and natural rubber. During exposure to air following irradiation in vacuum, oxidation products continued to form up to 95 days. These reactions were indicated by the growth of strong hydroxyl and carbonyl bands. Oxidation products were formed in postirradiation oxidation that were different from those produced by irradiation in oxygen. To prevent oxidation, polymers irradiated in vacuum were kept in a helium atmosphere during spectral measurements.

Irradiation of polystyrene at high doses in vacuum produced a wholesale disruption in which both the aromatic and aliphatic components were affected equally. On the other hand, on comparing GR-S and polybutadiene at equal dosages, the butadiene component of GR-S showed a greater per cent change than did pure polybutadiene.

All polymers showed significant changes in the double-bond regions as a result of irradiation. In polyethylene, $R_1R_2C{=}CH_2$ groups disappeared as *trans* $RCH{=}CHR_1$ groups formed. In GR-S and polybutadiene the number of terminal vinyl groups decreased, and unsaturation in the hydrocarbon chain of GR-S and natural rubber was decreased. Irradiation increased the number of *trans* $RCH{=}CHR_1$ groups in natural rubber as it did in polyethylene. Conjugated and unconjugated unsaturation were produced in polyvinyl chloride.

Radiation Stability of Ceramics. – The effect of reactor radiation on the elastic constants of a selection of ceramic materials was studied. A resonance method of measurement was employed. The frequency fell between 1500 and 5000 cps; the temperature was 25°C. In the case of some of the materials there is evidence that fast-neutron-produced displacements are dominant in causing changes; for other materials either ionizing radiation or thermal neutrons are more important; and still other materials are unchanged for the periods of exposure which were given. The change in the dynamic torsional modulus is of the same order as the change in dynamic Young's modulus. Little change was observed in internal friction for all the materials except cordierite and forsterite. The x-ray diffraction patterns for irradiated ThO_2 showed some lattice expansion. Annealed specimens of irradiated partially stabilized ZrO_2 showed a strengthening in the monoclinic phase and disappearance of the lattice expansion.

Effects of Annealing on Irradiated Zirconia. – X-ray studies of irradiated zirconia indicate that cubic (stabilized) ZrO_2, which is the stable form at high temperatures, is relatively stable when irradiated to 2×10^{20} fast neutrons/cm^2. The monoclinic phase, which is changed to cubic by irradiation, can be restored by annealing. Annealing the irradiated cubic phase counteracts the lattice expansion produced by irradiation.

X-Ray Examination of Irradiated Thoria. – Ceramic disks of ThO_2 and of ThO_2 + C exposed to a total integrated flux of 4×10^{19} *nvt* showed a lattice expansion of 0.4% in a_o and no particle-size broadening.

RADIATION METALLURGY

HRP Radiation Metallurgy. – Subsize Izod results from an 8½% nickel steel showed that the energy for fracture was decreased 40 to 80% by an irradiation of 10^{20} *nvt* (fast).

Ductility of Nickel Alloys. – The ductility minimum in monel in elevated-temperature tension tests was investigated; the existence of the minimum depends upon strain rate. The minimum in higher speed tests is at about 1000°F. At slow testing speeds the ductility is generally lower, except at 1000°F where it coincides with the values from higher speed tests.

CHEMICAL EFFECTS OF NUCLEAR REACTIONS

Pyridinium Borate. – An attempt to prepare metaboric acid by dehydration of orthoboric acid with pyridine resulted in the preparation of a new compound, pyridinium borate, $C_5H_5N{\cdot}3HBO_2$. The compound has been characterized by chemical analysis and by its x-ray diffraction pattern. The density is 1.448 ± 0.014 g/cm^3.

Yields of the Chemical Elements in Thermal-Neutron Fission of U^{235}. – The yields of most of the chemical elements occurring in thermal-neutron fission of U^{235} have been calculated as functions of irradiation time for the interval 10^2 to 10^7 sec. The results are presented graphically.

SPECIAL PROJECTS

Resistivity Changes in Alpha Brass as a Function of Neutron Irradiation. – The resistivity of an alpha-brass wire (12.9 at. % zinc) was measured periodically during a neutron irradiation lasting 29 weeks in the center of the ORNL Graphite Reactor. Following a rapid decrease in resistivity, there was a gradual linear increase of 0.23×10^{-4} μohm-cm/hr, which amounted, at the end of the 29-week irradiation, to about 1% over the initial resistivity value.

Effect of Neutron Radiation on the Precipitation-Hardening Reaction. – A neutron irradiation of the precipitation-hardening alloy, Ni-Be, at 300°C for three weeks in the ORNL Graphite Reactor has indicated an increase in the precipitation. The amount of precipitation as indicated by a shift in the measurement of the ferromagnetic Curie temperature is considerably greater than the precipitation in a control sample held at 300°C. A study was also made of the precipitation process in samples previously irradiated and subsequently heat treated at 450°C. In these samples there appears to be a lag in the initial precipitation in the irradiated samples.

A High-Temperature Furnace for Growing Alloy Crystals. – Construction of a versatile high-temperature furnace for growing alloy crystals is nearly complete.

Small-Angle X-Ray Scattering Technique. – A simple technique has been developed for making reproducable quantitative studies of small-angle x-ray scattering from such materials as Al-Ag in the region $2\theta = 0° 30'$ to $2\theta = 3°$.

Effect of Neutron Radiation on Precipitate Growth in Al-Ag. – Neutron irradiation is seen to retard precipitate growth in Al-Ag during heat treatment at 100°C following irradiation at approximately 40°C.

Paramagnetic Resonances in Unirradiated MgO. – A complex paramagnetic resonance spectrum has been observed in three single crystals of MgO. The center of the spectrum has a g value of 2.00 ± 0.01. The spectrum is composed of six major lines with satellites, the number of satellites per major line being 2 in two of the crystals and 4 in the third. Five additional lines are observed, one of which is apparently common to the three crystals, and this one has been attributed to excess oxygen.

The regularities of the six major lines indicate that they may be the hyperfine splitting arising from a nuclear spin of $\frac{5}{2}$. Several possible sources of the six-line spectrum are indicated.

Paramagnetic Resonances in Irradiated Fused and Crystalline Quartz. – Measurements have been made on the narrow resonance found in irradiated silica, indicating that the asymmetry of the resonance does not arise from two lines. Measurements at 23,000 Mc, compared with those at 9,000 Mc, show no resolution. The asymmetry of the line is apparently the same at both frequencies.

A broad resonance has also been observed in the Vitreosil and in the Corning silica. Its width at the inflection points is approximately 15 gauss and its g value is 2.010 ± 0.005.

Resonances found in natural and in synthetic quartz cut with the long axis parallel to the 110 and 001 planes reveal an orientation dependence. When the relative intensities and spread in g values of the lines are compared with the narrow resonance in the silica, it is suggestive of the conclusion that the resonance in the silica is the envelope of the narrow lines in the crystal summed over random orientations of regions of short-range order.

The temperatures of irradiation were approximately 250°C and approximately 320°C. On the basis of high-temperature stability of the narrow and broad resonance in silica, the apparent similarity of the narrow resonances in the fused material, the crushed crystal and the crystal given 3.3×10^{20} nvt, the correspondence of g values in the fused material and the crystals, the lack of hyperfine structure, and the dissimilarities of impurities in the six materials (Vitreosil, Corning silica, G-E silica, Amersil, natural crystal, and synthetic crystal), it is tentatively concluded that these two resonances do not arise from impurities but from some effect of irradiation on the basic SiO_4 tetrahedra.

An estimate of the total number of unpaired spins in the two resonances is 37% less than the number found by magnetic-susceptibility measurements for specimens of the same material irradiated at the same time and in the same irradiation facility.

Displacements from a Pile-Neutron Spectrum: Calculation for Germanium. – A calculation was made of the number of atoms displaced by a pile-neutron spectrum. The spectrum chosen was a sum of $1/E$ distributions extending to each element of a fission spectrum. This was applied to the case of germanium and was found to agree within a factor of 4 with the results of low-temperature irradiations.

Initial Expansion of LiF Under Neutron Irradiation. – The initial expansion of an LiF single crystal was measured during neutron irradiation at 60°C by the strain-gage technique. The linear expansion was $(9.9 \pm 0.3) \times 10^{-5}$ per 10^{15} thermal neutrons/cm^2, which indicates roughly 1400 displacements per (n,α) reaction. Displacement theory predicts 1900. These data indicate that little annealing occurred at 60°C.

Annealing of Quenched-In Lattice Defects in Au-Cd. – Measurement of dimensional changes induced in the beta-phase Au-Cd alloy by quenching have been extended to include strain changes. By the use of this technique, a determination of the activation energy for defect motion has been made. The value 0.5 ev, thus evaluated, is in good agreement with that obtained from electrical-resistivity measurement, namely, 0.6 ev. This fact, together with the rough agreement between the estimates of the number of vacancies produced upon quenching from 450°C, is taken as further indication that electrical and dimensional changes arise from the same mechanism and that vacancies constitute the defect produced by the quenching.

A Rocking-Curve Adapter for the X-Ray Diffractometer. – An adapter for use with a conventional x-ray diffractometer has been constructed so that rocking curves of single crystals can be obtained. Interchangeable sample holders make it possible to examine a variety of sample types. Provision is made for alignment of the specimen – the sample holder can be removed from the shaft and attached to a two-circle goniometer. The control mechanism permits either manual or automatic rocking.

Structural Studies in Irradiated Nonmetals. – Structural studies of neutron-irradiated nonmetals are presented. The behavior of fused-quartz single crystals under bombardment is similar to normal thermal behavior. A radiation-induced phase transition in ZrO_2 presents possible implications of the thermal-spike mechanism. Examples of neutron-induced amorphism in several silicate crystals are given. Two positive effects on the coherent x-ray reflections in neutron-irradiated single crystals are shown. Annealing studies on bombarded diamond powders reveal that both the rate of thermal recovery and the amount of residual damage are higher in the more heavily irradiated samples.

Effect of Radiation on Electrical Insulation. – It has been demonstrated that the radiation effects on lead-wire insulation are due to changes in the bulk of the insulation and that the effect of surface leakage was negligible.

Radiation Effects in Barriers. – Irradiations of point-contact germanium rectifiers and germanium transistors have been conducted in the ORNL Graphite Reactor and in a Co^{60} gamma source. The lattice dislocations in germanium due to Co^{60} gamma irradiation reported by Crawford and Cleland were observed. The behavior of the barrier change under gamma irradiation, however, was different from that observed under reactor irradiation.

Correlations were noted between the behavior of the back characteristic of a diode and the collector of a transistor, as well as between the emitter of a transistor and the forward direction of a diode. The correlation between the collector resistance change and amplification change was noted.

The need for complete families of characteristic curves as a function of exposures is indicated.

Thermal Conductivity of Dielectrics at Low Temperatures. – The effect of lattice defects in crystals is being studied by measurement of the thermal conductivity of a quartz crystal before and after successive periods of neutron irradiation and of a separate crystal before and after Co^{60} gamma irradiation. The measurements were made at low temperatures (2 to 100°K).

A single crystal of high-purity germanium was studied before and after two successive neutron irradiations, and an indication of partial annealing of the defects was found, as evidenced by thermal-conductivity measurements.

Other crystals presently under similar investigation include MgO, Al_2O_3, CaF_2, and KCl.

SOLID STATE REACTIONS

THERMAL-NEUTRON IRRADIATION OF INDIUM ANTIMONIDE

J. W. Cleland J. H. Crawford, Jr.

In a preliminary report[1] on the effect of slow neutrons on the electrical properties of InSb, it was indicated that a Szilard-Chalmers type of reaction might be detected in this material. Data were given which indicated that approximately one donor resulted for each slow neutron incident on the specimen, assuming a certain calculated value of the slow-neutron flux, and that further changes in carrier concentration upon extended high-temperature vacuum annealing were attributable to the annealing of fast-neutron-produced interstitials and vacancies. It was consequently concluded that activated atoms, if displaced at all, return to normal lattice positions at reactor ambient exposure temperature or that interstitial transmuted atoms contribute to the carrier concentration in a manner analogous to that of normal impurity atoms.

Further experiments have been performed in order to make certain that gamma-recoil effects are the only ones being observed. A determination of the relative neutron flux of the slanted animal tunnel of the ORNL Graphite Reactor was made by the Activation Analyses Group. Gold foil was used in the flux determination, and a value of 98.0×10^{-24} cm^2 for the activation cross section of the reaction $Au^{197}(n,\gamma)Au^{198}$ was used in calculating the flux value. The results of these measurements showed the flux to be $1.36\ (\pm 0.02) \times 10^9$ neutrons·cm^{-2}·sec^{-1}. The determination of the fast-neutron flux in this position was also attempted, but the sample employed was not activated above the background count of the very sensitive detection system used in this determination.

A further check of the possible fast-neutron flux in this location was made by means of high-purity germanium specimens. It was found from the total concentration of lattice defects that, as an upper limit, the ratio of all displacement processes (including those induced by fast neutrons and gamma rays) to the recoil effect is considerably less than 1%. In addition, the cross section for atomic displacements in germanium[2] by gamma rays has been determined to be approximately 1.5×10^{-26} cm^2, which is only approximately 10^{-3} times that for fast-neutron irradiations. Companion experiments on samples of InSb indicate an even smaller cross-section value for gamma-ray irradiations. It may therefore be concluded that fast neutrons and gamma rays are not present in sufficient concentration in this reactor position to affect the slow-neutron-produced changes in carrier concentration reported here.

In Table 1 are summarized the changes in carrier concentration obtained for a series of irradiations, and also indicated are the total changes in carrier

[1] J. W. Cleland and J. H. Crawford, Jr., *Solid State Semiann. Prog. Rep. Aug. 30, 1955*, ORNL-1945 p 12.

[2] J. W. Cleland, J. H. Crawford, Jr., and D. K. Holmes, "Effects of Gamma Radiation on Germanium," this report.

TABLE 1. CHANGE IN CARRIER CONCENTRATION ON IRRADIATING INDIUM ANTIMONIDE WITH THERMAL NEUTRONS

Sample	Change in Carrier Concentration (cm^{-3}), Δn	Incident Thermal Flux (neutrons·cm^{-2}), $(nvt)_{th}$	Carrier Removal Rate, $\Delta n/(nvt)_{th}$
N-6	6.01×10^{14}	4.37×10^{14}	1.37
	7.07×10^{14}	4.83×10^{14}	1.46
	9.10×10^{14}	7.35×10^{14}	1.24
			Av 1.36
N-8	6.92×10^{14}	4.84×10^{14}	1.43
	7.20×10^{14}	5.48×10^{14}	1.31
	1.13×10^{15}	8.24×10^{14}	1.37
	1.81×10^{15}	1.33×10^{15}	1.36
			Av 1.37
P-6	2.64×10^{15}	1.52×10^{15}	1.73
	2.10×10^{15}	1.33×10^{15}	1.58
	3.06×10^{15}	1.97×10^{15}	1.55
			Av 1.62
P-7	3.40×10^{15}	1.97×10^{15}	1.72
	3.18×10^{15}	1.96×10^{15}	1.62
			Av 1.67
		Total	
N-6	1.76×10^{15}	1.22×10^{15}	1.44
N-8	4.28×10^{15}	2.70×10^{15}	1.59
P-6	1.18×10^{16}	7.28×10^{15}	1.62
P-7	3.87×10^{16}	2.49×10^{15}	1.55
			Av 1.54

concentration obtained for the total irradiation and for subsequent vacuum annealing. The flux value measured by the gold-foil technique mentioned above was used in the calculation of the data.

It is evident from the results in Table 1 that more than one current carrier is added or removed for each slow neutron incident on the specimen. In fact, for every incident slow neutron, the average rate of addition of current carriers is approximately 1.37 for n-type material, and the average rate of removal of current carriers is approximately 1.65 for the p-type samples. The average removal or addition rate subsequent to total exposure and vacuum annealing, however, is approximately 1.54 per incident slow neutron. Subtraction indicates that approximately 11% of the slow-neutron-produced electron donors do not become effective in n-type material until after the vacuum anneal; whereas approximately 7% of the acceptors produced in p-type material by slow-neutron irradiation are removed by vacuum annealing.

If approximately 11% of the Sn^{116} atoms produced as a result of the Szilard-Chalmers type of reaction which follows slow-neutron irradiation of n-type InSb remain in an interstitial position at reactor ambient exposure temperature (~30°C), then it might be assumed that such interstitial impurity atoms do not ionize and, therefore, cannot contribute to the donor concentration. Vacuum annealing, however, would return these donor-type impurity atoms to the normal lattice where they could ionize and contribute to the donor concentration. The approximately 7% of the Sn^{116} atoms that appear to remain in an interstitial position in p-type material would be expected to ionize and contribute electrons to the indium vacancies, and this increases their hole-trapping efficiency; in addition, the indium vacancies themselves might be expected to contribute an electron. The net result, therefore, would be a greater trapping efficiency of holes as a result of some interstitial Sn^{116} atoms, which would be decreased if these atoms were returned to normal lattice positions as a result of vacuum annealing.

It may therefore be concluded that the experiments performed thus far indicate the possible existence of a Szilard-Chalmers type reaction in InSb at reactor ambient exposure temperature, and this effect should be greatly enhanced in experiments conducted under low-temperature-irradiation conditions. The disagreement between the calculated carrier-concentration change, in which the slow-neutron-flux data as determined by gold activation were used, and the carrier-concentration change, as measured by the Hall coefficient, is not understood, however, and future experiments will be made in order to investigate this discrepancy further.

EFFECTS OF GAMMA RADIATION ON GERMANIUM

J. W. Cleland J. H. Crawford, Jr.
D. K. Holmes

Recently, Dugdale[3] presented evidence that high-energy photons (Co^{60} gamma rays) enhance the ordering rate of disordered Cu_3Au in much the same manner, but to a considerably less degree, that fast-neutron bombardment does.[4] He explains this behavior as the result of the generation of atomic displacements by energetic Compton electrons and photoelectrons which result from gamma-ray absorption in the alloy. These resultant defects enhance the diffusion rate, and the rate of ordering is thereby increased.

Reported here are the results of studies of the effect of gamma radiation on the electrical properties of germanium. This material was chosen because of its very great sensitivity to fast-particle bombardment. In high-purity specimens, whose extrinsic carrier concentrations are in the neighborhood of $10^{13}/cm^3$, the presence of as few as 5×10^{11} displaced atoms per cubic centimeter may be detected with good precision by Hall coefficient and resistivity measurements. Five years ago, at the suggestion of K. Lark-Horovitz, attempts to observe gamma-ray effects in germanium were made, but the purity of available material at that time was too poor and the intensity of the Co^{60} source used was too low to yield positive results.

Both n- and p-type specimens cut in the form of Hall plates ($10 \times 3 \times 1$ mm) were exposed to 1.17- and 1.33-Mev gamma rays of equal intensity from a 900-curie Co^{60} source. The temperature of exposure was approximately 20°C. Before irradiation and after subsequent exposure, the resistivity ρ and the Hall coefficient R were measured as a function of temperature over the range 77 to 300°K.

[3] R. A. Dugdale, *Conference on Defects in Crystalline Solids*, p 246, Physical Society, London, 1955.

[4] T. H. Blewitt and R. R. Coltman, *Phys. Rev.* **85**, 384 (1952); *Acta Met.* 2, 549 (1954).

The photon flux was estimated from both geometrical considerations and water-decomposition measurements,[5] and the two methods yielded values that were in satisfactory agreement with each other.

Exposure of n-type germanium to gamma rays decreases the extrinsic electron concentration at an initial rate of approximately 1.4×10^{-3} electron per photon at liquid-nitrogen temperature (a rate only about 10^{-3} times as great as for fast neutrons). In a high-purity specimen (2×10^{13} electrons/cm^3) rapid saturation is apparent; but in a more impure sample (7×10^{14} electrons/cm^3) the effect is approximately linear up to an exposure of 5×10^{18} photons/cm^2. The high-purity specimen has been converted to p-type by gamma radiation, and the results obtained are summarized in Fig. 1, in which log R is plotted against reciprocal temperature for several of the exposures. Curve I, obtained before exposure, exhibits the expected behavior for a high-purity specimen. After 1.6×10^{16} photons/cm^2, two electron trapping levels exist, a deep one which is completely occupied throughout the entire extrinsic range, and a shallow state which is ionized at the higher temperature but is completely occupied at low temperature. The shallow level is responsible for the step in the extrinsic portion of curve II. A closer examination of curves of this type, in a range where the concentrations of exposure-produced levels are not sufficient to remove all the chemical donor electrons, reveals that the two levels are produced in approximately equal concentration. After additional bombardment, the shallow level controls the temperature dependence of the extrinsic electron concentration, as shown by curve III. The slope of this curve indicates that the shallow level lies approximately 0.2 ev below the conduction-band edge. These findings are virtually identical with those for fast-neutron bombardment of n-type germanium.[6]

Further exposure converts the specimen to p-type, and the slope indicates the presence of an acceptor (presumably the deep electron trap) at approximately 0.26 ev above the valence-band edge. This acceptor ionization energy is somewhat larger than that estimated for fast-neutron bombardment (~0.18 ev), but the difference may arise from the nonuniform distribution of defects and from a tendency for clustering of interstitials, indications of which are found in reactor-irradiated specimens.[6,7] This supposition is supported by the low-temperature-annealing behavior of the gamma-irradiated specimen. After 90 min at 120°C, the sample of Fig. 1 showed a marked decrease in Hall coefficient toward low temperature, and the slope of the curve indicates an acceptor ionization energy of approximately 0.16 ev.

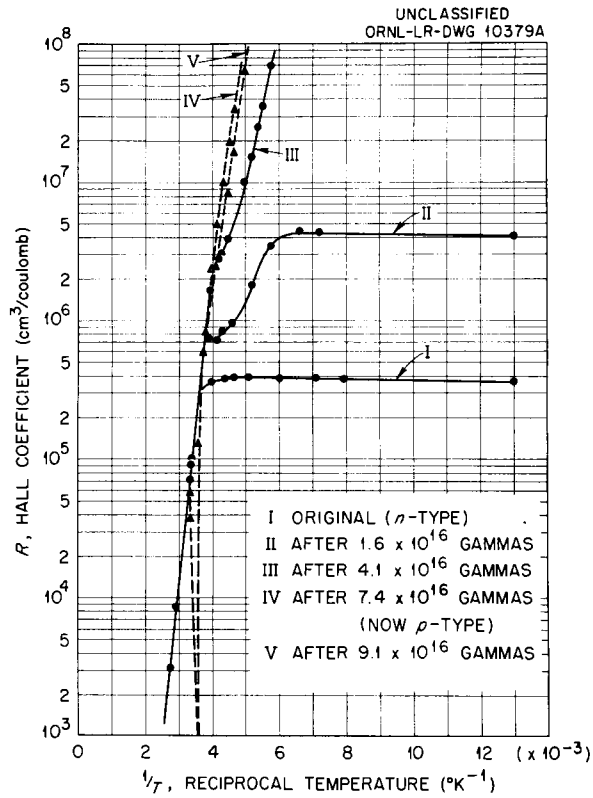

Fig. 1. Hall Coefficient vs Reciprocal Temperature of Initially High-Purity Germanium After Successive Exposures to Co^{60} Gamma Radiation.

These results suggest that gamma radiation indeed produces lattice defects in germanium. Moreover, the correspondence of these states with those of neutron-bombarded specimens and the apparent absence of complications expected from clustering and nonrandom distribution of defects

[5] This calibration was made by C. J. Hochanadel of the Chemistry Division.

[6] J. W. Cleland, J. H. Crawford, Jr., and J. C. Pigg, *Phys. Rev.* 98, 1742 (1955).

[7] J. W. Cleland, J. H. Crawford, Jr., and J. C. Pigg, *Phys. Rev.* 99, 1170 (1955).

would strongly suggest that individual interstitial-vacancy pairs are uniformly produced throughout the volume of the specimen.

The behavior of p-type germanium, although not so clear-cut as that of high-purity n-type specimens, is consistent with expectations based on the n-type results. Exposure decreases the hole concentration over the entire extrinsic range for a specimen whose initial concentration is approximately $1 \times 10^{13}/cm^3$, and the decrease saturates after prolonged exposure. The rate of carrier removal and the total decrease after saturation are considerably smaller than for n-type germanium. In view of the large ionization energy of the bombardment-produced acceptor level and the expected presence of hole traps,[7] a decrease in hole concentration is expected over the temperature range 77 to 200°K. After appreciable saturation, the hole concentration was considerably greater in magnitude and possessed a much smaller temperature dependence than did the converted n-type specimen (curve V, Fig. 1).

If it is assumed that at liquid-nitrogen temperature two electrons, one for each type of trap, are removed for each displaced atom the cross section σ_γ for displacing atoms by Co^{60} photons in germanium may be readily obtained from the initial rate of electron removal. The value of σ_γ has been found to be approximately $1.5 \times 10^{-26} cm^2$. The observed σ_γ is evidently the sum of the contributions resulting from the various gamma-ray absorption processes. Since, at these photon energies (1.17 and 1.33 Mev), pair production is negligible and since the cross section for direct interaction of the gamma ray with the nucleus is very small, the effect must be caused primarily by the Compton and the photoelectric processes.[3] It should be mentioned that the mechanisms suggested by Seitz[8] and Varley[9] to account for photon generation of defects in ionic crystals do not seem applicable to germanium. Evaporation of defects from dislocations by an exciton energy transfer process[8] does not seem probable because of the small exciton energies in germanium. Moreover, Varley's mechanism, which depends on the ejection of a multiply ionized anion from its lattice site by the crystal potential, is not expected to operate in a homopolar, covalent crystal.

Compton electrons and photoelectrons with energies greater than a threshold value, that is, with sufficient energies to transfer more than the necessary displacement energy E_d to a lattice atom, can displace atoms by coulombic interaction with the nucleus. In this regard, disordering of solids by gamma rays is essentially the same as by electron bombardment,[10] except for two factors: (1) a distribution of electron energies results from the Compton process, and (2) lattice damage can be produced uniformly throughout a relatively thick specimen by gamma-ray bombardment, whereas it is produced by electron bombardment only within the short electron range. The first factor renders this method of introducing defects relatively ineffective for precise determinations of E_d, but the second is quite desirable experimentally, since it permits the introduction of a uniform distribution of Frenkel defects for bulk property studies, without the limitation of sample dimensions imposed by electron range. Kinchin and Pease[11] have suggested an additional process, namely, atomic displacement by recoil during photoelectron ejection. For the photon energies involved here, however, the electrons are ejected predominantly in the forward direction with respect to the absorbed photon,[12] and, hence, the momentum transferred to the emitting atom is usually so small that the recoil energy is less than the displacement energy in the case of germanium.

The necessary information for calculating the contributions of the Compton electrons and the photoelectrons to σ_γ is summarized by Bethe and Ashkin.[13] If the expression for the electron-displacement cross section, based on the theory of Mott[14] as modified by McKinley and Feshback[15] and by Dugdale and Green,[16] is used and if an

[8] F. Seitz, *Revs. Mod. Phys.* 26, 7 (1954).

[9] J. H. O. Vorley, *J. Nuclear Energy* 1, 130 (1954).

[10] E. E. Klontz and K. Lark-Horovitz, *Phys. Rev.* 86, 643 (1952).

[11] G. H. Kinchin and R. S. Pease, *Reports on Progress in Physics*, vol. 18, p 1, Physical Society, London, 1955.

[12] A. Hedgran and S. Hultberg, *Phys. Rev.* 94, 498 (1954).

[13] H. A. Bethe and J. Ashkin, *Experimental Nuclear Physics*, ed. by E. Segre, vol. 1, p 166, Wiley, New York, 1953.

[14] N. F. Mott, *Proc. Roy. Soc. (London)* A 124, 425 (1929); A 135, 429 (1932).

[15] W. A. McKinley, Jr., and H. Feshback, *Phys. Rev.* 74, 1759 (1948).

[16] R. A. Dugdale and A. Green, *Phil. Mag.* 45, 163 (1954).

E_d of 25 ev is assumed, then on integration over both the energy distribution and range of electrons, a total value for both processes of approximately 1.3×10^{-26} cm^2 is obtained for σ_γ. In view of uncertainties in the photon flux and in the approximations in the calculation, this value is considered to be in satisfactory agreement with the observed σ_γ. A recent determination of E_d for germanium indicates that 23 ev is perhaps its upper limit.[17] This smaller value of E_d would increase the calculated σ_γ several per cent.

An interesting consequence of the calculation is that, contrary to expectation, the contribution of the photoelectrons is found to be approximately the same as that of the Compton electrons. This results from the fact that the electron-displacement cross section increases rapidly with energy and that the energy of photoelectrons is essentially that of the absorbed photon, whereas the effective Compton electrons have energies ranging from the threshold value to a maximum which is appreciably less than the photon energy (0.54 to 1.12 Mev).

MAGNETIC SUSCEPTIBILITY OF *n*-TYPE SILICON

D. K. Stevens

The temperature dependence of the magnetic susceptibility of two *n*-type single-crystal silicon specimens has been measured, and that of a pure single-crystal *p*-type specimen[18] has been remeasured. The results are shown in Fig. 2, where the top curve is for a phosphorus-doped 0.007 ohm-cm *n*-type specimen (RR-174), the middle curve is for a 35 ohm-cm *p*-type specimen (35-P), and the bottom one is for a phosphorus-doped 0.023 ohm-cm *n*-type sample (RR-176). The different symbols on a given curve indicate separate temperature runs. By use of the mobility data of Morin and Maita,[19] the electron concentrations in the first and last specimens were calculated to be 2×10^8/cm^3 and 7×10^{17}/cm^3, respectively.

The room-temperature concentration of holes in the 35 ohm-cm *p*-type specimen is 4.1×10^{14}/cm^3,

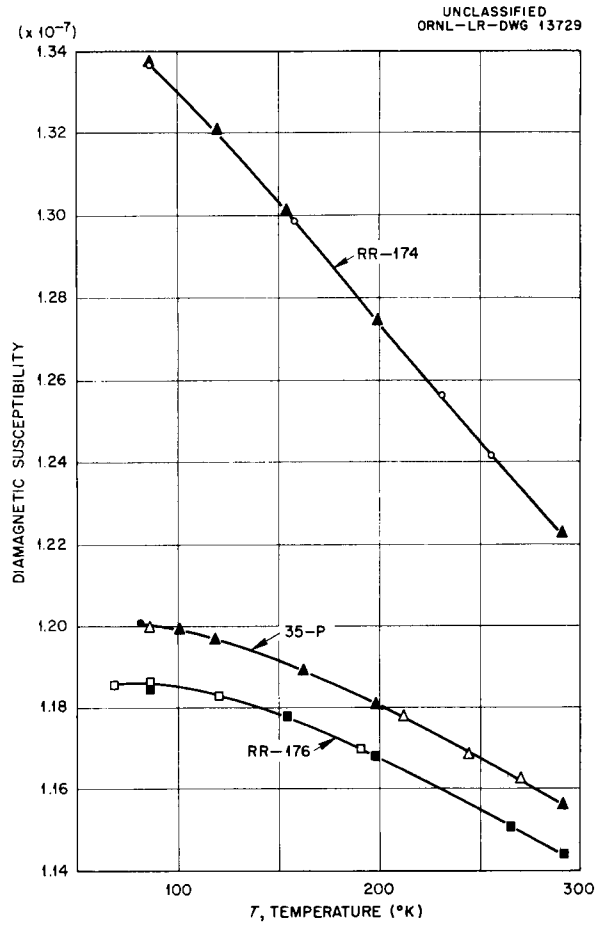

Fig. 2. Magnetic Susceptibility of Single-Crystal Silicon Specimens as a Function of Temperature.

and, therefore, their contribution to the total susceptibility is below the limit of resolution of this apparatus. The curve for this sample is considered to be that of the host silicon lattice. It is noteworthy that the temperature dependence is similar in degree and in kind to that of pure germanium.[20] For a more extensive discussion of the temperature dependence, see the next section of this report. The susceptibility-temperature curve for a fairly high-purity specimen of *n*-type silicon previously reported[21] does not correspond with the presently reported curve for the high-purity specimen. Re-examination of the old data reveals that

[17] J. J. Loferski and P. Rappaport, *Phys. Rev.* 98, 1861 (1955).

[18] W. W. Tyler and W. C. Dash of the General Electric Co. Research Laboratory, Schenectady, N. Y. and C. S. Fuller of the Bell Telephone Laboratories, Murray Hill, N. J. supplied the silicon samples and information concerning the carrier concentrations of each.

[19] F. J. Morin and J. P. Maita, *Phys. Rev.* 96, 28 (1954).

[20] D. K. Stevens *et al.*, *Solid State Semiann. Prog. Rep. Aug. 30, 1955*, ORNL-1945, p 17, esp. p 23; *Phys. Rev.* 100, 1084 (1955).

[21] D. K. Stevens, ORNL-1677, p 47 (Feb. 28, 1954) (Secret).

the specimen was polycrystalline and that some question existed as to the purity. The room-temperature magnetic data were field-dependent in a manner suggestive of ferromagnetic impurities. The presence of such impurities would explain the disagreement between the two curves, at least in part. Since the 35 ohm-cm p-type specimen is a single crystal, since it has a higher room-temperature resistivity, and since its carrier concentration at room temperature is known to be low ($\sim 4 \times 10^{14}$), it is considered to be the more reliable specimen for use in the determination of the silicon lattice susceptibility.

If the difference between the curves for a given specimen and a pure specimen is attributed to the susceptibility contribution of the carriers in the less pure specimen, the square of the reciprocal mass-ratio tensor for motion of these carriers in a magnetic field, $\overline{f_e^2}$, can be evaluated in a manner previously described for the case of germanium.[20] When this analysis is carried out for the n-type sample RR-174, which has approximately 2×10^{18} electrons/cm^3 in the conduction band, a value of 14.4 is obtained for $\overline{f_e^2}$. A value for $\overline{f_e^2}$ of 12.82 is obtained if the values for the effective masses of electrons in silicon, obtained by means of cyclotron-resonance techniques at liquid-helium temperatures,[22] are inserted into the expression

$$\overline{f_e^2} = \frac{2m_t + m_l}{3m_t^2\, m_l} ,$$

where m_t and m_l are the transverse and longitudinal effective masses, respectively. The agreement between the values obtained by the two methods is surprisingly good in view of the large number, and thus highly degenerate character, of carriers involved in the static susceptibility measurement.

With respect to position and curvature, the curve for the second n-type sample is anomalous. This curve was expected to fall intermediate to the RR-174 and the 35-P curves. The reason for this anomaly has not been determined, although it is to be remembered that in the early work on the susceptibility of germanium some samples failed to exhibit the expected behavior.[23] Failure at that time was attributed to impurity gradients and inhomogeneities in the sample.

[22] R. N. Dexter *et al.*, *Phys. Rev.* 96, 222 (1954).

[23] D. K. Stevens, J. H. Crawford, Jr., and J. W. Cleland, ORNL-1606, p 71 (Aug. 31, 1953) (Secret).

DIAMAGNETISM OF PURE GERMANIUM AND SILICON

J. H. Crawford, Jr. D. K. Stevens

In previous reports,[24] the anomalous temperature dependence of the magnetic susceptibility of germanium and silicon has been noted, and definite evidence for similar behavior in InSb has been discussed. In pure specimens of germanium and silicon, whose carrier concentrations are too small to make a measurable contribution, the diamagnetic susceptibility of the lattice atoms decreases with increasing temperature – at 300°K, $d\chi/dT = 2.4 \times 10^{-11}$ cgs units for germanium and 2.7×10^{-11} cgs units for silicon. This appreciable temperature dependence was puzzling, since the atomic diamagnetism is expected to be essentially independent of temperature. Another puzzling feature of the data was the fact that the absolute magnitude of the lattice susceptibility was considerably smaller than the susceptibility calculated from the mean-square atomic radius.

Krumhansl and Brooks[25] have explained these anomalies in terms of the superimposed temperature-independent (nominally) Van Vleck paramagnetism, which in the case of certain molecules has been shown to be of the same order as the induced diamagnetism. The expression for the Van Vleck paramagnetism involving only one excited state j has the form[26]

$$\chi_{vv} = \frac{2N}{\rho} \frac{|(j|\mu_z|0)|^2}{\Delta} ,$$

where N is the number of atoms per cubic centimeter, ρ is the density, Δ is the energy separation between the ground state and the excited state, and $(j|\mu_z|0)$ is the magnetic-moment matrix element connecting the two states. The energy separation Δ is expected to be temperature dependent, similar in extent to that for direct optical transition from the valence band to the conduction band; but the magnitude of Δ may be considerably greater than the optical gap, since at the center of the Brillouin zone the moment is zero.

[24] D. K. Stevens *et al.*, *Solid State Semiann. Prog. Rep. Aug. 30, 1955*, ORNL-1945, p 17, esp. p 23; *Phys. Rev.* 100, 1084 (1955).

[25] J. A. Krumhansl and H. Brooks, paper to be presented at the Pittsburgh Meeting of American Physical Society, March 1956.

[26] C. Kittel, *Introduction to Solid State Physics*, p 354, Wiley, New York, 1953.

If it is assumed that $\chi_{vv} \ll \chi_{dia}$ in diamond – this seems to be a reasonable assumption because Δ in diamond should be quite large and χ_{vv} quite small – much can be learned about the magnitude of χ_{vv} in germanium and in silicon by considering the homologous series diamond, silicon, and germanium. A check of the assumption within an order of magnitude can be made by calculating the diamagnetic susceptibility of the valence electrons in diamond from the equation

$$\chi_M = Nn \cdot \frac{e^2}{6mc^2} \cdot \overline{r^2} ,$$

where r, the radius of the valence electrons, is taken as one-half the interatomic distance d_0, χ_M is the molar susceptibility, N is Avagadro's number, n is the number of valence electrons, m is the mass and e is the charge of the electron, and c is the velocity of light. For diamond, one half the interatomic distance is 7.7×10^{-9} cm, and $n = 4$. Hence

$$\chi_M = -6.70 \times 10^{-6} \text{ cgs units/gram-atom} ;$$

the observed value is -5.5×10^{-6} cgs units/gram-atom. Since the chosen value for r^2 is expected to be somewhat high, in view of the nonspherical nature of the bonding orbitals, the agreement with observation is considered satisfactory.

In order to compare the various contributions to the susceptibility for these elements, it is assumed that the valence-electron diamagnetism is proportional to the square of the interatomic distance. If the estimated core electron contribution is used,[27] the total atomic diamagnetism for each element can be obtained relative to diamond. Comparison of these with the observed values yields the Van Vleck term. The results are tabulated in Table 2. Column 2 lists the values of d_0^2; in column 3 are presented the estimated valence-electron contributions; column 4 gives Van Vleck's estimate of the core contributions; and column 6 lists the observed atomic susceptibilities at 300°K. The Van Vleck term at 300°K, obtained by subtracting column 5 from column 6, is given in column 7. Hence it appears from this approximate treatment that on a specific-susceptibility scale (cgs units/g) $\chi_{vv} = 3.9 \times 10^{-7}$ for silicon and 1.90×10^{-7} for germanium. These values, even though approximate, indicate that the Van Vleck term is comparable in magnitude to the induced diamagnetism.

[27] J. H. Van Vleck, *Theory of Electric and Magnetic Susceptibilities*, p 224, Clarendon Press, Oxford, 1932.

OPTICAL ABSORPTION BEHAVIOR OF IRRADIATED SILICA

C. M. Nelson J. H. Crawford, Jr.

In a previous report,[28] preliminary studies of optical behavior in fused silica were discussed. This work has been continued with most of the attention being concentrated on high-purity Corning silica, which is of great interest in optical-coloration studies because of its great resistivity to coloration by high-energy photons. The absorption spectra for the Corning material are compared with those of Vitreosil, a commercial silica glass, in Fig. 3. Here the optical density for specimens of the same thickness is plotted against wavelength for two Co^{60} gamma-ray exposures: 1.5×10^7 r (solid curve) and 1.5×10^8 r (dashed curve). The short exposure strongly colors the Vitreosil over the entire range (2000 to 8000 Å), while the Corning specimen is only very slightly colored below 2500 Å. The second exposure produces a weak but well-defined band in the Corning specimen at 2150 Å, while the Vitreosil absorption is increased

[28] C. M. Nelson, *Solid State Semiann. Prog. Rep. Aug. 30, 1955*, ORNL-1945, p 32.

TABLE 2. A TABULATION OF THE COMPONENTS OF THE MOLAR SUSCEPTIBILITIES OF DIAMOND, SILICON, AND GERMANIUM

Element	$d_0^2 \times 10^{16}$ (cm^2)	$\chi_M \times 10^6$				
		Valence Electrons	Core	Total	Observed	Van Vleck
C	2.37	−5.33	−0.15	−5.48	−5.48	
Si	5.53	−12.40	−2.10	−14.50	−3.24	11.26
Ge	5.91	−13.27	−8.53	−21.80	−8.00	13.80

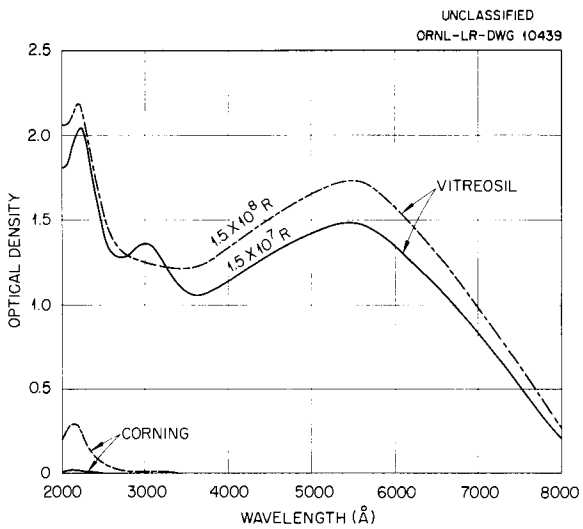

Fig. 3. Optical Absorption Spectra for Silica Irradiated with Co^{60}.

only slightly over most of the range, indicating that the short exposure has appreciably saturated the available color centers in this material. It is interesting to note that the heavy exposure has caused the 3000-Å Vitreosil band to disappear. This behavior was previously observed by Mitchell and Paige.[29]

Since the visible coloration in Vitreosil is patchy in nature, an effect which may be caused by an inhomogeneous impurity distribution, it is interesting to know whether a similar coloration inhomogeneity occurs in Corning silica. Specimens of either type were transmission-photographed by exposing densely colored ones backed by a photographic plate to wavelengths which were appreciably absorbed. The transmission photograph of the Corning specimen showed uniform coloration, whereas that of the Vitreosil sample reflected the patchiness. Hence, it may be concluded that the 2150-Å band in the Corning specimen is not associated with inhomogeneities in the specimen.

The Corning absorption spectrum developed by fast-neutron bombardment has been previously discussed.[28] One major absorption band at 2120 Å is prominent, and there is a second unresolved band at 2570 Å. In addition, the unsymmetrical nature of the 2120-Å band on the short-wavelength side is taken as evidence that there is additional absorption below 2000 Å. In contrast, the absorption spectra produced by Co^{60} gamma irradiation give much less indication of the 2570-Å band. An attempt to calculate the oscillator strength of the 2120-Å band in neutron-irradiated specimens has been reported;[28] Smakula's formula was used, and the unpaired electron concentration was determined magnetically. A re-examination of the data has revealed an error in the values previously reported. The correct one, under the same assumptions, is approximately 0.2, rather than 0.08. However, in view of the suspected additional absorption below 2000 Å, such a calculation would be in error, and, hence, the actual oscillator strength is perhaps much nearer unity.

A study of the rate of buildup of coloration has been performed on specimens exposed to both gamma rays and neutrons. The increase of extinction coefficient E, defined by the expression

$$\frac{I}{I_o} = 10^{-Ed} ,$$

where I_o and I are the incident and transmitted intensities of a given wavelength and d is the specimen thickness, is plotted against integrated exposure expressed in roentgens in Fig. 4. The two curves refer to specimens from two batches, and it is evident that the coloring susceptibility varies from one batch to the other. The curves can be fitted to a first-order buildup equation,

$$E = E_\infty (1 - e^{-k't}) , \quad (1)$$

where E_∞ is the saturation extinction coefficient, k' is the first-order rate constant, and t is the exposure time. Since the intensity of gamma radiation is constant during the exposure period, t may be expressed in terms of roentgens. The value of k' may be obtained from a knowledge of E_∞ and the initial slope A, since $E_\infty = A/k'$. The solid curves of Fig. 3 were calculated according to Eq. 1, and the points are experimental. The parameters required for the fit are $E_\infty = 4.86$ cm^{-1} and $k' = 4.8 \times 10^{-9}$ r^{-1} for specimen I and $E_\infty = 3.21$ cm^{-1} and $k' = 3.4 \times 10^{-9}$ r^{-1} for specimen II. Hence, it appears that past history of the specimen batch has an important bearing on the colorability of Corning silica also. Specimens from a given batch, however, all exhibit very nearly the same optical behavior; that is, the rate of color buildup is virtually the same.

[29] E. W. J. Mitchell and E. G. S. Paige, *Proc. Phys. Soc. (London)* B 67, 262 (1954).

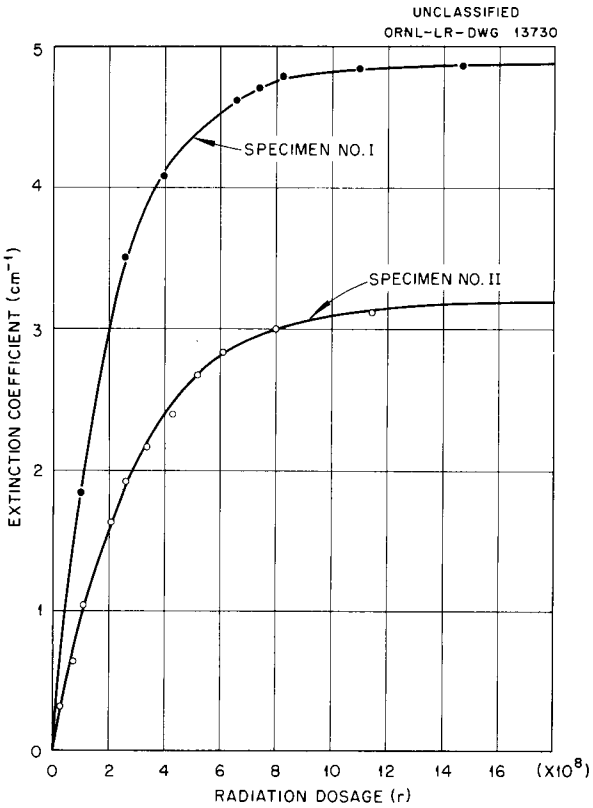

Fig. 4. Corning Silica Irradiated with Co^{60}. Curves are plotted as a first-order process.

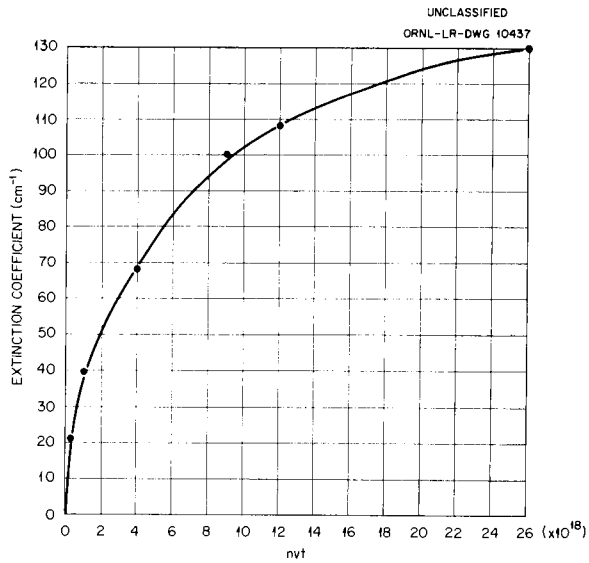

Fig. 5. Corning Silica Irradiated with Fast Neutrons.

Coloration of specimens with fast neutrons has also been investigated in greater detail. In a previous report (Fig. 30, ref. 28), evidence was presented which seemed to indicate that during neutron bombardment E did not saturate in a simple fashion but, rather, passed through a maximum value. Closer examination has shown this not to be the case, and the highest exposure point was found to be in error, as regards *nvt*. A more recent absorption vs exposure-time curve for neutron bombardment is shown in Fig. 5. It is apparent that for the same total exposure as used in Fig. 30 (ref. 28) there is no evidence for a maximum. Also worth mentioning is the fact that the curve of Fig. 5 cannot be fitted by the first-order buildup equation. This is perhaps due to the rapid initial saturation of those sites in the crystal which produce color centers, during gamma-ray exposure, superimposed on a color-center production process (as yet unknown) which results from fast-neutron bombardment. In order to study the neutron coloration process in greater detail, an irradiation facility for exposing specimens in the active lattice of the LITR has been fabricated and installed.

The primary reason for the interest in the 2150-Å band in fused silica is its similarity to a corresponding band in crystalline quartz. Moreover, the band seems to be independent of impurity content, whereas the visible bands are not; hence it is associated with damage to the crystalline network, or in this case the vitreous network. Since the glassy state has no long-range order, color centers cannot be identified with lattice defects in the usual sense. According to accepted ideas, the only order in silica glass is the fundamental SiO_4 tetrahedra; each oxygen atom acts as a bridge between two such tetrahedra or is common to them. Consequently, the only entities which can be conceived as responsible for color centers are impurity atoms which may trap electrons or holes and broken covalent bonds. It is the latter that are of concern here. Hence, in chemical terms, it appears reasonable to assume that free radicals are responsible for the coloration of pure vitreous quartz. According to this hypothesis, coloration by photons presents a problem because if the bonds are ionized by the radiation they would be expected to re-form in a period of approximately 10^{-8} sec unless prevented by some mechanism. Moreover, if the 2150-Å band is not associated with

impurity content, the effect of past history on E_∞ and the rate of coloration must be accounted for.

It appears reasonable to resolve these points on the basis of microscopic quenching strains produced during manufacture of the glass. Because of the high viscosity of vitreous SiO_2 in the region of the melting point, it is difficult for the SiO network to assume an unstrained configuration during solidification. Hence the amount of strain will be a sensitive function of the rate of cooling through the viscous range. If a given SiO bond which is under stress is ruptured, stress relaxation by separation of the nuclei is expected to occur in a short time, as compared with that required to reestablish the bond. Thus, the formation of a stable covalent bond may be prevented. This process would seem to explain the differences in susceptibility to coloration between different batches of Corning silica. The very large colorability at 2150 Å of Vitreosil is perhaps due to the much less rigid control of rates of cooling during manufacture.

In order to test this hypothesis, specimens of Corning SiO_2 were annealed at high temperature and cooled slowly. Figure 6 shows the rate of gamma-ray coloration of these specimens at 2150 Å. Although different specimens were used, they were obtained from the same batch; and previous experience had shown that such specimens should give essentially the same coloration behavior. It is evident that annealing at 700°C for 1 hr perceptibly reduces the rate and saturation value of coloration, and the 1000°C anneal has an even greater effect. In view of these studies, it appears that the colorability of pure silica glass by gamma rays may, indeed, be decreased by annealing. Further annealing experiments at higher temperatures are planned.

Another annealing study has been carried out which throws light on the effect of fast-neutron bombardment. It has been found that annealing at 700°C completely removes the absorption in previously irradiated specimens. Two colored Corning specimens, one exposed in the reactor until $E \sim 110\ cm^{-1}$ and one exposed to gamma rays until $E \sim 4\ cm^{-1}$, were thermally bleached at 700°C for a short period (1 hr). These specimens were then colored by gamma radiation, and the results are shown in Fig. 7. The specimen previously exposed to gamma radiation colors in the expected fashion, whereas the one previously bombarded with fast neutrons shows a very sharp initial rise

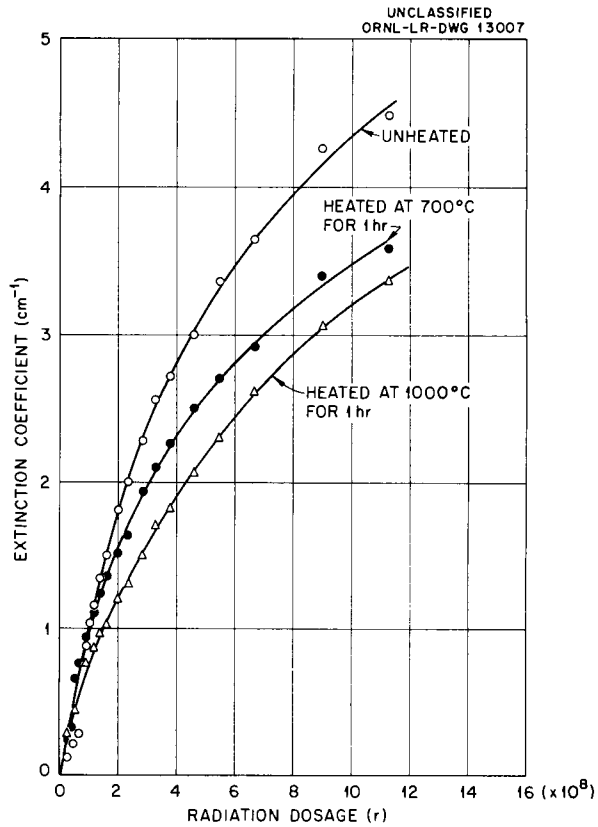

Fig. 6. Effect of Heat Treatment on Corning Silica Coloration.

of absorption, which is then followed by a more normal rate of coloration. These results indicate strongly that the effect of neutron bombardment is the manufacture of sites available for color-center formation, not all of which are removed by the thermal-bleaching process. It appears reasonable to assume that these sites are associated with displaced atoms which rupture the SiO_4 tetrahedra.

In addition to the 2150-Å band, fast-neutron bombardment produces very weak absorption centered near 6000 Å (Fig. 8). The intensity of this band is only approximately 0.0002 of that at 2150 Å. It is interesting to note that this band completely developed at an exposure of 4×10^{18} *nvt*, further bombardment tending to bleach it. This behavior of radiation in the bleaching of the visible absorption is similar to that reported[29] for impure material for the band at 5500 Å, and, hence, it is concluded that the absorption at 6000 Å represents an impurity band.

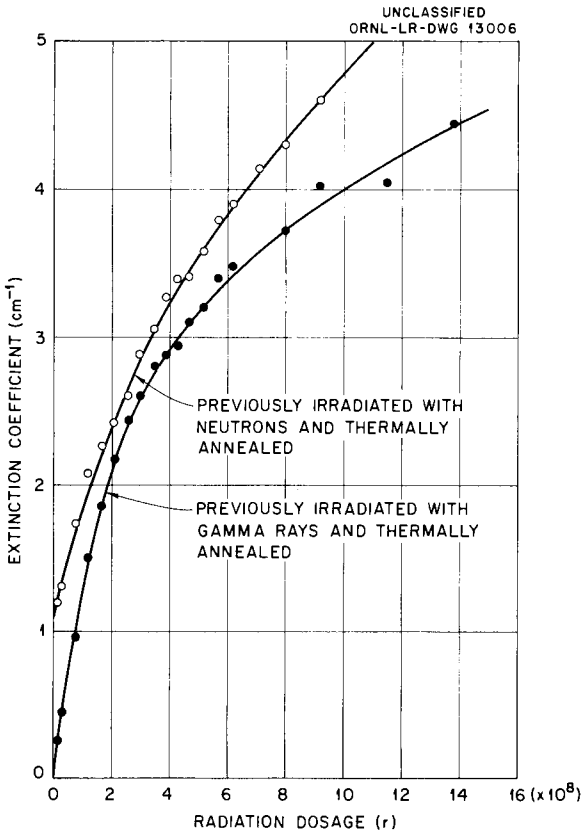

Fig. 7. Absorption Curves for Corning Silica Specimens Irradiated with Co^{60}.

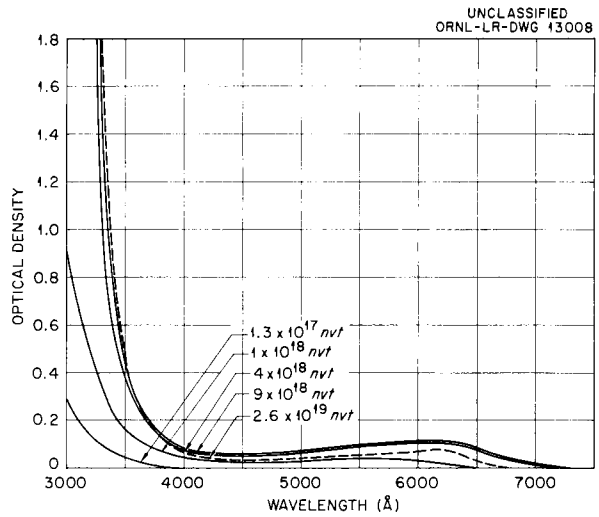

Fig. 8. Visible Coloration in Corning Silica Irradiated with Fast Neutrons.

ENGINEERING PROPERTIES

O. Sisman

INFRARED SPECTRA OF PLASTICS AND ELASTOMERS AFTER IRRADIATION

W. C. Sears W. W. Parkinson
O. Sisman R. L. Towns

Although it is well known that the physical properties of plastics and elastomers are changed greatly by nuclear irradiation,[1,2] the mechanism of irradiation effects and the resulting chemical reactions are still under investigation.[2-6] In the present study, the infrared spectra of polymers before and after irradiation have been measured in order to obtain an indication of changes in molecular structure resulting from irradiation. All infrared spectra were measured with a Perkin-Elmer model 21 infrared spectrophotometer.

The polymers shown in Table 3 were irradiated with the indicated dosages. The formulations of the cured elastomer films, which were supplied by

[1] C. D. Bopp and O. Sisman, *Radiation Stability of Plastics and Elastomers*, ORNL-1373 (Feb. 1, 1954).

[2] C. D. Bopp and O. Sisman, *Nucleonics* 13, No. 7, 28 (1955).

[3] D. S. Ballantine *et al.*, *Further studies of the Effect of Gamma Radiation on Vinyl Polymer Systems*, BNL-294 (1954).

[4] M. Dole, C. D. Keeling, and D. G. Rose, *J. Am. Chem. Soc.* 76, 4304 (1954).

[5] A. Charlesby, *Proc. Roy. Soc. (London)* A 231, 521 (1955).

[6] D. L. Loughborough *et al.*, *Report to Wright Air Development Center by the B. F. Goodrich Co. on Project 1GE* (Oct. 29, 1954).

TABLE 3. IRRADIATION DOSAGES OF POLYMERS FOR INFRARED SPECTRA

Polymer	Irradiation Exposure ($\times 10^8$ rads)				Average Sample Thickness (in.)
	Co^{60} Gamma, $\sim 10^6$ r/hr		Graphite Reactor, $\sim 10^6$ r/hr	LITR, $\sim 10^8$ r/hr	
	In Oxygen	In Vacuum	In Vacuum	In Vacuum	
Polystyrene[a]	11	2.3, 11	1.5, 16, 23, 31, 35	1000, 1000, 1500	0.0018
Polyalphamethyl styrene[a]	0.39, 6.9	6.6[b]	7.0		0.002
Polyethylene[c]	0.39, 3.9	1.2, 2.3, 6.2	3.4		0.0012[d]
Polybutadiene[e]		3.8, 6.1, 8.9	4.0[c], 14, 18		
GR-S[e]	0.72, 6.5	3.8, 6.1, 8.9	3.8, 13, 20		0.002
Natural (Hevea) rubber[e]		1.4, 8.9	4.8[f], 16		
Extracted Hevea[e]		1.4, 8.9	16, 22		
Polyvinyl chloride[e]	0.39, 0.72, 3.9	3.9, 5.2, 8.9	12, 40[b]		0.002
Polymethyl methacrylate[c]	0.39, 6.9	6.5[b]	2.0, 6.5		0.0004
Teflon[g]	0.72	3.8, 6.1	16, 22		0.0006
Mylar[g]	0.39, 6.9	2.3, 6.2	16, 17		0.00025
Nylon[g] resin No. 63	0.72	1.4, 6.1	22		0.0015

[a] Supplied by Dow Chemical Co.
[b] Sample crumbled, making measurement impossible.
[c] Commercial film.
[d] Also 0.008 and 0.030 in. exposed to 0.12×10^9 rads.
[e] Supplied by B. F. Goodrich Co.
[f] Tube cracked during irradiation.
[g] Supplied by E. I. du Pont de Nemours & Co., Inc.

the B.F. Goodrich Co., are indicated in Table 4. The vulcanizing compounds have three of their bands superimposed on the polymer spectra of polybutadiene, GR-S, and natural rubber; and during irradiation, these foreign bands nearly vanished.

The polymer films, after having been cemented on a 2.9 × 1.1 cm rectangular aluminum-wire frame, were evacuated for 2 to 5 hr and were then measured to provide a preirradiation spectrum. Films were irradiated in vacuum and in oxygen atmospheres as listed in Table 3. The films to be irradiated in vacuum were evacuated for 3 to 5 days at 0.2 μ and were sealed in vacuum in pyrex or quartz tubes prior to irradiation. These sample tubes were packed with aluminum foil in aluminum cans for irradiation. The polymers were irradiated by one or more of the following facilities: (1) Co^{60} gamma source, (2) water-cooled hole No. 19 of the ORNL Graphite Reactor, and (3) lattice position C-46 in the LITR. The maximum permissible dosage was limited in some polymer films by the formation of open slits caused by shrinkage and by loss in film strength. It was found that the dosage on polystyrene, polyvinyl chloride, mylar, and polymethyl methacrylate could be increased by irradiating them as unmounted films.

The discovery of postirradiation oxidation occurring in irradiated polymers during air exposure necessitated the opening of the vacuum tubes containing the irradiated samples in a helium atmosphere. An evacuable box fitted with arm ports and rubber gloves and recently constructed for the Solid State Division was used for manipulating the infrared samples in an inert atmosphere. For spectral measurement, each sample after irradiation was placed inside an infrared gas-absorption cell filled with helium. Measurement of the infrared spectrum was then repeated after extended exposures to air.

Polystyrene Irradiated in Vacuum

From the standpoint of change in physical properties, hydrogen evolution during irradiation, and change in infrared spectrum, polystyrene[1] is one of the most radiation-resistant polymers. Exposures of roughly 10^{10} rads in vacuum were required to produce significant spectral change. Polystyrene (Fig. 9) irradiated in the LITR has a spectrum showing very marked postirradiation oxidation. The oxidation occurred during exposure to air for 23 days following the LITR irradiation and a two-week "cooling" period in vacuum. Oxidation is evidenced by the greatly increased intensity of the O–H stretching band at 3450 cm^{-1} and the C=O stretching band at 1700 cm^{-1}. An indication that the oxygen came principally from molecular oxygen in air instead of from water vapor was (1) that polystyrene which was subjected to 3.5 × 10^9 rads in the Graphite Reactor showed far greater O–H and C=O band intensities after exposure to an atmosphere of oxygen for 14 days than after exposure to saturated water vapor for the same length of time and (2) that the O–H absorption in polystyrene subjected to 10^{11} rads was not lessened by evacuation at 0.2 μ for four days.

An irradiation dosage of 10^{11} rads appears to start a wholesale disruption of the polystyrene molecule. For example, it greatly reduced the intensities of the aromatic bands at 3060, 3026, 1946, 1868, 1802, 1743, 1603, 1495, 756, and 698 cm^{-1} as well as the aliphatic bands at 2924, 2850, and 1450 cm^{-1}. The 3060- and 3026-cm^{-1} bands are assigned to aromatic C–H stretching vibrations; the 1946-, 1868-, 1802-, and 1743-cm^{-1}

TABLE 4. FORMULATIONS OF ELASTOMERS

Polymer	Compound Added (wt %)						
	Stearic Acid	Zinc Oxide	Sulfur	Benzothiazyl Disulfide	Phenyl β-Napthylamine	Tetramethyl Thiuram Disulfide	Lead Stearate
Polybutadiene	1	5	2			0.3	
GR-S		5	2	1.75			
Crude Hevea	1	5	2.5	1	1		
Extracted Hevea	1	5	2.5	1	1		
Polyvinyl chloride							1

bands are overtone and combination bands of monosubstituted benzene; the 1603- and 1495-cm^{-1} bands are associated with conjugated double bonds; the strong 756- and 698-cm^{-1} bands arise from hydrogen atoms being deformed out of the plane of the benzene ring. The radiation stability of polystyrene has been attributed in part to its phenyl groups.[1] Although polystyrene is more resistant to radiation than other hydrocarbon polymers, the spectrum indicates that the aromatic ring undergoes damage at a rate comparable with that for the main hydrocarbon chain. Loss of aliphatic hydrogen during irradiation appears to result in the formation of double bonds in the chain, as evidenced by increased absorption at 1650 cm^{-1} for C=C stretching and at 965 cm^{-1} for hydrogen bending in *trans* $RCH{=}CHR_1$. The formation of new chemical compounds, having overlapping spectra, tends to obscure the spectra of individual compounds.

Polyethylene in Vacuum

During the summer of 1954, the spectra of polyethylene were measured and are generally in agreement with the results of Dole *et al.*[4] Both results indicate that during irradiation double bonds of the type $R_1R_2C{=}CH_2$ vanish, and double bonds in the polymer chain are formed. Polyethylene shows very little postirradiation oxidation at a dosage of 6.2×10^8 rads with Co^{60}.

Polybutadiene in Vacuum

The polybutadiene spectrum in Fig. 10 indicates that irradiation produces a sizable reduction in the number of double bonds at the ends of the polymer chain and very little, if any, decline in the number of double bonds in the chain. These irradiation effects are shown at 911 and at 990 cm^{-1}, which are characteristic of the hydrogen bending in $RCH{=}CH_2$, and at 965 cm^{-1}, which is assigned to hydrogen bending in *trans* $RCH{=}CHR_1$. The double-bond stretching band at 1640 cm^{-1} and the first overtone of the 911-cm^{-1} band at 1822 cm^{-1}, likewise, are reduced in intensity. A decrease in the terminal vinyl groups is indicated by the fact that the two characteristic C–H stretching bands at 3020 and at 3060 cm^{-1} diminish in intensity.

As a result of chain cleavage, a major reduction takes place in the strength of the 722- and 685-cm^{-1} bands, which are assigned to vibrations of the carbon chain. Irradiated polybutadiene exhibits a small postirradiation oxidation at 1708 and at 3400 cm^{-1} for C=O and O–H stretching vibrations, respectively. The band at 1540 cm^{-1}, which cannot be assigned to the polymer, appears to arise from the stearate ion.[7]

GR-S in Vacuum

Since GR-S is a copolymer of butadiene and styrene in the ratio 71/29, it might be expected to have better radiation stability than polybutadiene or natural rubber because it has phenyl groups attached to the chain. Comparison of the change in physical properties of GR-S and natural rubber[2] indicates no advantage for GR-S.

Irradiation causes changes in the double-bond regions of the spectrum of GR-S (Fig. 11) which are similar to those in polybutadiene. At a dosage of 2.0×10^9 rads, the terminal double bonds in GR-S, originating from 1,2-butadiene polymerization, have nearly vanished; and the number of *trans* $RCH{=}CHR_1$ groups has declined. These conclusions are substantiated by the decrease in intensity of both the C=C stretching band at 1640 cm^{-1} and the C–H stretching bands at 3020 and at 3060 cm^{-1}.

The preirradiation GR-S spectrum is a composite spectrum of its butadiene and styrene components. Qualitatively it appears to be the spectrum of a specimen consisting of a physical mixture of polybutadiene and polystyrene in the same proportion as in GR-S. A comparison of the spectra of GR-S and polybutadiene after each polymer has had a dosage of about 1.3×10^9 rads reveals (1) that the number of terminal vinyl groups appears to decrease at least as rapidly in GR-S as in polybutadiene, (2) that there appears to be no reduction in intensity of the bands associated with either the aliphatic (1455 cm^{-1} for CH_2 deformation) or aromatic parts of the styrene component of GR-S, and (3) that methylene groups (at 1445 cm^{-1}) from the butadiene component of GR-S are disrupted by irradiation, whereas they are stable in polybutadiene.

The bands at 722, 1400, and 1540 cm^{-1}, which almost vanish during irradiation, are due to the vulcanizing compounds. A big postirradiation oxidation effect, not shown in Fig. 11, also occurs in GR-S.

[7] N. Sheppard and G. B. B. M. Sutherland, *Trans. Faraday Soc.* 41, 261 (1945).

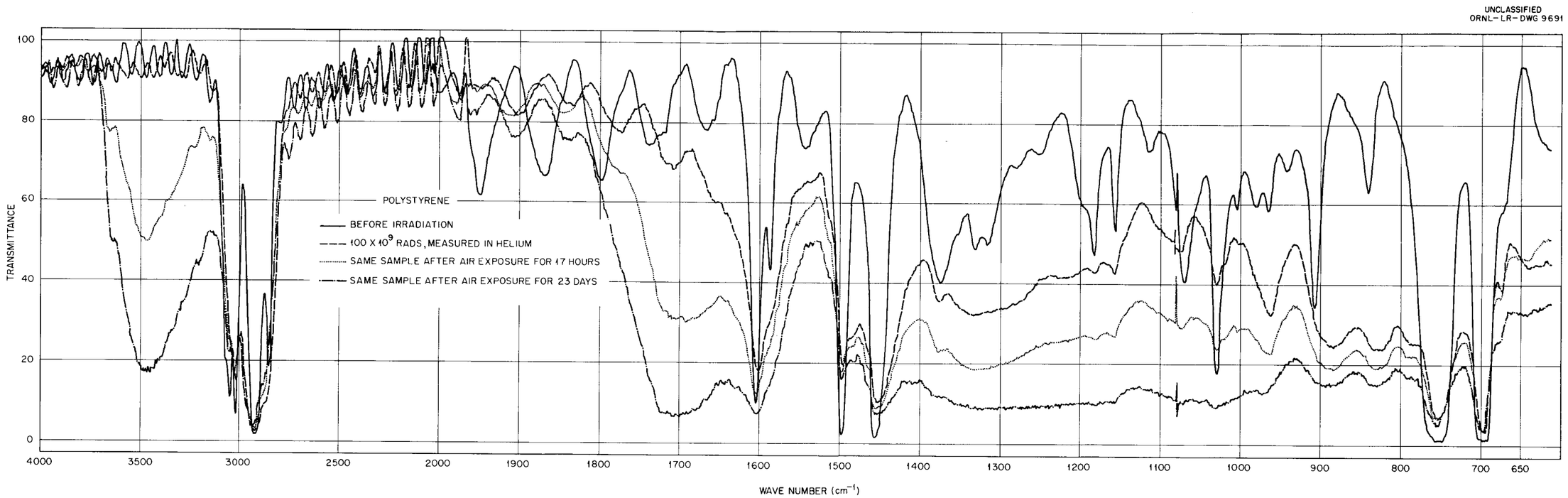

Fig. 9. Infrared Spectra of Polystyrene Irradiated in Vacuum.

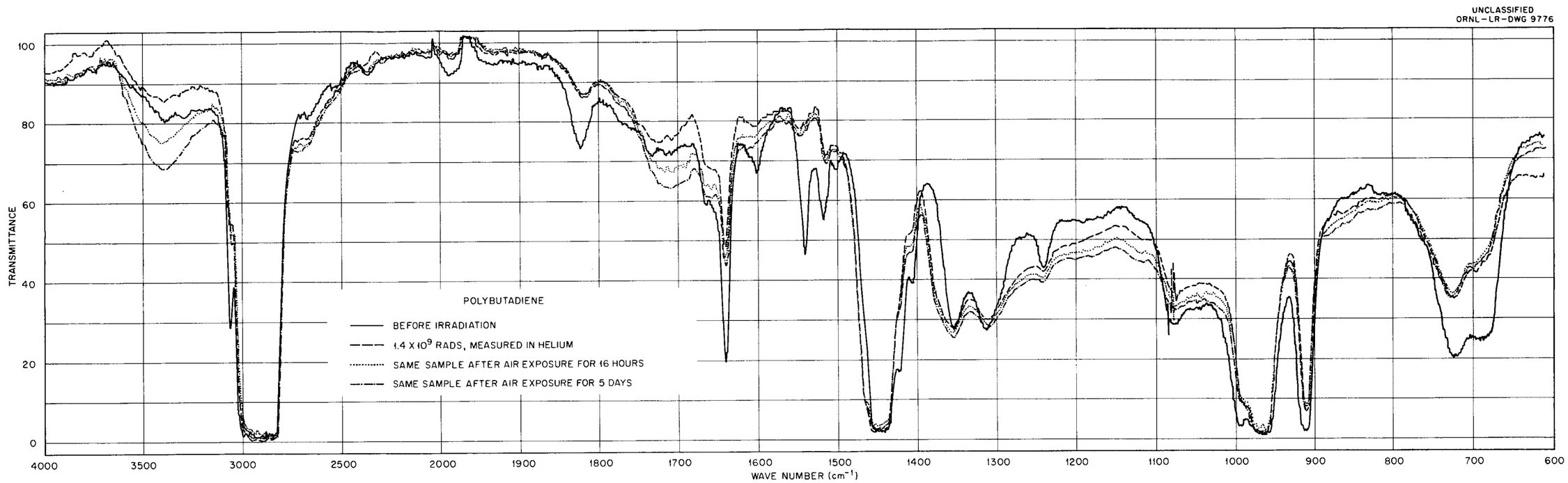

Fig. 10. Infrared Spectra of Polybutadiene Irradiated in Vacuum.

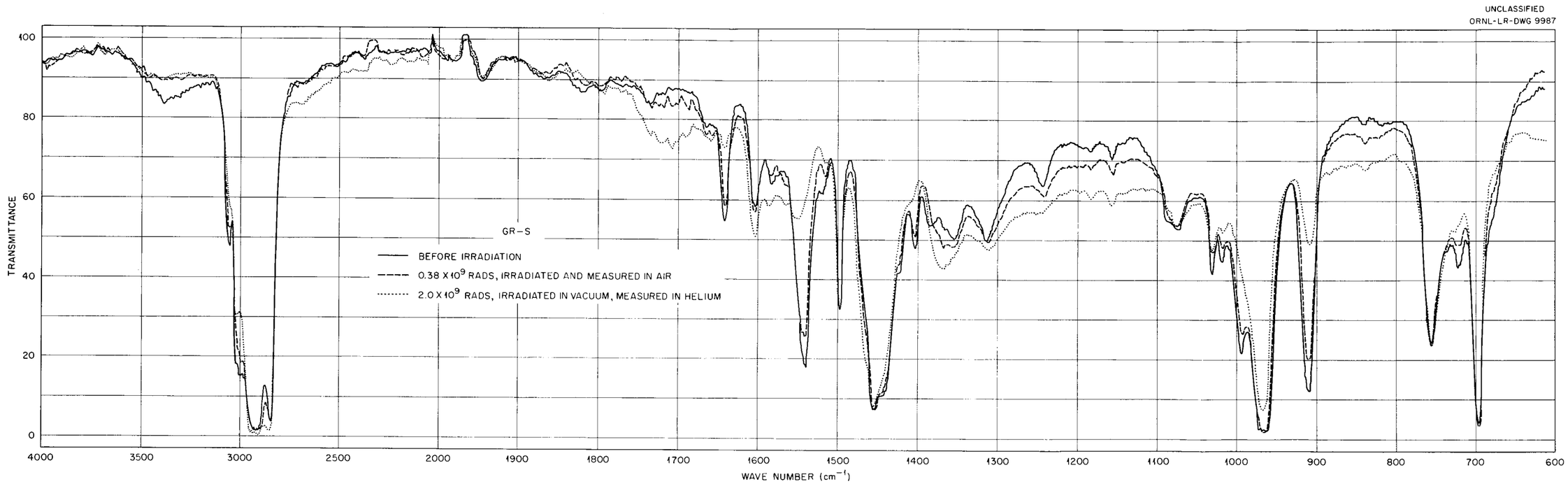

Fig. 11. Infrared Spectra of GR-S Rubber.

Natural Rubber in Vacuum

Natural (Hevea) rubber and Hevea extracted of most of its protein content were irradiated. The only significant difference in their spectra was that extraction reduced the intensity of the carbonyl stretching vibration at 1735 cm^{-1}. Some of the absorption at 1540 cm^{-1} is caused by the stearate ion.

The most important effects of irradiation on extracted Hevea, Fig. 12, were (1) the creation of unsaturation of the *trans* $RCH{=}CHR_1$ type, which is similar to the effect in polyethylene, as indicated by the new band at 965 cm^{-1}, (2) a decrease in the number of groups of the $R_1R_2C{=}CHR_3$ type (R_1 is a methyl group) as indicated at 835 cm^{-1}, (3) the activation of postirradiation oxidation at a dosage of 2.2×10^9 rads, comparable with that in polystyrene, (4) no apparent change in unsaturation at 835 cm^{-1} during oxidation, and (5) no loss of methyl groups from the polymer at 1377 cm^{-1}.

Polyvinyl Chloride in Vacuum

At dosages of 0.5×10^9 rads, changes occur in the infrared spectrum of polyvinyl chloride (Fig. 13) in the methylene deformation and C–H stretching regions. For example, for the polymer, methylene deformation absorption at 1432 cm^{-1} decreases in intensity, and a new methylene band appears at 1460 cm^{-1} which is associated with a chlorine-free alkyl structure. Corresponding changes in the C–H stretching frequency are observed as new bands which appear at 2850 and at 2940 cm^{-1} for alkyl methylene groups and at 3020 cm^{-1} for the $R_1R_2C{=}CHR_3$ group. Evidence for the formation of aliphatic conjugated double bonds is seen in the double-bond stretching band at 1600 cm^{-1}; this conjugation probably explains the reddish color formed in polyvinyl chloride. The $R_1R_2C{=}CHR_3$ stretching band is observed at 1655 cm^{-1}, and its hydrogen deformation band appears to result in the new band at 790 cm^{-1}. The decrease in intensity at 690 and/or at 635 cm^{-1} for the C–Cl stretching vibration may be an indication of loss of chlorine. Apparently the 965-cm^{-1} band does not indicate *trans* $RCH{=}CHR_1$ groups because such a strong band should have associated bands at 1650 and at 3020 cm^{-1}.

Although the postirradiation oxidation is comparatively slight, hydroxyl and carbonyl groups are formed after an exposure of 8.9×10^8 rads.

Other Polymers in Vacuum

For the maximum polymer dosages (Table 3), only minor changes were observed in the infrared spectra of polyalphamethyl styrene, polymethyl methacrylate, mylar, and nylon. Low film strength limited the dosage of polyalphamethyl styrene and polymethyl methacrylate. In order to prevent these films from being broken during irradiation, thicker, unmounted specimens might be used. Because of the high film strength of mylar, it may be able to withstand enough additional dosage to make some spectral change.

Bands in the nylon spectra between 1200 and 1700 cm^{-1} were poorly resolved because the specimens were too thick. The thickness was reduced from 2.5 to 1.5 mils by linear stretching. Thinner nylon film will be requested from du Pont.

Oxidation of Polymers Initiated by Irradiation

Polymers irradiated in an oxygen atmosphere do not form the same oxidation products as those which result from exposure to oxygen after irradiation. Probably, oxygen adds directly to the polymer during irradiation in oxygen. On the other hand, in postirradiation oxidation, several small molecular species and free radicals are formed first; these molecules together with the remaining polymer become oxidized. The fact that spectra of all oxidized polymers have such broad O–H and C=O stretching bands indicates that several different kinds of hydroxyl and carbonyl groups are formed. Table 5 compares the oxidation bands observed in polymers irradiated in oxygen with those formed by postirradiation oxidation.

Polymeric associated hydroxyl groups in alcohols give rise to a broad intense absorption stretching band between 3200 and 3500 cm^{-1}. Broad absorption between 2450 and 2800 cm^{-1} is believed to have its origin in the O–H stretching vibration of molecules of carboxylic acids which are associated as dimers. The corresponding C=O stretching vibration is found at about 1710 cm^{-1}. The 1695-cm^{-1} band in polystyrene may indicate aromatic ketones, and the bands at 1738 and 1763 cm^{-1} may indicate esters. Since the carbonyl frequencies characteristic of esters, ketones, and aldehydes overlap so much near 1710 cm^{-1}, it is almost impossible to identify each compound. Also, the C–O stretching and O–H deformation, δ(OH), are too variable for diagnostic purposes.

TABLE 5. OXIDATION BANDS INITIATED IN POLYMERS BY IRRADIATION

Polymer	Observed Frequencies (cm^{-1})					
	Irradiated in Oxygen			Postirradiation Oxidation		
	O–H	C=O	C–O and/or δ(OH)	O–H	C=O	C–O and/or δ(OH)
Polystyrene	2640	1695*	1183	3320	1685	
	3450*	1738	1280*	3450*		
	3550	1763	1320	3640	1700*	**
Polyethylene	2650	1713*	1125		1698*	
			1188*		1705*	
		1738	1288*	3400*	1715*	**
	3400*	1775	1415		1750	
Polybutadiene		1690		2400		
	3450*	1708*	1553	2520	1708*	**
		1720		2680*		
				3400		
GR-S	2600		1050*			1155*
			1175*	2600		1183*
		1713	1275	3400*	1708*	1310
	3400*		1375			1368
Extracted Hevea	2600	1708*		2600	1708*	
		1718	**	3380*	1770	**
	3380*	1770			1815	
Polyvinyl chloride	2600	1640				
	3400*	1720*	**	3450*	1715*	**

*Most intense bands.

**These absorption bands overlapped too much to permit resolution.

It seems safe to conclude that many of the oxidation products indicated previously, as well as alkyl ethers and anhydrides, may be formed. In discussing their spectra of polyethylene irradiated in oxygen, Ballantine *et al.*[3] refer to a "general rise in absorption" between 1000 and 1300 cm^{-1}. In the heat oxidation of polyethylene, Willis[8] concluded that aldehydes and ketones were formed because O–H and C=O, but no C–O, bands were observed.

Comments on Results

Unsaturation in polymer chains could be produced by loss of a hydrogen atom on each of two adjacent carbon atoms. Loss of a side chain and/or terminal unsaturation, as in polyethylene, polybutadiene, and GR-S, could accompany cross-linking, which is known to occur.[1] Since infrared spectra are fairly insensitive to changes in molecular weight, no specific indication of cleavage is found.

Apparently the extent of postirradiation oxidation depends critically upon the dosage. When each O–H band has grown to its maximum during air exposure, a quantitative measure of oxidation should be possible. Work is continuing on the analysis of the concentration of double bonds in the polymers.

[8]H. A. Willis, *Discussions Faraday Soc.* 9, 321 (1950).

RADIATION EFFECTS ON THE ELASTIC CONSTANTS AND THE INTERNAL FRICTION OF CERAMICS

C. D. Bopp O. Sisman R. L. Towns

The effect of radiation on the elastic constants and the internal friction of a number of ceramic

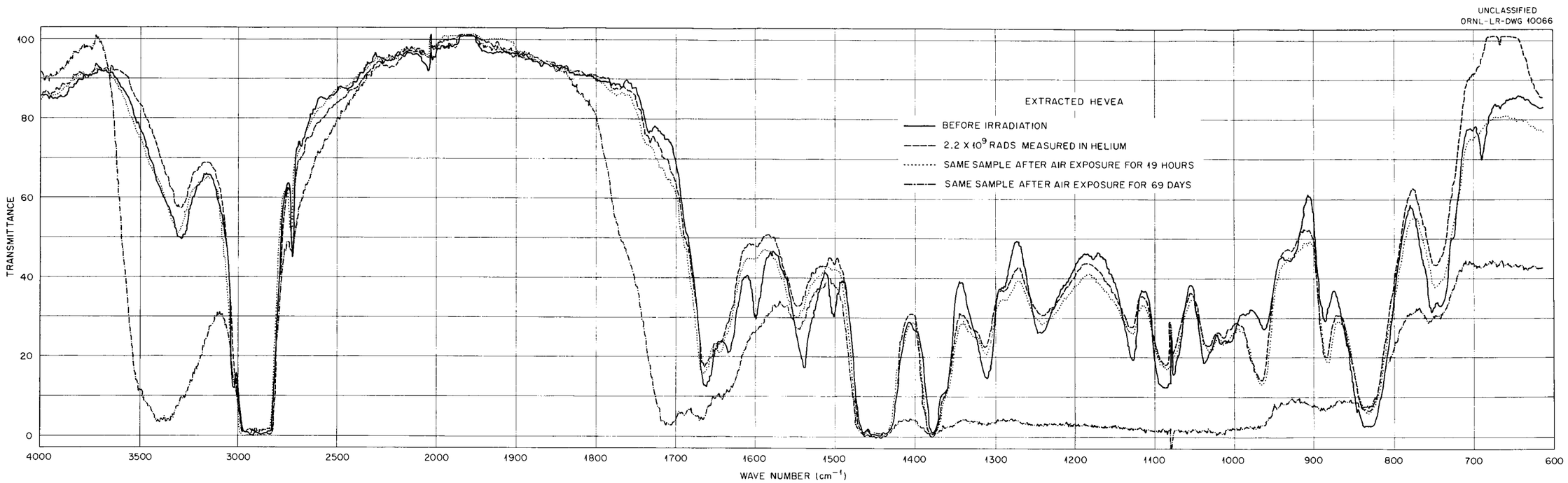

Fig. 12. Infrared Spectra of Extracted Hevea Irradiated in Vacuum.

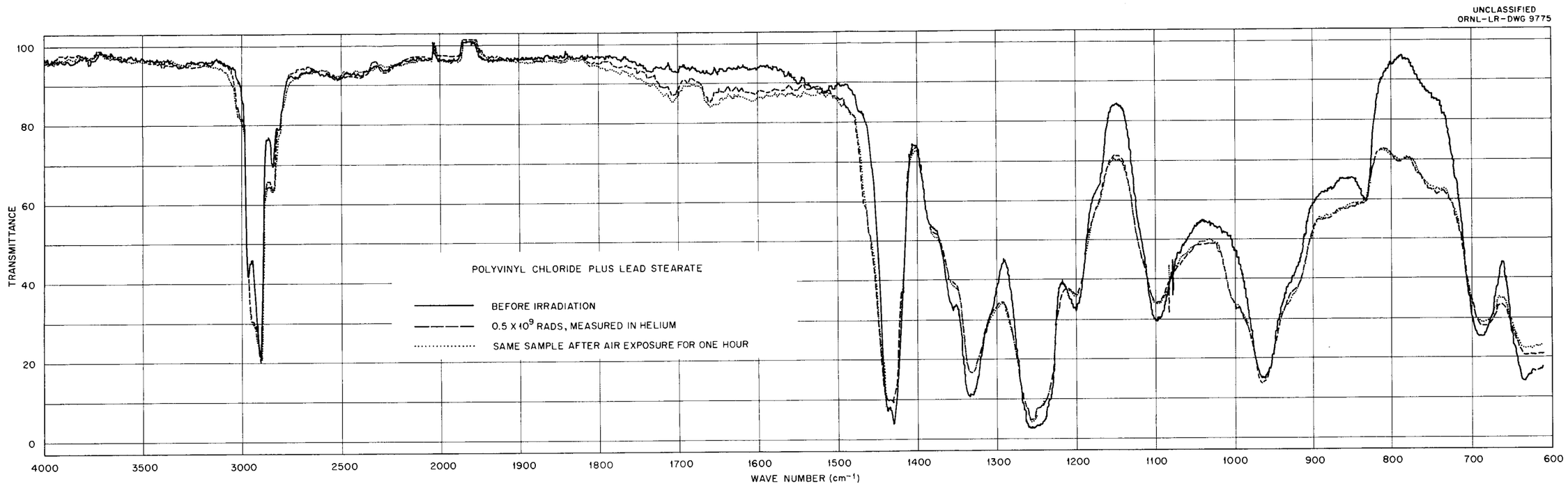

Fig. 13. Infrared Spectra of Polyvinyl Chloride Irradiated in Vacuum.

materials is shown in Table 6. These are the same materials for which the change in thermal conductivity and x-ray diffraction was reported.[9,10] Both the dynamic shear (or torsional) modulus and the dynamic Young's modulus were measured, and the friction was measured for both flexural and torsional modes of vibration; however, since within experimental error the changes for both moduli and for both types of friction are the same,[11] only the changes in Young's modulus and in the flexural friction are listed. The change in modulus is an apparent change, inasmuch as the radiation-produced change in density is not taken into account, but this is a small correction. The friction listed is higher than the absolute internal friction, since "background" is included as a result of the experimental method.[11]

With the exception of steatite, the materials which were homogeneous enough for a sensitive measurement of their elastic properties and which were decreased in thermal conductivity also decreased in modulus. Decreased elastic constants and thermal conductivity may result from the following processes: (1) displacement of atoms by fast neutrons, (2) introduction of impurities by thermal-neutron-induced transmutations, or (3) decomposition of molecules by ionizing radiation. Results are listed in Table 6 for three exposures – one conducted in the Materials Testing Reactor and the other two in a graphite-moderated reactor. For the MTR exposure, the integrated thermal flux

[9] C. D. Bopp, O. Sisman, and R. L. Towns, *Solid State Semiann. Prog. Rep. Aug. 30, 1955*, ORNL-1945, p 35.

[10] G. E. Klein, *Solid State Semiann. Prog. Rep. Feb. 28, 1955*, ORNL-1852, p 35.

[11] The measurements for zircon were more sensitive than for the other materials partly because of more uniform dimensions and partly because of the larger effect of radiation. In this case, Young's modulus changed about 25% less than the shear modulus.

TABLE 6. EFFECT OF REACTOR RADIATION ON THE DYNAMIC YOUNG'S MODULUS AND ON THE INTERNAL FRICTION OF SOME CERAMIC MATERIALS*

Exposure	Reactor	Integrated Epithermal Flux, 10^{19} *nvt*	Integrated Thermal Flux, 10^{19} *nvt*
A	Graphite	8	10
B	Graphite	16	20
C	MTR	3–6	30–60

Material	Decrease in Young's Modulus (%)			Friction (Q^{-1}) × 10^3			
	A	B	C	0**	A	B	C
Al_2O_3, single crystal		<10	<10	5		5	5
Al_2O_3, sintered		<10	<10	4		4	4
TiO_2 192			<5	4			4
Forsterite 243	10	11	21	4	3	4	5
Cordierite 202	22	27	46	12	5	5	5
Steatite 228		<5	<5	5	5	5	5
ZrO_2 550		<10	<10	6		6	6
Zircon 475	42	45	34	4	4	4	4
Silica glass		<5	<5	4		4	4
Plate glass		<5	<5	4		4	4

*At 25°C and at a resonant frequency in the range from 1500 to 5000 cps.

**Nonirradiated.

and the energy absorption from gamma radiation were greater, and the integrated epithermal flux was less than for the exposure in the graphite reactor. This difference provided a means of assessing whether displacements produced by fast neutrons are dominant in producing changes. In the case of the present data, there appears to be no means of distinguishing whether changes which do not follow the epithermal flux result from thermal neutrons or from ionizing radiation.

For many of the materials, the thermal conductivity and the elastic constants appear to have reached saturated values, since the values are nearly the same for all three exposures. The change in x-ray diffraction is not saturated, however, and follows the integrated epithermal flux in accord with a fast-neutron effect. An exception to this pattern is shown by cordierite, spinel,[12] forsterite, and steatite,[13] which show little change in x-ray diffraction but show a large change either in thermal conductivity or in elasticity. In this case, the change is not saturated but is greatest for the exposure with highest integrated thermal and gamma fluxes, in accord with an effect from radiation-introduced impurities. A check on this interpretation will be given by annealing experiments which are planned, since impurity-produced changes will not anneal as readily as fast-neutron effects.

A magnetostrictive driver was used to vibrate the specimen as is shown in Figs. 14 and 15. The amplitude of vibration was measured by the change in capacitance between the specimen and a charged plate which was placed close to the specimen. The specimen was made conductive by painting it with a suspension of graphite in ethyl acetate. The edge of the specimen is placed in a narrow, shallow slot in a brass block which is pivoted so that its weight holds the specimen against the driver. The driver is located to one side of the center of the specimen because this position will induce both flexural and torsional resonances. (In addition, double peaks[14] in the flexural resonance occurred less frequently when the driver was not centered.) The driving force is adjusted by tilting the block so that the position of its center of gravity is altered with respect to its pivot. The resonant frequency is nearly independent of the driving force, but the amplitude increases with the driving force.

The nodes move continuously along the specimen as the frequency is varied;[15] resonance occurs

[12] In the case of spinel a sensitive measurement of the elastic constants was not obtained because of the presence of small cracks.

[13] In the case of steatite there was no measurable change in elastic constants but a large change in thermal conductivity.

[14] G. Pickett, *Am. Soc. Testing Materials, Proc.* 45, 846 (1945).

[15] W. Elasser, *Ann. Physik* Series 4, 13, 791 (1904).

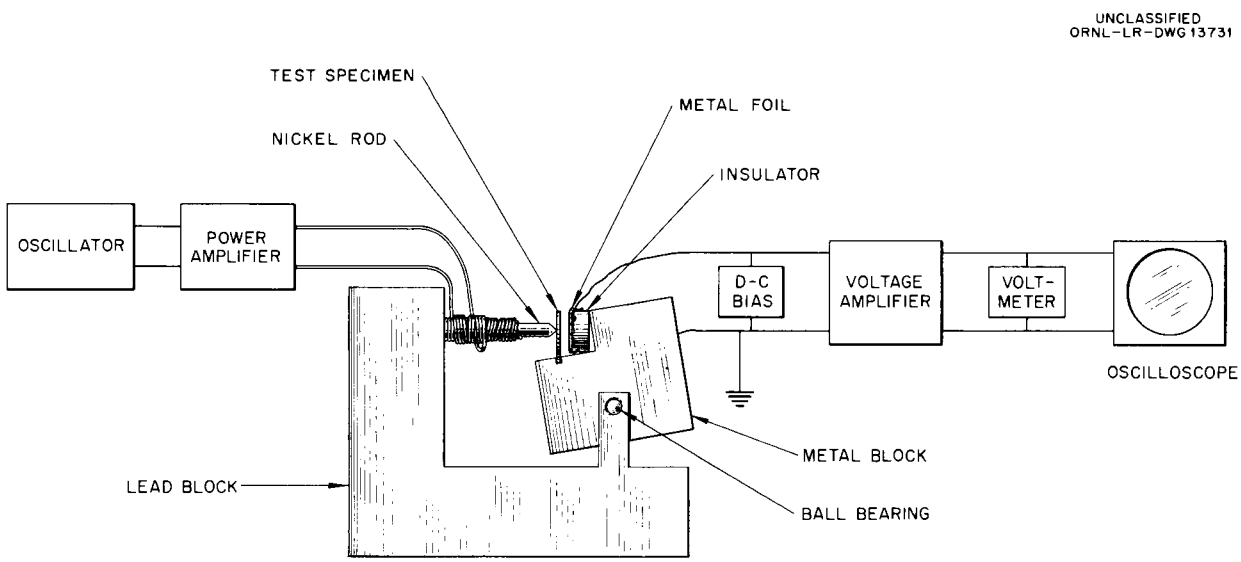

Fig. 14. Resonant-Frequency Measuring Apparatus.

Fig. 15. Resonant-Frequency Driver and Pickup Mounting.

when a node coincides with the position of the driver. At resonance the equation for free vibration holds approximately if the energy expended as friction (the energy supplied to the driver) is small compared with the total potential energy and kinetic energy alternately stored up by the specimen. The equation of vibration does not permit an exact solution for bars with variable cross section; even an approximate solution is difficult if the boundary conditions are complicated. By comparison of the results obtained from the present specimens (disks $\frac{3}{4}$ in. in diameter by 20 mils thick) and from specimens with uniform cross section (rectangular), it was determined, however, that the resonant frequencies of the present specimens are, for a limited variation in frequency, proportional to the quotient of the elastic modulus and the density (the same result as is given by solving the vibration equation for uniform bars). The changes listed in Table 6 are apparent changes, inasmuch as the radiation-induced change in density is not taken into account. By the use of stainless steel specimens of a suitable range of dimensions, it was determined that if the radiation-induced change in density is isotropic this correction is too small to have much of an effect on the results in Table 6. This effect is not predictable from simple theory, since the position of clamping is involved.

The mode of vibration associated with a particular resonance was identified from the effect that a change in position of the driver produced on the frequency and amplitude. For a torsional mode, the amplitude is increased as the driver is moved from the center of the specimen toward one side, but the frequency may not be much affected; however, for a flexural mode, the amplitude is not changed as much, but the frequency is affected. Invariance of the frequency for the torsional mode is taken as evidence that the torsional mode is not significantly coupled with the flexural mode; the shift in frequency for the flexural mode results from a change in the bending shape. Three resonances were readily detectable above the interfering resonances from various parts of the apparatus. For all the materials tested, the three frequencies were in the ratio (4.2–3.4):(2.5–2.0):1. By the method of identification just described, the lowest frequency is for a flexural mode, and the intermediate and the highest frequencies are for a torsional mode. Additional information was gained by moving the driver away from the clamp toward the free end of the specimen. The frequencies for the flexural mode and the torsional mode of lower frequency are raised; the frequency for the torsional mode of higher frequency is lowered. This associates the first two with a clamped-free bar which is driven near the clamped end, and the third, with a clamped-free bar which is driven near the free end.

The amplitudes of the two modes of lowest frequency are an order of magnitude stronger than those for the torsional mode of higher frequency or for any interfering resonances; therefore, there can be no significant coupling that would alter the frequencies of these lowest frequency modes other than the coupling between themselves. As already mentioned, there is evidence that there is not significant coupling between these two modes. Reproducibility of frequency measurements on individual specimens is limited by dimensional nonuniformity. For specimens which are not machined to close tolerances, best results are obtained by averaging several readings. (The specimen is reoriented each time so that a different portion is clamped.) In the most favorable cases, reproducibility was within 3%. For metals machined to close tolerances, the limiting factor is nonhomogeneity in elastic properties. Occasionally one or the other of the resonances was absent for some orientation of an individual specimen, or

there was a double peak in one of the resonance curves. This is attributed to nonhomogeneity. No attempt was made to analyze such cases, and the orientation was changed.

The friction was measured for both the flexural mode and for the torsional mode of lower frequency. The ratio of the bandwidth of the resonance curve to the resonant frequency, Q^{-1}, is listed in Table 6. (The bandwidth is the difference in the two frequencies where the amplitude is reduced to $1/\sqrt{2}$ of its maximum value.) The dependance of the amplitude on friction proved to be small for the small amplitudes which were used. Background friction from surface friction with air, from energy absorbed by the clamp, and from the Q which is characteristic of the magnetostrictive driver is less than 2×10^{-3}, since this value was measured for both 2S aluminum and stainless steel specimens. In order to study the mechanism of a change in internal friction, it would be advantageous to vary the temperature and frequency at which the friction is measured. In the present method, the frequency measurement is limited to the resonant frequency of the specimen, but it is planned to measure the temperature dependance. This type of measurement should be more sensitive than a comparison of absolute measurements at a single temperature, since the absolute value of friction often varies about 10 to 30% for different specimens of the same material.

RADIATION STABILITY OF CORDIERITE 202

In the previous report[16] the preirradiation thermal conductivity of cordierite was incorrectly reported as 23×10^{-4} cal·sec^{-1}·cm^{-1}·°C^{-1}. This value should have read 77×10^{-4} cal·sec^{-1}·cm^{-1}·°C^{-1}.

EFFECT OF ANNEALING ON IRRADIATED ZIRCONIA

G. E. Klein

Previous work on the x-ray study of irradiated zirconia ceramic specimens[17] showed that, for a partially stabilized ZrO_2 containing both the monoclinic and cubic phases before irradiation, the x-ray pattern of the monoclinic phase decreased in intensity and almost completely disappeared upon irradiation with 2×10^{20} fast neutrons/cm^2, while the cubic phase remained intact except for a 0.28% expansion in its lattice dimensions.

Next, the irradiated specimens were annealed at 1100°C (which is above the temperature at which normal monoclinic ZrO_2 transforms to the tetragonal form) for 1 hr. In the bottom curve in Fig. 16, it can be seen that the lines of the monoclinic phase partly return after the anneal, while the cubic portion of the pattern shows that the expansion produced by irradiation has been annealed out.

It would appear that cubic (stabilized) ZrO_2, which is the stable form at high temperatures, is relatively stable to irradiation (at least to 2×10^{20} neutrons/cm^2). The monoclinic phase which is changed to cubic by irradiation[18] can be restored by annealing. The effect of temperature on the irradiated cubic phase is to counteract the lattice expansion produced by irradiation.

X-RAY EXAMINATION OF IRRADIATED THORIA

G. E. Klein

Ceramic disks composed of both ThO_2 and ThO_2 + C were exposed to a total integrated flux of 4×10^{19} neutrons/cm^2 and were examined with the shielded x-ray diffractometer. The radiation from each sample was measured and was found to be approximately 4 r/hr at 1 cm.

Both samples show a lattice expansion of 0.4% in a_o after irradiation. No particle-size broadening is found in the irradiated specimens.

[16] C. D. Bopp, O. Sisman, and R. L. Towns, *Solid State Semiann. Prog. Rep. Aug. 30, 1955*, ORNL-1945, p 35.

[17] G. E. Klein, *Solid State Semiann. Prog. Rep. Feb. 28, 1955*, ORNL-1852, p 59.

[18] M. C. Wittels, Solid State Division Information Meeting, Dec. 1955.

Fig. 16. Effect of Radiation and Heating on Partially Stabilized ZrO_2.

RADIATION METALLURGY

J. C. Wilson

HRP RADIATION METALLURGY

R. G. Berggren J. C. Wilson

The results of notch-bar impact tests on subsize Izod specimens of an 8½% nickel steel (ASTM A353) are shown in Fig. 17. The mill analysis of this steel was: 0.10% carbon, 0.76% manganese, 0.23% silicon, and 8.58% nickel. The specimen stock was double-normalized from 1650 and 1450°F and tempered at 1050°F to produce maximum low-temperature toughness.[1] The grain size of the heat-treated steel was ASTM 8.

This steel has high toughness at low temperatures, and, thus, it is being studied in order to determine whether this high initial toughness improves resistance to brittle fracture at higher temperatures after irradiation. This steel in the unirradiated condition does not exhibit a sharp ductile-brittle transition in notch-bar impact tests at temperatures as low as −392°F; therefore, it cannot be directly compared with steels, such as the ASTM A212B steel reported previously,[2] which exhibit a sharp drop in impact strength as the testing temperature is lowered. Thus, it has not been possible with this steel to check the linear dependence of change of transition temperature on integrated fast-neutron flux that was observed in the ASTM A212B steel.[2]

The ASTM A353 steel is of interest also because of its high content (about 12%) of retained austenite in the heat-treated condition. It will be of interest to determine whether or not irradiation accelerates the rate of transformation of retained austenite. Elevated-temperature irradiations are in progress, and data from these experiments may provide an answer to this question.

One six-notch impact specimen was irradiated in the HB-3 facility of the LITR at a temperature of about 140°F to a calculated integrated fast-neutron flux ranging from 0.7 to 2.5 × 10^{19} *nvt* (>1 Mev). Two six-notch impact specimens were irradiated in the HB-3 facility of the MTR at a maximum temperature of 185°F to calculated integrated fast-neutron fluxes ranging from 1.0 to 3.8 × 10^{20} *nvt* (>1 Mev). The lower notch-bar impact strengths associated with greater integrated fast-neutron fluxes are apparent in Fig. 17.

An experiment containing impact and tensile specimens of a variety of steels has been assembled and is at the MTR for insertion in an HB facility of that reactor. Specimen temperatures in this experiment will be less than 200°F. Construction of an experiment designed for elevated-temperature irradiation of specimens in the MTR will begin soon. An experiment, for use in the MTR, in which impact and tensile specimens of titanium and Zircaloy will be irradiated at 575°F is now being designed.

Superficially the stress-strain curve at yielding in austenitic stainless steels after neutron irradiation is similar to curves produced by straining in tension, unloading, and reloading of unirradiated metal. The drop-in-beam type of yield point observed in unirradiated type 304L stainless steel

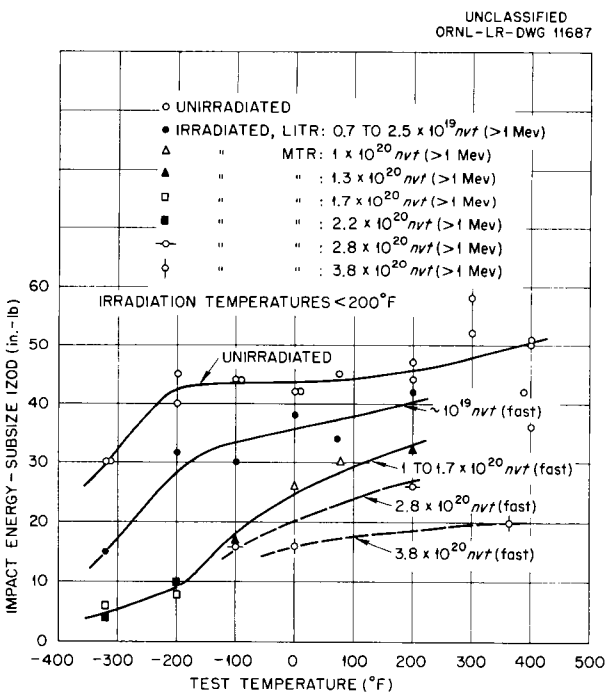

Fig. 17. Effect of Radiation on Impact Energy of 8½% Nickel Steel.

[1] G. R. Brophy and A. J. Miller, *Trans. Am. Soc. Metals* 41, 1185 (1949).

[2] R. G. Berggren and J. C. Wilson, *Solid State Semiann. Prog. Rep. Aug. 30, 1955*, ORNL-1945, p 37.

has been studied. At room temperature the drop-in-beam yielding is observed only after large amounts of plastic deformation (or irradiation); the unirradiated tension specimen is pulled until the stress is about 95% of the ultimate stress before a noticeable yield point is observed on reloading. Only partial unloading (about 10%) before reloading is required to bring forth the yield point. If the structure causing the yield point is formed by a diffusion process, the process must be very rapid, because the yield point can be made to appear in an unloading and reloading interval of less than 10 sec.

DUCTILITY OF NICKEL ALLOYS

T. C. Price J. C. Wilson

The ductility minimum that frequently occurs in tension tests of nickel alloys in the neighborhood of 1000°F is being studied. First the effect of strain rate is being measured. To date, fairly complete data have been obtained for monel, and work on Nichrome and Inconel is under way.

The gage-length portion of the tension specimens is 0.1500 ± 0.0005 in. in diameter and 0.60 ± 0.05 in. long. Two strain rates were used: 2 and 0.002 in./min. Test temperatures ranged from 800 to 1400°F. The ultimate and yield strengths at both strain rates seem to vary linearly with temperature. There was, however, a large non-linear decrease in elongation and in percentage reduction of area in the region 900 to 1000°F at the faster strain rate (Fig. 18). This anomaly was not observed at the slower strain rate.

At the lower strain rate (Fig. 19), the ductility values are lower than those obtained at the faster rate. At about 1000°F, the ductility values nearly coincide for both strain rates, so the processes responsible for the behavior are independent of strain rate at this temperature. At higher and lower temperatures, the curves tend to diverge, with the higher-strain-rate curves showing greater ductility.

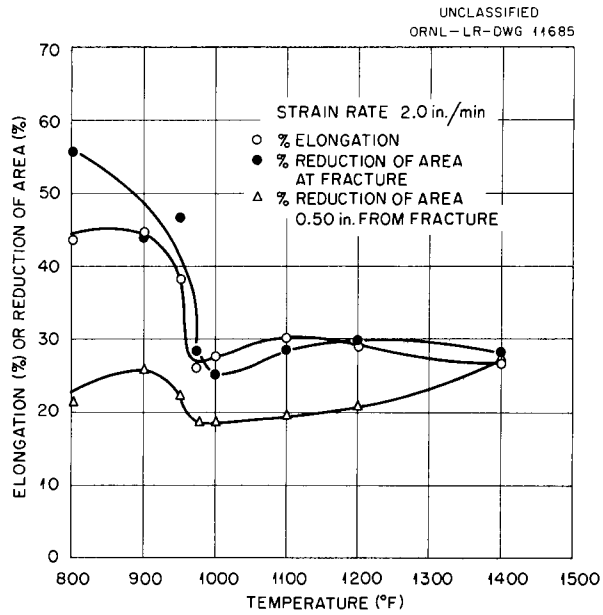

Fig. 18. Effect of Temperature on Tensile Ductility in Monel at a Strain Rate of 2.0 in./min.

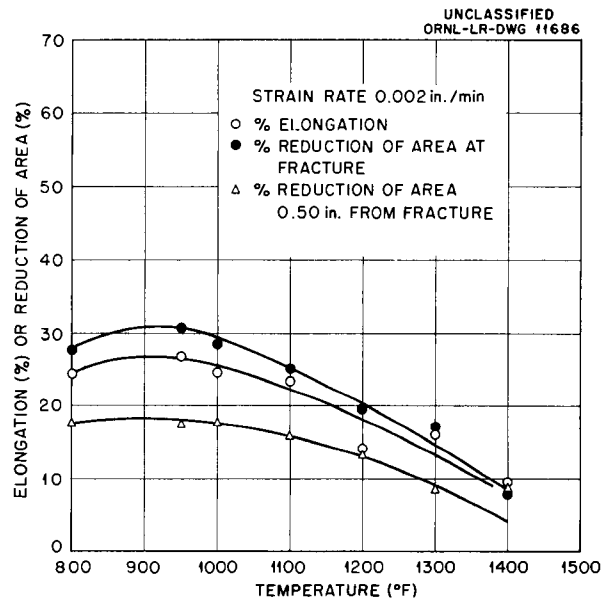

Fig. 19. Effect of Temperature on Tensile Ductility in Monel at a Strain Rate of 0.002 in./min.

CHEMICAL EFFECTS OF NUCLEAR REACTIONS

PYRIDINIUM BORATE

M. T. Robinson

A program for studying the effects of reactor radiation on the heterogeneous reactions between water vapor and the solid compounds in the boron oxide–water system has been initiated. It has been recently reported[1] that water could be extracted from orthoboric acid, H_3BO_3, by either pyridine or dioxane, producing either metaboric acid, HBO_2, or so-called pyroboric acid, $H_2B_4O_7$, depending on the temperature of extraction. This claim was based solely on the determination of the volume of hydrogen released by treating the resulting solutions with calcium hydride, the gas being attributed entirely to extracted H_2O. An attempt was made to use such an extraction as the basis of a new method for the preparation of metaboric acid.

The apparent solubility of H_3BO_3 in dioxane and in pyridine was determined at three different temperatures. Duplicate runs were made at each temperature. Each sample was prepared by placing powdered H_3BO_3 in a 2-oz polyethylene bottle, filling the bottle with the organic solvent, and sealing the screw cap with paraffin wax. For periods of from one to three weeks, the bottles were rotated end-over-end at 1 rpm in a water bath maintained at a temperature constant to ±0.1°C. The content of each bottle was rapidly filtered at the bath temperature, and two aliquots were withdrawn for analysis. These samples were diluted with the same solvent to prevent crystallization of solid. The solutions were analyzed for boron by inserting them in a paraffin block containing a Po-B source and measuring the reduction in neutron density.[2] The results are shown in Fig. 20. The large scatter in the results from the pyridine experiments is believed to be due to the chemical reaction of H_3BO_3 with pyridine:

$$(1)\quad C_5H_5N_{(liq)} + 3H_3BO_{3(cryst)} \longrightarrow C_5H_5N{\cdot}3HBO_{2(cryst)} + 3H_2O_{(soln)}$$

The relative amounts of the two phases govern the water content of the solvent and the solubility therein of pyridinium borate.

The solid phases separated from the solutions were examined both by chemical analysis and by x-ray diffraction. The solid in equilibrium with saturated dioxane solutions was shown to be unchanged H_3BO_3. The solid in equilibrium[3] with saturated pyridine solutions exhibited a very different x-ray diffraction pattern. Chemical analyses

[1] K. V. Astakhov, A. G. Elitsur, and K. M. Nikolaev, *Zhur. Obschei Khim.* 21, 1753–63 (1951).

[2] W. A. Brooksbank, G. W. Leddicotte, and J. E. Strain, *A Rapid Analytical Method Based Upon Neutron Absorption*, ORNL-1961 (to be issued).

[3] Because of the chemical reaction (1), the pyridine solutions are a three-component system. The boric acid content of the solution is not determined by the temperature alone, since it will also depend on the water content of the liquid phase.

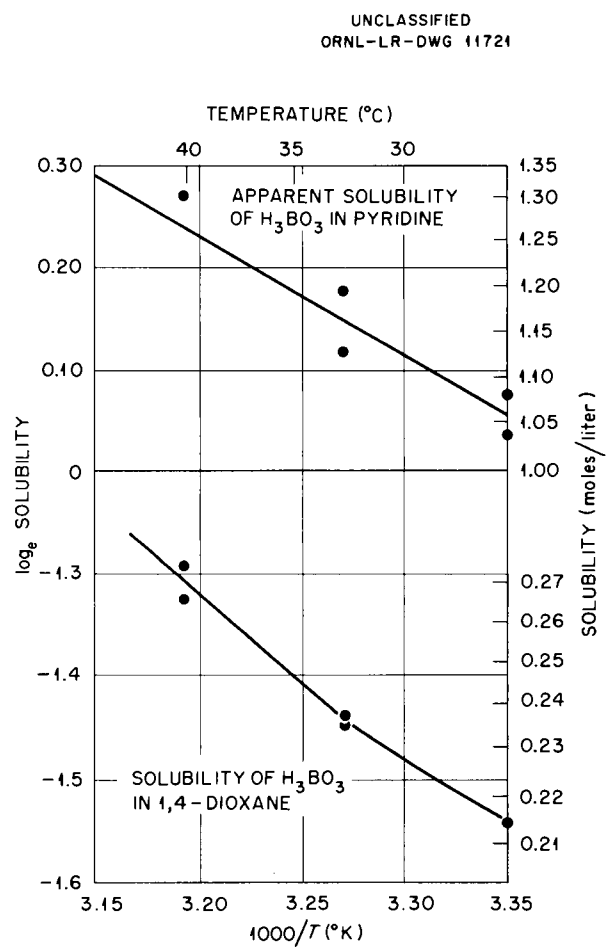

Fig. 20. Apparent Solubility of H_3BO_3 in Pyridine and in Dioxane.

presented in Table 7 support the composition $C_5H_5N{\cdot}3HBO_2$, which is perhaps better written[4] as $(C_5H_5NH)^+(H_2B_3O_6)^-$.

At all temperatures from 0°C to the boiling point of pyridine (115°C), crystalline orthoboric acid absorbs pyridine very rapidly, always producing the same product. The reaction proceeds so rapidly that the crystalline powder sinters to a coherent mass in a matter of a minute or less. The product separated by filtration of a slurry of pyridinium borate in pyridine contains about 20 wt % excess solvent, which is easily removed by subjecting it at room temperature to any of the following conditions: 1 hr at 10 μ Hg, 20 hr at 1 mm Hg, or 24 hr at 1 atm. The pyridinium borate produced in this way is probably identical with the unidentified compound described by Gebauer-Fülnegg and Riesenfeld.[5]

The x-ray diffraction pattern of pyridinium borate has not yet been completely analyzed. The substance appears to be orthorhombic, with some 18 to 20 formula weights per unit cell. The density, as measured by displacement of cyclohexane and of toluene, is 1.448 ± 0.014 g·cm^{-3} at room temperature. It is intended to extend this work to include other pyridine bases as an aid in the analysis of the x-ray diffraction pattern.

When heated in a sealed tube, the compound melts incongruently at about 148°C to a white solid and a very volatile, colorless liquid. In a thermal decomposition study, a sample was heated at 124°C for about 20 hr at a pressure of about 10 μ Hg. Chemical analyses showed that almost all the 16% weight loss was water. X-ray diffraction showed that the resulting product was amorphous.

[4] X-ray diffraction data indicate that HBO_2 is always trimerized in the solid state: see H. Tazaki, *J. Sci. Hiroshima Univ.* **A10**, 55 (1940), and W. H. Zachariasen, *Acta Cryst.* 5, 68 (1952).

[5] E. Gebauer-Fülnegg and F. Riesenfeld, *Deutsches Reich Patent 482,266* (Dec. 24, 1925).

YIELDS OF CHEMICAL ELEMENTS IN THE THERMAL-NEUTRON FISSION OF U^{235}

M. T. Robinson J. F. Krause[6]

The yields of most of the chemical elements occurring in thermal-neutron fission of U^{235} have been calculated from data compiled by Blomeke[7] on the mass yields, radioactive half lives, and decay schemes of fission-product nuclides. Desk-computer methods were used to solve the conventional growth-and-decay differential equations for each mass chain from 72 to 161 for the irradiation-time range 10^2 to 10^7 sec (2 min to 116 days). The amount of each element was obtained by summing the values for each of its isotopes. Finally, the

[6] On loan from Pratt & Whitney Aircraft.

[7] J. O. Blomeke, *Nuclear Properties of U^{235} Fission Products*, ORNL-1783 (Oct. 21, 1955).

TABLE 7. CHEMICAL ANALYSES OF PYRIDINIUM BORATE[a]

Sample No.	Composition (wt %)					
	Carbon[b]	Hydrogen[b]	Boron[c]	Boron[c]	Pyridine[d]	Water[e]
PB-15b	29.7	3.6	16.1	15.3	34.6	53.7
PB-15c	29.7	3.7	16.0	15.3	34.2	53.3
PB-15d	28.9	3.6	16.1	15.3	35.5	52.8
PB-15e	29.4	3.8	15.8	15.3	35.3	52.8
			Calculated			
	28.5	3.8	15.4		37.6	51.3

[a] $C_5H_5N{\cdot}3HBO_2$.

[b] Determined by combustion.

[c] The two sets of boron analyses were determined at different times by different groups at ORNL.

[d] Determined by distillation of pyridine, followed by titration.

[e] Karl Fischer method – includes water produced by the reaction $HBO_2 + 3CH_3OH \rightarrow (CH_3O)_3B + 2H_2O$.

yield of each element was gotten by dividing the quantity of the element by the total number of fissions which had occurred up to the time in question. The following assumptions were made in performing the calculations:

1. The fission rate was taken to be independent of time; that is, burnup of U^{235} was ignored.
2. Nuclides having half lives less than about 1 min were neglected.
3. Nuclides having half lives greater than about one year were assumed to be stable.
4. With the exception of Cs^{136}, shielded nuclides and their descendants were neglected.
5. Neutron capture (and delayed-neutron emission) by the fission products was neglected, except in the case of Xe^{135}.
6. Isomeric states with half lives that are short compared with the ground state were neglected, except where decay directly to the daughter is known to occur.
7. For calculations involving Xe^{135}, the thermal-neutron flux was assumed to be sufficiently high that no decay to Cs^{135} occurred.

In Fig. 21 the yields of the chemical elements are plotted against atomic number for three different irradiation times. The familiar double-maximum mass-yield curve is reflected in the two irregular blocks in each plot. Superimposed on this is a strong even-odd alternation, owing to the fact that the elements with even atomic number have many more stable and nearly stable isotopes than do the elements with odd atomic number.

The complete results will be published elsewhere.[8]

[8] M. T. Robinson and J. F. Krause, *J. Nuclear Sci. Eng.* (to be published).

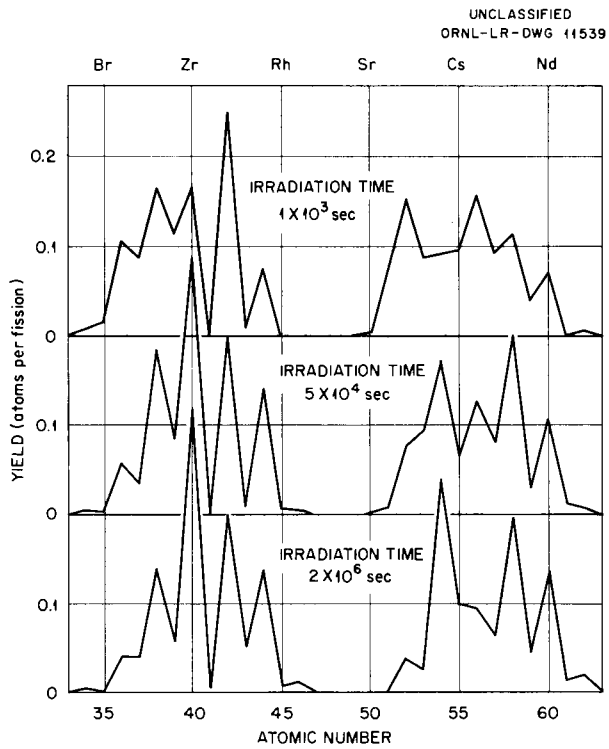

Fig. 21. Yields of Chemical Elements in Thermal Neutron Fission of U^{235}.

SPECIAL PROJECTS

RESISTIVITY CHANGES IN ALPHA BRASS AS A FUNCTION OF NEUTRON IRRADIATION

R. H. Kernohan D. S. Billington

The in-pile measurement of the resistance of a brass wire, described in the previous semiannual report,[1] was continued. After a total irradiation of 29 weeks in a hollow fuel element (hole 1968) in the Graphite Reactor, the experiment was terminated.

In this experiment, a well-annealed brass wire containing 12.9 at. % zinc was irradiated at ambient pile temperature, and resistance and temperature readings were taken periodically. All resistance readings were corrected to 20°C and are plotted as a function of accumulated reactor power in Fig. 22.

A minimum occurs in the resistance after a dosage of 2×10^6 kwhr – an integrated neutron flux of about 2×10^{18} neutrons/cm^2. Thereafter, the resistance seems to increase linearly with time in the reactor. The brass wire had an original resistance of 41,440 μohms at 20°C. Percentage changes in resistance of the wire may be found by multiplying the ordinate values, that is, the change in resistance in μohms, by 2.42×10^{-3}. Thus, the minimum represents a decrease of about 0.85%; and at the end of the experiment, the resistance had increased 1.00%. The geometry of the wire was such that if the resistance is multiplied by 1.02×10^{-4} the resistivity is obtained in μohm-cm; the original wire then measured 4.23 μohm-cm: it decreased 0.036 μohm-cm at the minimum and increased 0.043 μohm-cm above the original value by the time the wire was withdrawn from the reactor.

From the data on the linear part of the curve, a root-mean-square line was calculated. If ΔR is the change in resistance in μohms, and P is the increment of reactor power in millions of kilowatt-hours, then

$$\Delta R = -539 + 63.9P ,$$

or in terms of resistivity,

$$\Delta\rho = -0.0550 + 0.00652P ,$$

or in terms of the number of hours t in the reactor,

$$\Delta\rho = (-550 + 0.228t) \times 10^{-4} \ \mu\text{ohm-cm} .$$

A calculation of the number of radioactive atoms produced during the irradiation shows that about 35×10^{-4} at. % impurities were added. It is estimated that these impurities would increase the resistance 25×10^{-4} μohm-cm by the end of the irradiation period.

It is interesting to compare the linear rate of increase of the resistivity obtained in the brass-wire sample, 0.23×10^{-4} μohm-cm per hour, with the increase obtained by Blewitt in a sample of the same brass irradiated for one week at 20°K. Blewitt observed no decreases at all, but he did observe a linear increase of 46×10^{-4} μohm-cm in 150 hr. This rate of increase is 0.31×10^{-4} μohm-cm per hour of irradiation at 20°K. The estimated flux in the hollow fuel element is probably twice that which Blewitt had available.

Calculations are now being made on the nonlinear decreasing part of the resistance curve.

[1] R. H. Kernohan and D. S. Billington, *Solid State Semiann. Prog. Rep. Aug. 30, 1955*, ORNL-1945, p 63.

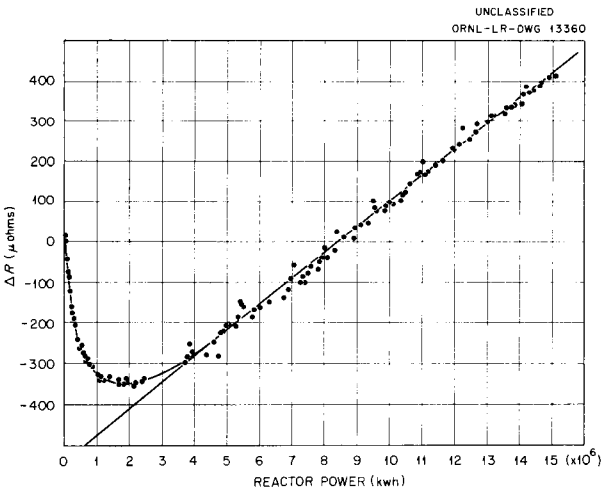

Fig. 22. Resistance Change in Alpha Brass vs Reactor Irradiation.

EFFECT OF NEUTRON RADIATION ON THE PRECIPITATION-HARDENING REACTION

R. H. Kernohan D. S. Billington
A. B. Lewis

The study of the precipitation process in the alloy Ni-Be has been continued; the ferromagnetic Curie temperature is used as an indication of the amount of precipitate formed. Previously reported

results[2,3] indicated that neutron irradiation at about 35°C had no effect on the Curie temperature but that irradiation at a temperature of 300°C, or about 200°C below the normal precipitation range, did, indeed, increase the amount of beryllium precipitated.

New techniques, recently introduced, have permitted a more rapid determination of Curie temperature, the use of smaller samples, and the construction of an in-pile experiment. Formerly, the Curie temperature was measured by inserting an Ni-Be sample in the center of a coil and measuring the change in inductance of the coil. The present technique is to use the Ni-Be sample as the core of a microtransformer. The transformer windings are No. 30 glass-covered copper wire wound on a Lavite (nonmagnetic and heat resistant) coil form. Less than 0.5 v of regulated 60-cycle ac is impressed on the primary, and the secondary output is led to a vacuum-tube voltmeter, rectified, and impressed on one pen of a two-pen Brown recorder. The microtransformer and specimen are placed in a noninductively wound oven whose temperature is slowly increased. A thermocouple adjacent to the specimen is connected to the second pen on the recorder. As the oven temperature goes up through the Curie temperature of the sample, the output of the secondary drops precipitously, and the reading may be taken from the recorder chart.

Since the microtransformer is less than 0.5 in. in diameter and 1 in. in length, specimens can be made rather small, and the microtransformer and surrounding oven can be placed in a reactor. At present the Ni-Be specimens being used are 0.3 cm in diameter and 3.5 cm in length. A number of these were heat-treated at 1125°C for 2 hr and water-quenched in order to retain all the beryllium in a supersaturated state.

A small oven to hold a microtransformer was constructed to fit in a hollow channel in the center of the ORNL Graphite Reactor. A duplicate apparatus was constructed to be used for a control sample outside the reactor. Both the irradiated experiment and the control were held at 300 ± 2°C. Periodically the ovens were shut down and allowed to cool. The apparatus was then connected to a recorder, and the Curie temperature was measured. The shutdown, cooling off, measurement, and warmup to 300°C could be accomplished in a little over 1 hr.

The results of the in-pile experiment at 300°C are shown in Fig. 23. The experiment had to be terminated at the end of three weeks because of a breakdown in the wiring in the experiment inside the reactor. However, these results agree very well with those obtained previously[3] on a before-after experiment which was run at 300°C for four weeks.

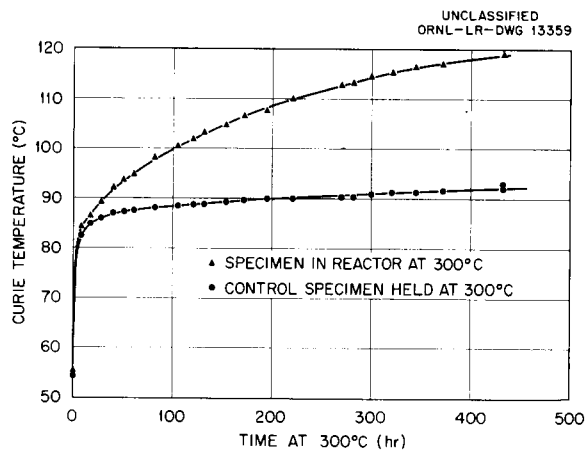

Fig. 23. Curie Temperature of Ni-Be Heat Treated at 300°C.

There is a linear dependence between Curie temperature and the amount of beryllium dissolved. If θ is the Curie temperature in degrees centigrade and A the amount of beryllium in solution, then

$$A = \frac{358 - \theta}{20.83} .$$

In addition to the above experiment, considerable data were gathered on specimens heat treated at 450°C. Typical data are shown in Fig. 24. During the first few minutes at 450°C, the Curie temperature rises quickly, and about 2 at. % beryllium is indicated as having precipitated. Presumably this is grain-boundary precipitation. Thereafter, the Curie temperature increases more slowly, and from the graph it would appear to approach a maximum value. This part of the precipitation is probably intragranular in nature.

[2] R. H. Kernohan and D. S. Billington, *Solid State Semiann. Prog. Rep. Feb. 28, 1955*, ORNL-1852, p 48.

[3] R. H. Kernohan, A. B. Lewis, and D. S. Billington, *Solid State Semiann. Prog. Rep. Aug. 30, 1955*, ORNL-1945, p 65.

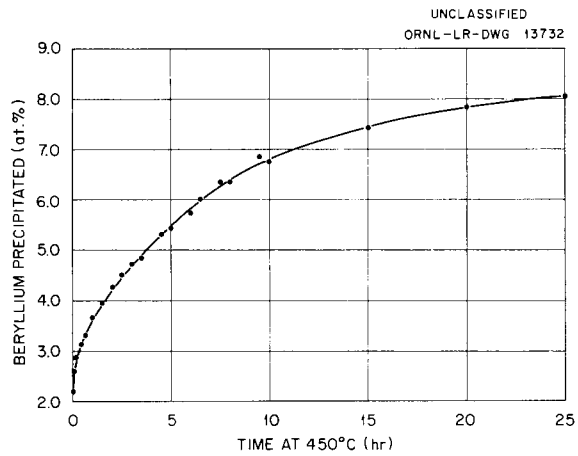

Fig. 24. Typical Curve Showing Precipitation of Beryllium from Ni-Be at 450°C.

A specimen which had been irradiated in the ORNL Graphite Reactor for a month (2×10^{18} *nvt*) at ambient reactor temperature and a control specimen were given the precipitation heat treatment at 450°C. The irradiated specimen is designated as *Y* and the control as *X* in Fig. 25. After the irradiation, specimen *Y* had the same Curie temperature as *X* and was apparently unchanged. However, the initial stage of its heat treatment at 450°C was very slow by comparison with the control specimen *X*.

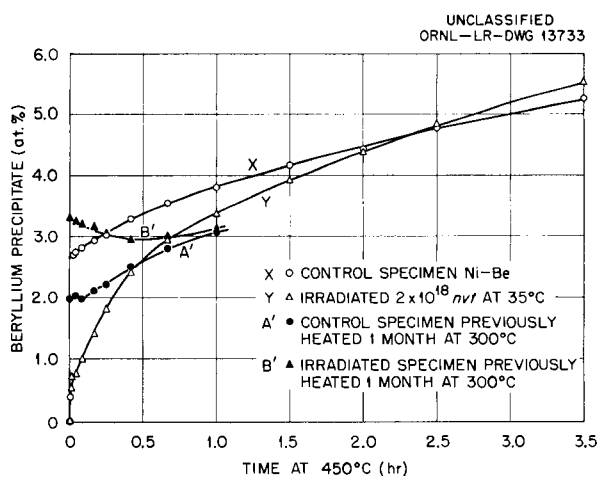

Fig. 25. Precipitation of Beryllium from Several Ni-Be Specimens at 450°C.

In addition, the precipitation heat treatment at 450°C was given to two other specimens *A′* and *B′*, which had previously been heat-treated for a month at 300°C. Specimen *B′* had also been irradiated during the heat treatment at 300°C. These curves are also shown in Fig. 25. Explanation of the peculiar behavior of specimens *A′* and *B′* will depend on further heat treatment and on the accumulation of more data.

Information is now being gathered on the normal precipitation heat treatment of specimens at three different temperatures in order to determine activation energies for the precipitation process. A further study of precipitation in samples irradiated at ambient reactor temperature and heat treated at different temperatures is also planned.

A HIGH-TEMPERATURE FURNACE FOR GROWING ALLOY CRYSTALS

R. E. Jamison

Construction of a versatile high-temperature crystal-growing furnace is nearly complete. The furnace will permit the growing of single crystals of alloys whose melting points are as high as 1400°C, such as alloys of nickel which are of particular interest in certain neutron-irradiation-effect studies at this laboratory.[4] The furnace will be of particular value in the growing of alpha-brass single-crystal tensile specimens with which there has been considerable difficulty because of dezincification and of relative thermal contraction of the crystal in the crucible just after growth.

SMALL-ANGLE X-RAY SCATTERING TECHNIQUE

R. E. Jamison

The camera described previously,[5] which is used to obtain pictures of small-angle x-ray scattering, has been in use periodically during the past two years and is satisfactory for strictly qualitative work. However, as others have found,[6] quantitative measurements by film techniques are not practical.

---

[4] R. H. Kernohan, A. B. Lewis, and D. S. Billington, *Solid State Semiann. Prog. Rep. Feb. 28, 1955*, ORNL-1852, p 50; *Solid State Semiann. Prog. Rep. Aug. 30, 1955*, ORNL-1945, p 65.

[5] R. E. Jamison, ORNL-1677, p 70 (Feb. 28, 1954) (Secret).

[6] A. Guinier, *Small-Angle Scattering of X-Rays*, p 168, Wiley, New York, 1955.

A Geiger-counter technique is much preferred, except in some cases where the scattering pattern is not symmetrical about the central beam. In general, in the photographic method, the camera must be aligned before each set of exposures; the film must be exposed for relatively long periods (18 hr minimum in this case); and a photomicrograph trace must be taken of the developed film. There are many chances for error (the exposure may not be in the linear region of the intensity vs exposure curve for the film; the development process has many inherent variables associated with it, etc.), so that even comparative intensity measurements are nearly impossible.

The first attempt, which was the simplest one possible, with Geiger-counter technique, has proved to be quite satisfactory. Results are consistant and easily reproduced. Accurate comparative measurements have been made, and absolute intensity measurements (by use of a standard scatterer) are planned.

A two-slit collimation system was used with the same Ross filter[5] that was used on the film camera, and the unit was adapted to a commercial Norelco x-ray diffractometer (Fig. 26).

No change was made in the diffractometer itself. A spare sample holder (easily removable from the unit) was adapted for use by constructing a combination sample holder and adjustable slit which is fastened to the holder by the same screws that ordinarily hold the sample clip. Both the slit opening and the position are adjustable. The position is adjusted to the center of rotation of the sample holder so that the rotation of the holder does not affect the scattering pattern.

By means of associated commercial equipment, the scattering intensity is recorded on chart paper, as shown in Fig. 27. The deflection on the chart is proportional to the intensity. The slit at the window of the Geiger tube is rotated slowly ($\frac{1}{8}$ deg/min) so that the curve obtained from the chart corresponds very closely to the type of curve that would be obtained by actually counting the sample at various angles for specific time intervals.

The nickel-filter intensity and the cobalt-filter intensity are plotted on the same chart, and the difference between the two (the monochromatic reading) is then easily measured and plotted on a graph as log intensity vs angle.[6] Such plots will be presented in the following report.

Some of the errors in the technique are obvious. There is scattering from the air between the sample and the counter, and there is scattering from the second slit. These errors have been measured and are small compared with the scattering by the sample within the angles which are of interest (> 30 min). In some materials, there is fluorescent radiation from the sample itself. An oxide layer on the surface of the sample can give rather high-intensity scattering, so that the surface condition of samples cannot be ignored. Errors due to beam height and to the fact that the radiation is not strictly monochromatic are also present and can be calculated when the scattering particle is known to be spherical in shape.

UNCLASSIFIED
ORNL-LR-DWG 13734

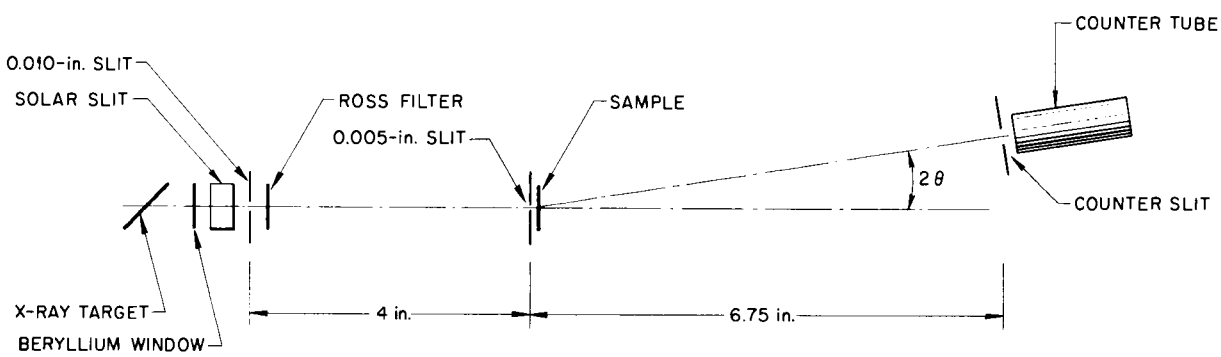

Fig. 26. Schematic Diagram of Experimental Arrangement for Small-Angle X-Ray Scattering.

UNCLASSIFIED
ORNL-LR-DWG 13735

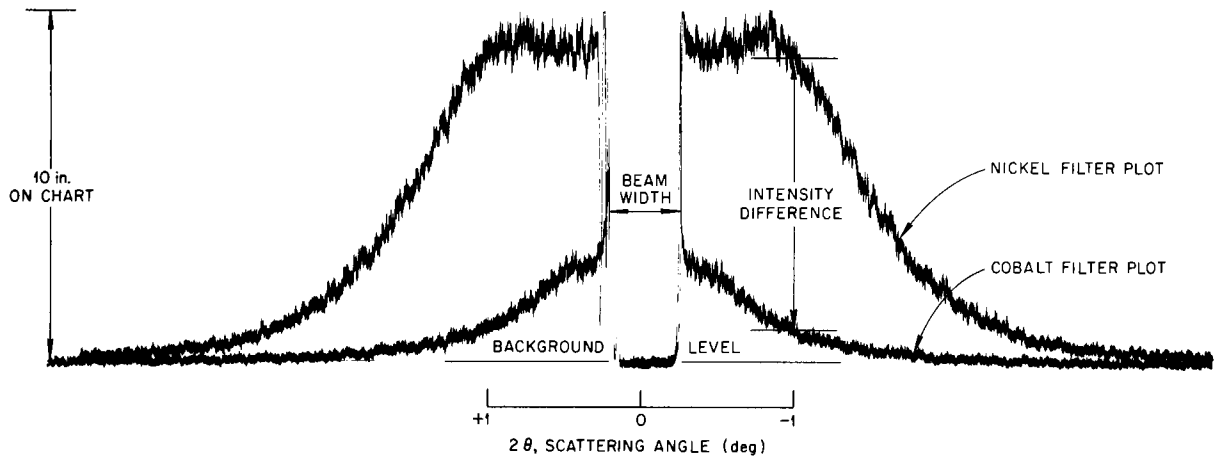

Fig. 27. Typical Recording of Small-Angle X-Ray Scattering Data.

As a check of accuracy, this arrangement was used to measure the cluster size of the precipitate in an Al-Ag sample which was furnished by J.-P. Jan of the University of Illinois and on which he had made measurements by a more elaborate technique. The results of the measurement [the slope of the log I vs $(2\theta)^2$ plot] agreed with his results to within a few per cent. A standard ovalbumin sample was made, and the scattering from it was measured, giving a particle size intermediate between that obtained by Jan and that obtained by Guinier.[7]

Thus, even though errors may be present, the technique seems to be a good one, and the fact that the measurements are conveniently made and easily reproduced makes it very satisfactory for use where comparative measurements of both particle size and relative intensity are desired.

EFFECT OF NEUTRON RADIATION ON AN Al-Ag PRECIPITATE ALLOY

R. E. Jamison

The 80 wt % Al–20 wt % Ag precipitate alloy has been chosen as a material for study because of the general interest in its aging process and because it is ideally suited to small-angle x-ray scattering studies, which can readily yield such information as the cluster size of the precipitate, the nature of the cluster, and the density of clusters. Another advantage in the use of this material for irradiation studies is that it ages only very slowly, if at all, at room temperature or even at ambient reactor temperature (40°C).

For the Al-Ag alloy in its first stage of aging, the accepted model[8] of the scattering configuration is a spherical silver-rich nuclei in a concentric silver-poor shell, all in the normal matrix. Such a model gives a ring-type scattering pattern, since the silver-poor shell subtracts from the scattered intensity near the origin. The normal behavior of the alloy at 100°C is seen in Fig. 28, which shows plots of the log of the x-ray intensity (on an arbitrary scale) vs the square of the scattering angle. The slope of the straight portion of such a plot is proportional to the square of the average radius of gyration of the scattering particles.[9] As aging proceeds, the slope of the curve increases, which indicates an increase in the precipitate size; and in some cases, apparently depending on the previous history of the sample, the ring diameter decreases, which probably indicates diffusion of silver into the silver-poor shell.

An increase in precipitate size due to irradiation was expected but has not as yet been seen in irradiated samples, even when exposed to 10^{19} nvt_f. The next step was to heat-treat the samples

[7] *Ibid.*, p 169.

[8] C. B. Walker and A. Guinier, *Acta Met.* **A1**, 568 (1953).

[9] A. Guinier, *Small-Angle Scattering of X-Rays*, p 127, Wiley, New York, 1955.

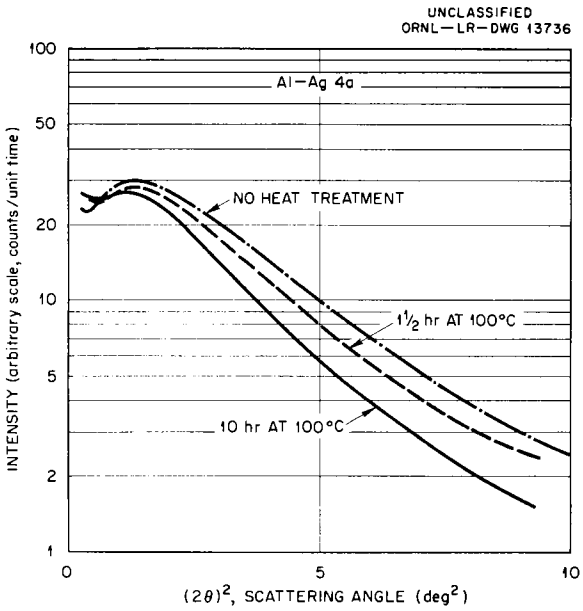

Fig. 28. Effect of Aging on Al-Ag Precipitate Alloy.

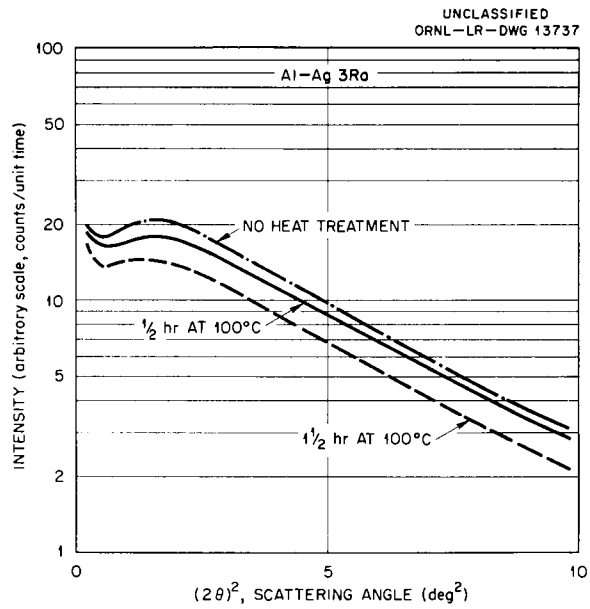

Fig. 29. Effect of Irradiation with 5×10^{18} nvt_f and of Subsequent Heat Treatment on Al-Ag Precipitate Alloy 3Ra.

after irradiation in order to see if the irradiation had an effect on the rate of aging. Figures 29 and 30 show the behavior of two irradiated samples during heat treatment at 100°C. Although there is a change of intensity with sample 3Ra, there is no change of slope. Sample 3Rb shows only slight changes of slope and intensity. There are large changes in the curves of both samples near the origin, which are interesting although not understood, but apparently the increases in average precipitate size during heat treatment of the irradiated samples are not so large as in unirradiated samples, typified by sample 4a in Fig. 28. The inconsistancies among irradiated samples with respect to intensity changes during heat treatment could be due to differences in sample history prior to irradiation.

Jan[10] has reported that cold work slightly retards the aging at 130°C of 70 wt % Al–30 wt % Ag and credits this to a combination of two effects: (1) an increase in the number of vacancies present, which should aid the precipitate growth, and (2) an increase in the number of dislocations present, which should hinder the growth, since

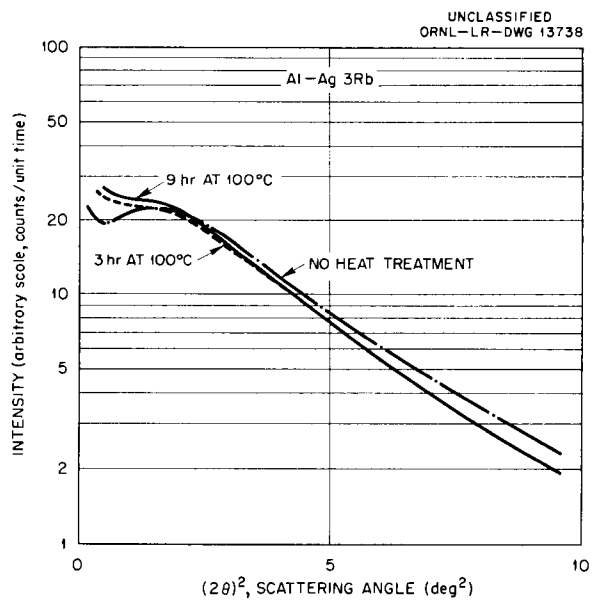

Fig. 30. Effect of Irradiation with 5×10^{18} nvt_f and of Subsequent Heat Treatment on Al-Ag Precipitate Alloy 3Rb.

[10] J.-P. Jan, *J. Appl. Phys.* 26, 1291, esp. 1294 (1955).

these dislocations would likely furnish nuclei for new precipitates and thus decrease the average precipitate size.

An explanation of the irradiation effect might be similar and would presuppose that the irradiation increases the number of nuclei, as cold work did in Jan's experiment.

PARAMAGNETIC RESONANCES IN UNIRRADIATED MgO

R. A. Weeks

In MgO it should be possible to observe the resonance of *f* centers without the complication of hyperfine splitting arising from the nuclear spin of the nearest neighbors of the *f* center. The one isotope of magnesium with a nuclear spin is Mg^{25}. Its natural abundance is 10%, and $I = 5/2$. The *f* center in MgO should have 10% of its nearest neighbors with a nuclear spin of $5/2$, and the remainder would have zero spin. The expected ideal shape of the paramagnetic resonance of such a center would be a narrow line occurring on top of a broad line of approximately 90% less intensity; the broad line would arise from those *f* centers which had one or more Mg^{25} atoms as nearest neighbors, and the narrow line would arise from those *f* centers which have no Mg^{25} atoms as nearest neighbors. Of course, some deviations from the ideal line shape would be expected to arise from contributions of next nearest neighbors and from more complex arrays of *f* centers, vacancies, and other crystal defects. The contribution of next nearest neighbors to the hyperfine splitting would be expected to fall off as $1/r^3$ and thus would not be nearly so important as the nearest neighbors. The effect of other crystal defects is much more difficult to assess.

Three different crystals of MgO have been used in the determination of resonance before irradiation, and all have had a complex spectrum: one was of unknown origin; one was a natural crystal; and the last was grown by the Norton Company. The impurities in the three were determined by spectral analysis and are listed in Table 8. The natural crystal has the greatest variety of impurities, and the other two have only four impurities which are detectable by the spectral method of analysis. On the basis of this analysis, there are only two impurities which are common to all three specimens; these are aluminum and calcium. The natural abundance of the isotope and its nuclear spin are also given in the table. The only calcium isotope with a nuclear spin is Ca^{43}, and its natural abundance is 0.13%. The isotope Al^{27} has a spin of $5/2$, and its natural abundance is 100%. The spectrum found in these three unirradiated crystals

TABLE 8. IMPURITIES IN MgO[a] CRYSTALS (SPECTRAL ANALYSIS)

Impurity	Abundance (%)	Nuclear Spin	Amount (wt %)		
			Unknown Crystal	Natural Crystal	Norton Crystal
Al^{27}	100	$5/2$	0.01 to 0.1	0.01 to 0.1	0.01 to 0.1
Ca^{43}	0.13	$7/2$	0.001 to 0.01	0.001 to 0.01	0.001 to 0.01
$Cu^{63,65}$	100	$3/2$		0.0001 to 0.001	
Fe^{57}				0.01 to 0.1	0.01 to 0.1
Mn^{55}	100	$5/2$		0.001 to 0.01	
Ni^{66}				0.001 to 0.01	0.001 to 0.01
Si^{29}	4	$1/2$	0.01 to 0.1	0.01 to 0.1	
Ta^{181}	100	$7/2$	0.01 to 0.1		
Ti^{41}	12	$1/2$		0.001 to 0.01(?)	
Ti^{48}	12	$5/2$		0.001 to 0.01(?)	
V^{51}	100	$7/2$		0.001 to 0.01(?)	

[a] Mg^{25}: 10% abundance, $I = 5/2$.

is shown in Fig. 31. The intensities of the lines are only approximate and are given only to show which are the major lines and which are the satellites. In all three crystals there are six lines of equal intensity which are approximately equally spaced from each other. The separation of these major lines in the Norton crystal is apparently greater than in the other two crystals. For the Norton crystal, the magnetic field was measured at the points indicated in Fig. 31. This was not done for the other two crystals. It was assumed that the sweep rate was constant for the measurements on the three crystals; however, the apparent difference in separation of the lines in the three crystals indicates that the sweep rates differed. The apparent decrease in the separation of the lines for increasing field H may also be due to a small change in sweep rate as H increases.

One difference that is evident is in the number of satellite lines. In two of the crystals there are two satellites per major line, and in the third crystal there are four. It can also be seen that the positions of the satellites change with increasing H. Another difference in the spectrum of the three crystals is in the number of additional lines that can be seen. In the crystal of unknown origin, there are four such lines. The most intense one apparently covers one of the satellite lines lying between the third and fourth line, counting from the low-field side. On the high-field side of the fourth line is another extra line of the same intensity as that of the six major lines. The two other additional lines lie at the extremities of the spectrum.

In the natural crystal there are apparently only two additional lines, one below (low field) and the other above (high field) the fourth major line. Both are quite weak compared with the major lines. In the Norton crystal, there is only one additional line. It can only be seen by noting that one of the satellite lines is somewhat stronger than its neighbor. This line occurs at approximately the same position as that of the additional line on the low-field side of the fourth major line in the other two crystals.

The crystal of unknown origin was irradiated with gamma rays from fission by-products. The dosage was 2×10^8 r. A faint, brown coloration was noted when the crystal was removed from the gamma source, and it faded in approximately 24 hr. There was no observable change in the spectrum after irradiation. The measurements were made approximately 48 hr after removal from the source. It is possible that paramagnetic centers generated by the gamma rays were related to the coloration; in this case, by the time the measurements were

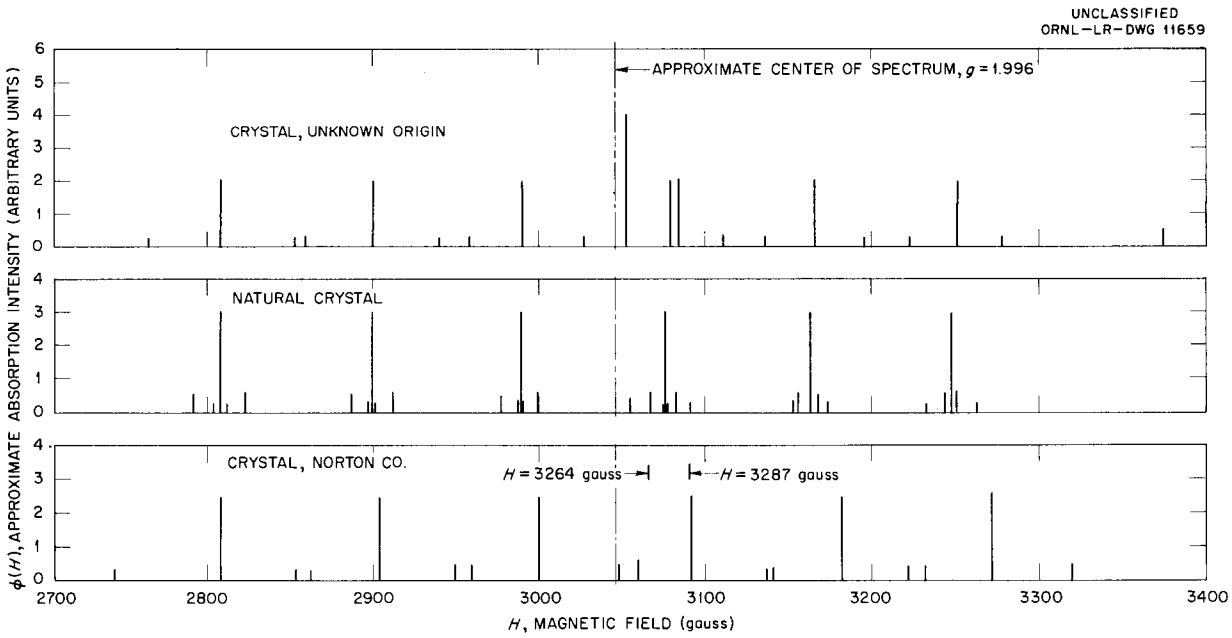

Fig. 31. Paramagnetic Resonance in MgO Crystals.

made, most of them would have been destroyed. One other experiment was performed with this crystal. It was annealed at 600°C for 2 hr in air. No change was observed in the spectrum. Wertz *et al.*[11] report that a line at a g value of 2.003 disappears when they heated their crystals in vacuum at 600°C; whereas heating in air increases its intensity. The additional line on the low-field side of the fourth line has approximately this g value. They[11] attribute this line to excess oxygen. They also report that exposure to x rays generates a line which has the same g value and which slowly decays.

As for the six-line spectrum, Wertz *et al.*[12] state that it is due to some impurity and suggest that this impurity may be excess magnesium (Mg^{25}: $I = 5/2$; natural abundance 10%). In the crystals used in the present work at ORNL, the impurity of greatest concentration, besides magnesium, is Al^{27} ($I = 5/2$; natural abundance 100%). The concentration of Al^{27} is of the same order of magnitude for the three crystals. In one of the crystals, manganese has been observed. This is a normally paramagnetic atom with an electronic spin $S = 5/2$ and nuclear spin $I = 5/2$. It has been suggested[13] that even an extremely small trace of manganese impurity, less than 0.0001%, will produce an observable spectrum. In respect to the manganese impurity, the total spread of the six lines in these crystals is approximately the same as that reported by Schneider and England[14] for dilute solutions of $MnSO_4$.

Since the spectrum of the unirradiated MgO crystals was so complex, little effort has been directed as yet toward a study of defects created by irradiation.

PARAMAGNETIC RESONANCES IN IRRADIATED FUSED AND CRYSTALLINE QUARTZ

R. A. Weeks

In a previous report,[15] some measurements were presented concerning a narrow resonance observed in Vitreosil and Corning silica after irradiation in a reactor. The asymmetry of the resonance indicated either (1) that there were two species of unpaired spins with g values that were almost the same or (2) that the splitting of the energy levels by the crystalline field was of the same order as the splitting arising from the magnetic field. The first situation was discussed in the preceding report. Since then, additional evidence has indicated that the second situation is probably the source of the asymmetry.

An additional resonance has been discovered. This resonance is also asymmetric; however, its asymmetry, width, and g value differ markedly from the narrow resonance discussed above. The width at the inflection points is approximately 15 gauss, and $g = 2.010 \pm 0.005$.

Measurements on the narrow resonance are summarized in Fig. 32. Curves I and II refer to Corning silica and Vitreosil. The apparent g value is 2.0017 ± 0.0005, and the width at the inflection points is approximately 1 gauss. A similar resonance has been observed in Amersil and in G-E silica. Curve VII, Fig. 32, is the integral of curve II. In order to decide whether the asymmetry of the resonance was due to two unresolved lines or to other factors, measurements were made[16] at 23,000 Mc. At this higher frequency, the absolute width of the lines remains the same, whereas the absolute separation increases. If two lines are present, then an increase in their resolution would be expected. The resonance was displayed on an oscilloscope, a photograph of which is shown in Fig. 33. The asymmetry is apparently the same as in curve VII, Fig. 32, and there is no indication of resolution into two lines.

A careful examination of the results obtained at 23,000 Mc revealed an additional broad resonance. A photograph of the oscilloscope display of this resonance is shown in Fig. 34. The narrow resonance is on the high-field side of the broad one. The r-f power required to bring this resonance into view partially saturated the narrow resonance. After the broad resonance at 23,000 Mc was found, it was possible to establish the conditions for observation at 9000 Mc. Figure 35 shows the derivative and Fig. 36 its integral. The narrow

[11] J. E. Wertz and J. L. Vivo, *Bull. Am. Phys. Soc.* 30, No. 8, 8 (1955).

[12] J. E. Wertz, J. L. Vivo, and B. Musulin, *Bull. Am. Phys. Soc.* 30, No. 8, 26 (1955).

[13] Private communication with R. Livingston, Oak Ridge National Laboratory.

[14] E. E. Schneider and T. S. England, *Physica* 17, 221 (1951).

[15] R. A. Weeks, *Solid State Semiann. Prog. Rep. Aug. 30, 1955*, ORNL-1945, p 67, esp. p 70–71.

[16] The measurements at 23,000 Mc were obtained through the assistance of R. Livingston, who provided the apparatus for this work.

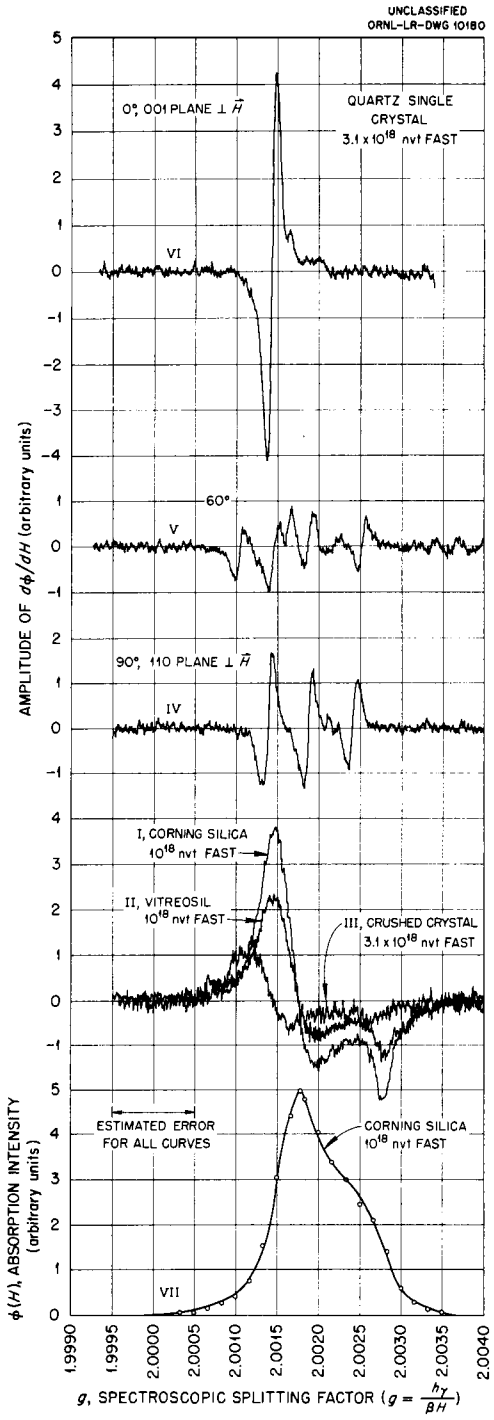

Fig. 32. Summary of Measurements Made on One of the Resonances Observed in Vitreosil, Corning Silica, and Natural Quartz. The modulation amplitude of the field was held to 0.2 or less of the half width of the resonance. The estimated g value applies to each curve.

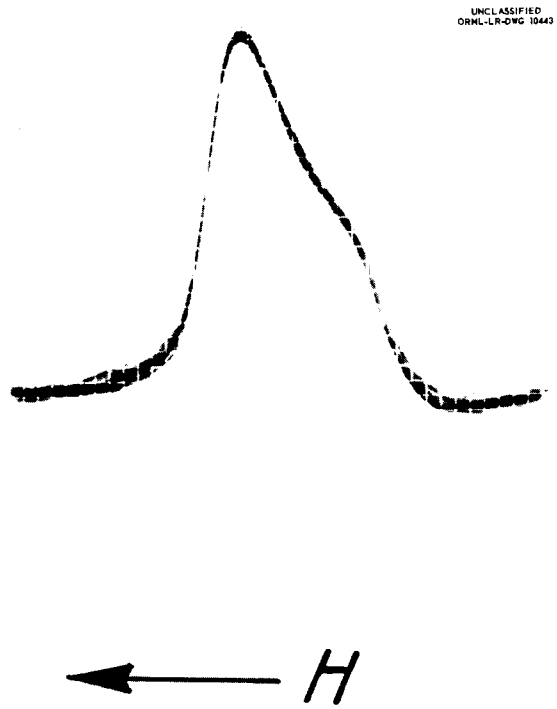

Fig. 33. Narrow Resonance in Vitreosil at 23,000 Mc. The magnetic field was swept with a 60 cps sine wave.

resonance saturated the preamplifier as soon as its signal was picked up. An approximate reconstruction of that portion of the broad resonance lying beneath the region dominated by the narrow resonance was possible, since two points on the integral of the derivative curve could be found. No additional lines have been found.

The crystalline specimens were both natural and synthetic crystals, which were cut so that one face parallel to the long axis of the specimen coincided with the 110 plane and the other face coincided with the 001 plane. Three measurements which show crystalline-field splitting at different orientations of the crystal to the magnetic field are presented in curves IV, V, and VI of Fig. 32. The resonance in the synthetic-crystal specimen exhibited the same behavior with rotation. A third single crystal was given a total dose of 3.3×10^{20} fast neutrons/cm^2. The resonance resulting from this large irradiation is shown in Fig. 37. The apparent g value, width, and shape of this resonance are the same as in the fused material. At approximately 10^{20} fast neutrons/cm^2,

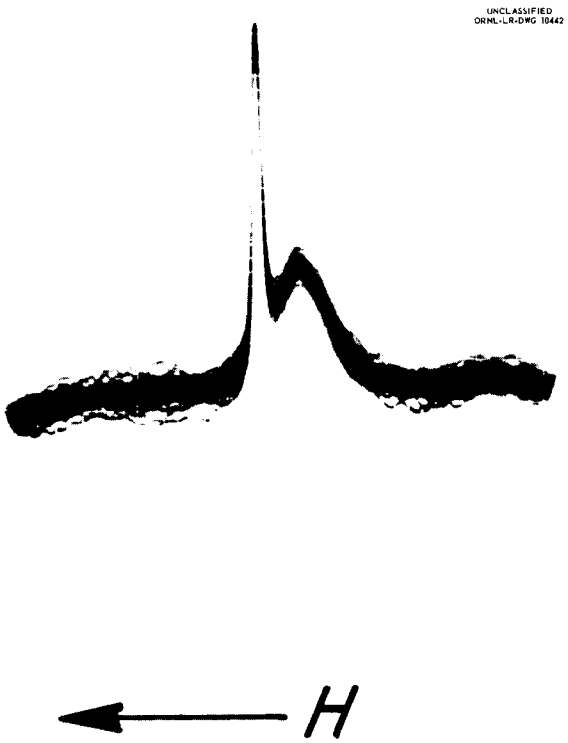

Fig. 34. Broad Resonance in Vitreosil Shown with the Narrow Resonance at 23,000 Mc.

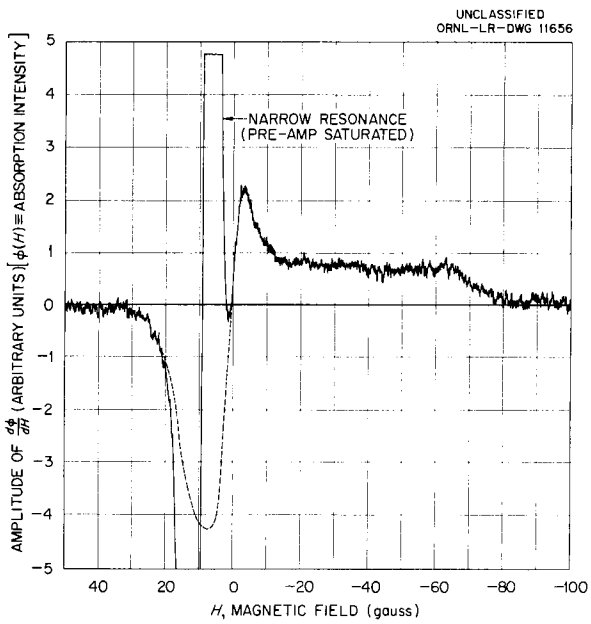

Fig. 35. Derivative of Broad Resonance at 9120 Mc in Irradiated Corning Silica.

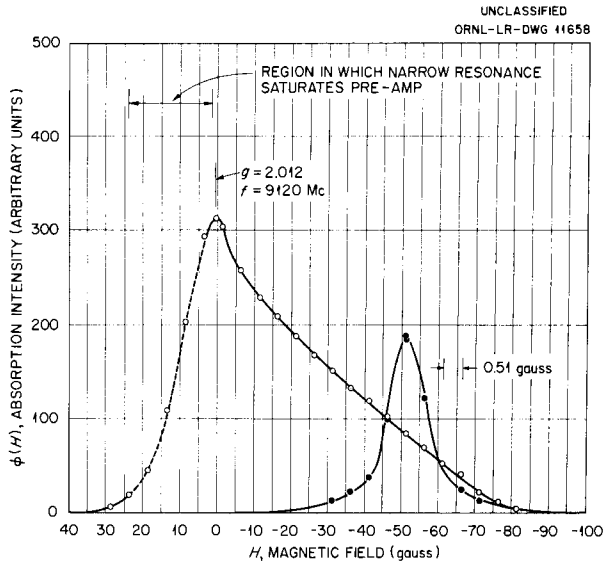

Fig. 36. Integral of Broad Resonance at 9120 Mc in Irradiated Corning Silica.

density measurements and x-ray diffraction patterns[17] of the crystal are characteristic of those obtained for fused silica. The results, shown in Figs. 32 and 37, suggest that the resonance observed in the fused material is the envelope of the very narrow lines in the crystal summed over random orientations of regions of short-range order. One of the crystals was crushed, and the resulting resonance is shown in curve III in Fig. 32. In support of the above suggestion, curves I, II, and III (Fig. 32) and the curve in Fig. 37 are seen to have nearly the same shape, width, and apparent g value.

An attempt was made to locate in the crystals a broad resonance similar to the one observed in the fused material. The attempt was not successful. Because of its width, this resonance could easily have been obscured by noise in the apparatus.

The approximate temperature of the specimens during irradiation was estimated to be 320°C for the natural crystals and 250°C for the Corning silica, Vitreosil, Amersil, G-E silica, and the synthetic crystals. Observations on paramagnetic resonances in irradiated silica and natural quartz by other workers have shown that the resonances are destroyed by annealing at 300°C or less.

[17] M. Wittels and F. A. Sherrill, *Phys. Rev.* 93, 1117 (1954).

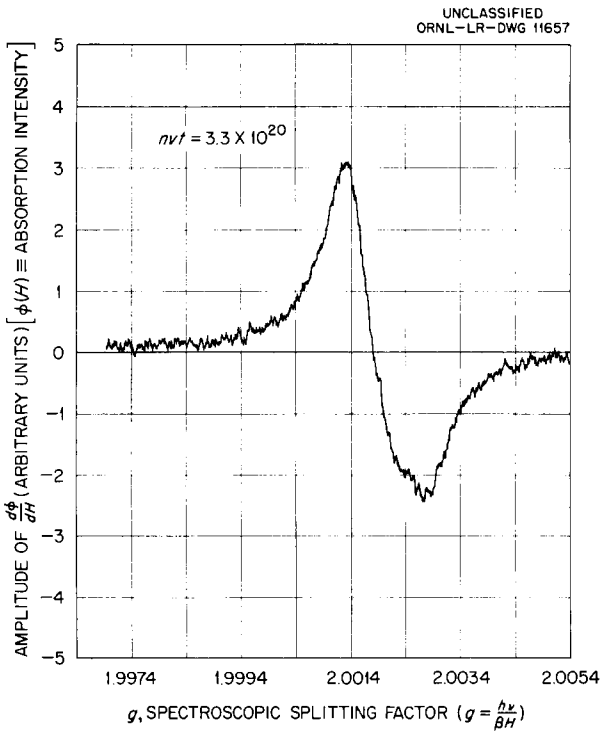

Fig. 37. Narrow Resonance in an Irradiated Quartz Single Crystal.

Griffiths *et al.*[18] have identified one group of resonances (six hyperfine lines plus lines due to crystalline-field splitting) as being associated with an Al^{27} impurity atom substituted for silicon. These resonances disappear when the specimen is annealed at 300°C. Combrisson and Uebersfeld[19] have observed a broad resonance in silica with a g value of approximately 2 that disappears at 150°C. Thus, it is improbable that these resonances are the same as those observed by the author. Because of (1) the high-temperature stability of the two resonances, (2) the apparent similarity of the narrow resonance in the fused material, the crushed crystal, and the crystal given 3.3×10^{20} nvt_f, (3) the correspondence of g values in the crystals to those in the fused material, (4) the dissimilarities of impurities,[20] and (5) the lack of any evidence of hyperfine splitting, it is tentatively concluded that the narrow resonance and the broad resonance do not arise from impurities but are due to some effect of the radiation on the basic SiO_4 tetrahedra.

The area under the broad resonance in one specimen has been compared with the area under the resonance of 100 μg of diphenylpicrylhydrazyl (DPH). This comparison suffers from one deficiency that is difficult to take into account. Whereas the resonance in DPH is almost symmetrical about its maximum, the resonances in the silica are asymmetrical and, if the tentative conclusion discussed above is correct, are composed of a group of lines arising from crystalline-field splitting. Therefore the DPH resonance should be compared with the area under each of the lines (suitably weighted) arising from the crystalline-field splitting. Nevertheless, some estimate of the number of centers can be gained from the comparison. In the one specimen on which measurements have been made, the number of centers contributing to the broad resonance is estimated to be 7×10^{18} unpaired spins/cm^3. If this number is added to the estimate for the number of centers contributing to the narrow resonance, the total is 1.7×10^{19} unpaired spins/cm^3. The total number of unpaired spins found by the magnetic-susceptibility measurements[21] is 2.7×10^{19}/cm^3. Hence, if it is assumed that the susceptibility measurement has only a small error, of the order of 1%, the error in the resonance measurement is 37%. In consideration of the inaccuracies in the resonance method, the agreement is rather good.

DISPLACEMENTS FROM A PILE-NEUTRON SPECTRUM: CALCULATION FOR GERMANIUM

D. Binder

The number of atoms displaced by a pile-neutron spectrum was calculated. The spectrum was computed by assuming a $1/E$ distribution extending

[18] J. H. E. Griffiths, J. Owen, and S. M. Ward, *Conference on Defects in Crystalline Solids*, p 81–91, Physical Society, London, 1955.

[19] J. Combrisson and J. Uebersfeld, *Compt. rend.* 238, 572–3 (1954).

[20] The impurities were measured by both spectral and activation analyses and were 0.001 to 0.01 wt % Al and 0.0001 to 0.01 wt % Mg in the natural crystal, and 0.0001 to 0.001 wt % Cu in the Vitreosil; in the Corning silica all the impurities were of the order of 10^{-5} wt % or less. The impurities in the G-E silica, Amersil, and synthetic crystals have not been determined.

[21] C. M. Nelson, *Solid State Semiann. Prog. Rep. Aug. 30, 1955*, ORNL-1945, Fig. 30, p 33.

to each differential element of the known fission spectrum,

$$\phi_o(E) = \sinh (2E)^{1/2} e^{-E} ,$$

and summing over these distributions. The resulting spectrum agrees within 6% with a $1/E$ distribution up to 1 Mev. The ratio of the resonance flux (0.4 ev $< E <$ 10^6 ev) to the fission flux ($>10^6$ ev) is 14. This calculated spectrum is used as an approximation to the neutron spectrum occurring in a graphite reactor.

In order to calculate the displacements, the method outlined by Kinchin and Pease[22] is extended to a flux spectrum. The method involves the usual assumptions: (1) that a minimum amount of energy e_d is necessary to displace an atom and (2) that there is a critical energy e_c for recoil atoms. Over e_c, all the energy of the atom is used for ionization; and under e_c, all the energy is used for elastic collisions. It is further assumed that the energy spectrum of the recoils is uniform from zero to the maximum energy,

$$e_{max} = \frac{4A}{(1 + A)^2} E ,$$

where A is the atomic weight, and E is the neutron energy. If one half the energy used for elastic collisions is effective in displacing atoms, then the fraction of atoms displaced by a neutron of energy E is

$$f_d = \frac{\sigma c_d E}{4e_d} , \qquad E < E_c ,$$

$$= \frac{\sigma c_d E_c}{4e_d}\left(2 - \frac{E_c}{E}\right) , \qquad E > E_c ,$$

where σ is the elastic-scattering cross section,

$$c_d = \frac{4A}{(1 + A)^2} ,$$

and

$$E_c = \frac{c_d}{e_c} .$$

Extending this to a flux spectrum $\phi(E)$,

$$f_d = \frac{\sigma c_d}{4e_d}\left[\int_0^{E_c} E\phi(E)\, dE + \int_{E_c}^{\infty} E_c \left(2 - \frac{E_c}{E}\right) \phi(E)\, dE\right] .$$

For insulators, e_c is assumed to be $\frac{1}{8}$ the energy of the recoil atom which has a velocity equal to the electronic velocity that is necessary to excite the first important absorption band.[22] Then

$$e_c = \frac{M}{m} \cdot \frac{I}{8} ,$$

where M is the atomic mass, m is the electron mass, and I is the energy of the absorption band.

For germanium, where I is 0.78 ev, E_c is 2.4×10^5 ev. This is well within the $1/E$ region of the neutron spectrum, and only a knowledge of the integrated fission flux is necessary. Analytically,

$$f_d = \frac{\sigma c_d}{4e_d}\left[\int_0^{E_c} c_r\, dE + \int_{E_c}^{10^6 \text{ ev}} E_c\left(2 - \frac{E_c}{E}\right) \frac{c_r}{E}\, dE + \int_{10^6 \text{ ev}}^{\infty} E_c\left(2 - \frac{E_c}{E}\right) \phi(E)\, dE\right] ,$$

where c_r/E is the resonance spectrum. To within 5%,

$$f_d = \frac{\sigma c_d E_c}{4e_d}\left[c_r\left(2 \ln \frac{10^6}{E_c} + \frac{E_c}{10^6}\right) + 2\int_{10^6 \text{ ev}}^{\infty} \phi(E)\, dE\right] .$$

If 3 barns is inserted for σ and 31 ev for e_d, as obtained by Klontz *et al.*,[23] then

$$f_d = 1.1 \times 10^{-22} \phi_r ,$$

[22] G. H. Kinchin and R. H. Pease, "The Displacement of Atoms in Solids by Radiation," *Reports on Progress in Physics*, vol XVIII, Physical Society, London, 1955.

[23] E. E. Klontz, R. R. Pepper, and K. Lark-Horovitz, *Bull. Am. Phys. Soc.* 30, No. 2, 12 (1955).

where ϕ_r is the total resonance flux,

$$\phi_r = \int_{0.4\,\mathrm{ev}}^{10^6\,\mathrm{ev}} \frac{c_r}{E}\, dE \ .$$

This may be related to the work of Cleland *et al.*,[24] who found that five electron traps were produced per "fast" neutron at approximately −155°C. A fast neutron was defined as one whose energy is greater than the threshold for displacements, $E > e_d/c_d$. Assuming two electron traps per displacement,[24] the result is equivalent to

$$f_d = 0.27 \times 10^{-22}\, \phi_r \ .$$

The agreement, within a factor of four, between the experimental and theoretical f_d values is satisfactory for an order-of-magnitude calculation of this type.

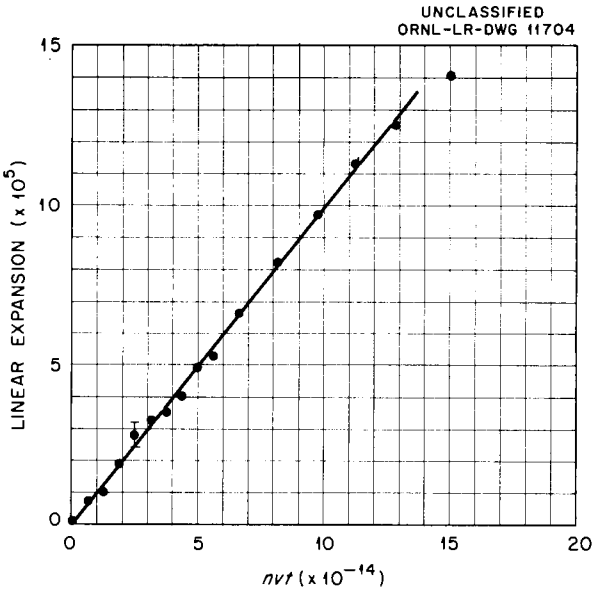

Fig. 38. Linear Expansion of LiF as a Function of Neutron Flux.

INITIAL EXPANSION OF LiF UNDER NEUTRON IRRADIATION

D. Binder W. J. Sturm

The initial expansion of an LiF single crystal was measured during neutron irradiation by means of the strain-gage technique. A Baldwin A5-1 strain gage was glued with Duco cement to both an LiF crystal (obtained from the Harshaw Chemical Co.) and a fused-quartz plate. Both specimens were ½ in. by 1 in., and the LiF crystal was thin enough to reduce neutron-attenuation corrections to 5% or less. These corrections were neglected. The Baldwin strain indicator used in the measurements gives the ratio of linear expansions of the two samples, and the quartz serves as a null both for temperature and for neutron irradiation.

The two samples were placed in hole 10 of the ORNL Graphite Reactor, along with a thermocouple for temperature corrections and a cobalt thermal-flux monitor. The results of the measurements are shown in Fig. 38, and the linear expansion is $(9.9 \pm 0.3) \times 10^{-5}$ per 10^{15} thermal neutrons/cm^2. If it is assumed, as a rough estimate, that 1% Frenkel defects cause a 1% linear expansion, then there were 1.4×10^3 displacements per alpha-triton pair. Seitz and Koehler[25] report 1.9×10^3 as a theoretical estimate. The agreement indicates that little annealing takes place at 60°C.

ANNEALING OF QUENCHED-IN LATTICE DEFECTS IN Au-Cd

W. J. Sturm M. S. Wechsler

It has been found that large metastable changes in several physical properties can be induced in the beta phase of the Au-Cd alloy (~50 at. %) by quenching from high temperature. Of these changes, the increase in electrical resistivity as a result of quenching has been investigated most extensively,[26] and the activation energies of formation and motion of the induced lattice defect have been obtained by this method. A second property, the density of the alloy, is also altered by the quenching process. Hydrostatic weighing measurements have shown that the density is decreased upon quenching.[27] In addition, observations of the amount of decrease in density as it varies with quenching temperature have led to an evaluation of the energy of formation of the defect. The direction of these changes is consistent with the assumption that the quenched-in

[24] J. W. Cleland, J. H. Crawford, Jr., and J. C. Pigg, *Phys. Rev.* 98, 1742 (1955).

[25] F. Seitz and J. S. Koehler, Univ. of Illinois Technical Report No. 6 (1955).

[26] M. S. Wechsler, *Solid State Semiann. Prog. Rep. Aug. 30, 1955*, ORNL-1945, p 73.

[27] W. J. Sturm and M. S. Wechsler, *Solid State Semiann. Prog. Rep. Aug. 30, 1955*, ORNL-1945, p 76.

defects are lattice vacancies. By application of the theoretical calculation of Jongenburger[28] to the electrical-resistivity change, the number of vacancies[26] produced by quenching from 450°C was estimated to be 0.7 at. %, which is in agreement within experimental error with that[27] determined from the density change (0.6 at. %), as estimated from Tucker and Sampson's elastic model.[29]

Studies of defect identification and reaction kinetics in the Au-Cd alloy have recently been extended to include the measurement of quenched-in changes in linear dimension by the use of strain gages. The strain gage is essentially a length of strain-sensitive wire which indicates changes in its length by changes in its electrical resistivity. A calibrated bridge circuit (Baldwin type L strain indicator) translates resistance data into linear measurement, and it has a sensitivity of about 2 parts in 10^6. The specimen of Au-Cd alloy that was used for these measurements was the same one on which density measurements were made (a cylindrical bar 2 in. in length and about ¼ in. in diameter). Paper-base strain gages (SR-4) were bonded coaxially to the alloy sample in such a way that changes in the length of the cylinder were measured by the bridge circuit.

The series of isothermal-annealing experiments required for the evaluation of the activation energy consisted of five measurements made in the temperature range 50 to 70°C. The Au-Cd alloy specimen at approximately 450°C was quenched in a water bath at about 40°C in order to introduce the dimensional change, and the strain gage was then mounted on the specimen with Duco cement. One hour was required, at room temperature, for the mounting process, and measurement of linear relaxation at the annealing temperature was begun immediately afterward. Earlier electrical-resistivity and density measurements had indicated that negligible annealing would occur at room temperature in this length of time. Measurements at the annealing temperature were continued until no further change in length was observed; a typical curve showing the isothermal decay at 60°C of quenched-in strain is given in Fig. 39. Qualitatively, the process resembles that determined by

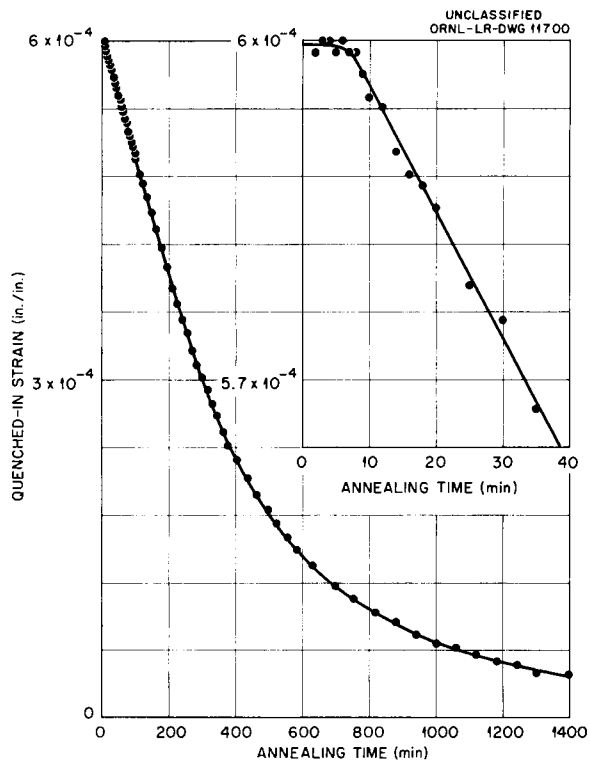

Fig. 39. Typical Strain Relaxation Curve for an Au-Cd Specimen Quenched from 450°C and Annealed at 60.0°C.

resistivity and density measurements[27] and consists of an initial period of incubation (see insert, Fig. 39) and a subsequent interval in which the defects are annihilated. Whether the incubation stage represents the nucleation of annihilation sites or a regrouping of vacancies preliminary to annihilation is not clear at this time. Certain quantitative differences between the relaxation curve as determined by strain methods and by electrical-resistivity methods are, however, apparent. Most strikingly, the time required to anneal the induced strain to half its total value is about three times as long as the corresponding time obtained by electrical-resistivity measurement; in addition, from the strain curve it appears that the incubation time is somewhat shorter. The significance of these quantitative variations will become more apparent with the completion of the series of electrical-resistivity measurements during isothermal annealing of the same specimen; this series is just being started. However, it must be borne in mind that variations of this sort may

[28] P. Jongenburger, *Appl. Sci. Research* **BIII**, 237 (1953).

[29] C. W. Tucker, Jr., and J. B. Sampson, *Acta Met.* 2, 433 (1954).

depend wholly on the fact that different samples were used for the electrical and dimensional measurements and thus that the variations may arise from small differences in composition or from differences in dimension.

As in the case of resistivity and density measurements, it is convenient to normalize the resulting curve and express the fraction of quenched-in strain after time t as

$$f = \frac{l - l_f}{l_i - l_f},$$

where l_i is the gage length of the sample immediately after quenching, and l_f is the final, fully annealed length. The resulting curve, with time plotted on a log scale, again emphasizes the qualitative similarity of all relaxation measurements and is shown in Fig. 40. A family of annealing curves of this type was determined at a series of temperatures between 50 and 70°C. A plot of the central, approximately linear, part of each curve (the portion between A and B in Fig. 40) yields the family of curves shown in Fig. 41. It is seen that each curve differs from that of Fig. 40 only in that it is translated along the time axis. As in the electrical-resistivity measurements, a characteristic relaxation time, τ, is defined such that

$$\tau = \tau_0 \, e^{\epsilon_M/kT},$$

where ϵ_M is the activation energy for motion; and since the ratio of times for equal values of f (Fig. 41) is nearly the same for all values of f, this ratio is called the time-scale adjustment factor. This factor may be written $\tau(T)/\tau(T_0)$, in

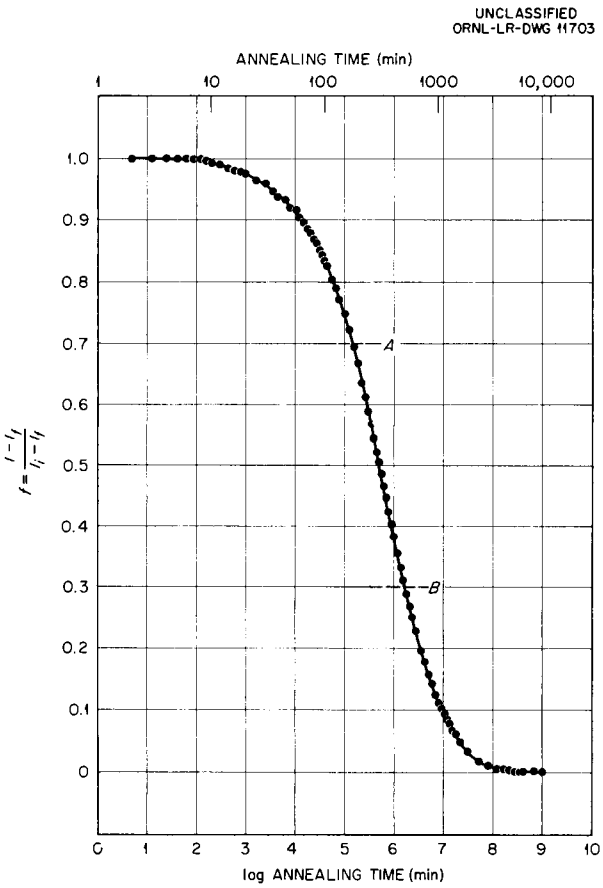

Fig. 40. Normalized Isothermal Relaxation Curve for an Au-Cd Specimen Quenched from 450°C and Annealed at 60.0°C.

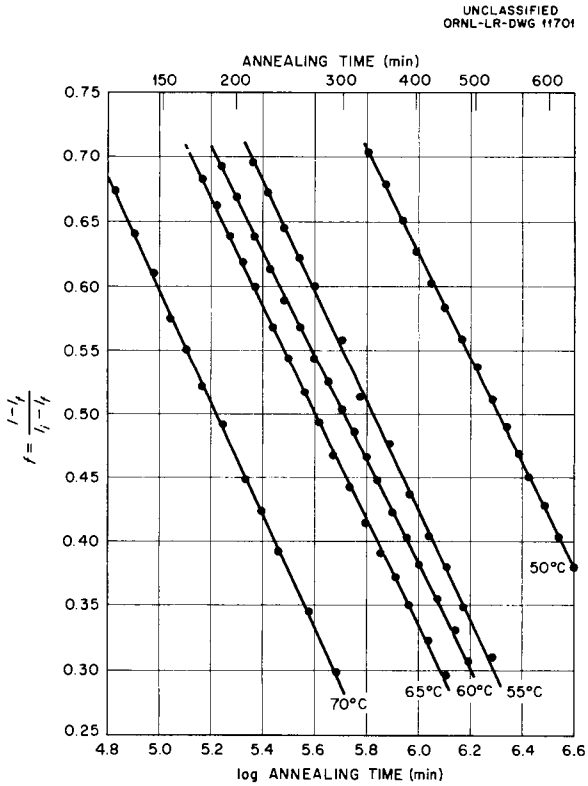

Fig. 41. A Family of Normalized Isothermal Relaxation Curves for an Au-Cd Specimen Quenched from 450°C. Annealing temperature is noted on each curve.

which T_0, the reference temperature, is 60°C (central curve in Fig. 41), and the characteristic times $\tau(T)$ and $\tau(T_0)$ correspond to 50% anneal. A plot of the logarithm of the time-scale adjustment factor vs $1/T$ will then lead to the evaluation of ϵ_M; this plot is shown in Fig. 42. The calculated value for the activation energy for motion is 0.5 ± 0.2 ev; the value determined by resistivity measurements[26] was 0.6 ev. Thus, the same mechanism apparently produces both electrical and dimensional effects.

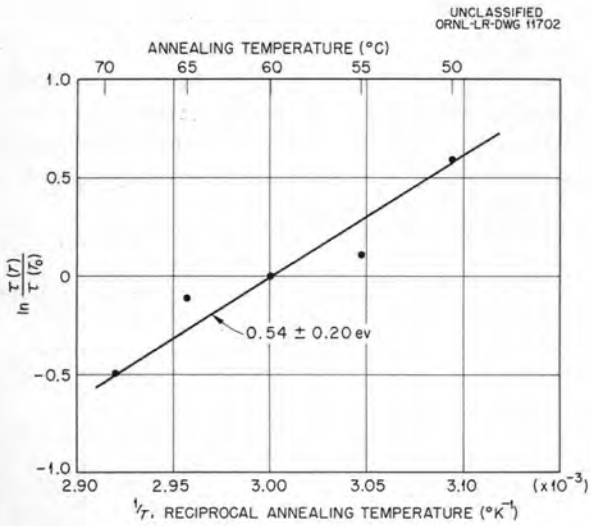

Fig. 42. The Log$_e$ Time-Scale Adjustment Factor as a Function of the Reciprocal Annealing Temperature for Au-Cd.

On the basis of the hypothesis that vacancies are responsible for these effects, it is possible to obtain an additional estimate of the number of vacancies produced by quenching from 450°C by the methods discussed earlier.[27] Since

$$\frac{\Delta V}{V} = 3\,\frac{\Delta l}{l},$$

where V is the volume and l is the length of the specimen, and since the value of $\Delta l/l$ obtained from strain measurements is 6×10^{-4}, calculation shows that 0.45 at. % vacancies are quenched in. This value is of the same order of magnitude but is somewhat lower than the 0.7 at. % determined by resistivity measurement and the value of 0.6 at. % from density-change data.

A ROCKING-CURVE ADAPTER FOR THE X-RAY DIFFRACTOMETER

G. E. Klein M. S. Wechsler

An adapter which enables rocking curves of single crystals to be obtained with a conventional x-ray diffractometer was designed by R. J. Fox and was constructed in the ORNL Research Shops.

The commercial diffractometer is designed primarily for powder diffraction work. The rocking-curve adapter permits data to be obtained from single crystals and is designed so that the degree of misorientation of mosaic-block regions in the single crystal will be shown and, moreover, so that the single-crystal-alignment procedure is facilitated in order to obtain accurate lattice-spacing values.

In normal operation the sample holder and the Geiger tube in the Norelco diffractometer rotate together. The rocking-curve adapter, as seen in Fig. 43, is substituted for the original sample

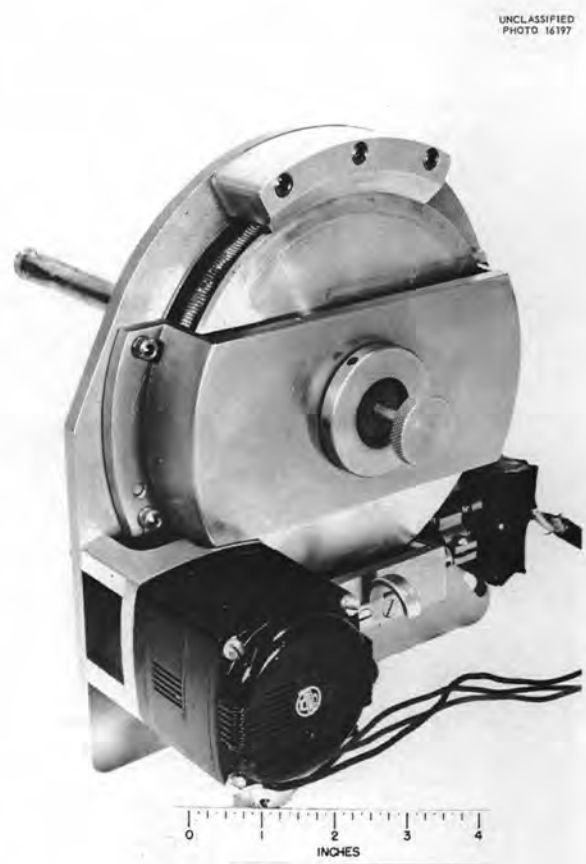

Fig. 43. Rocking-Curve Adapter.

holder and shaft in the diffractometer and consists of an accurately cut gear and calibrated vernier scale which are rotated or oscillated by the attached motor. When installed as an integral part of the diffractometer, the shaft carrying the new sample holder, as seen in Fig. 44, may be rotated independently of the Geiger counter or may be engaged by a knob at the rear of the instrument and rotated with the Geiger counter tube as in normal diffractometer procedure. If desired, the Geiger tube may be rotated while the sample remains stationary.

A variety of sample holders can be quickly attached to the end of the shaft in order to accommodate various sample types. The sample holder shown in the photograph can be removed from the shaft and attached to a two-circle goniometer for accurate alignment of the single-crystal specimen. The control mechanism provides for either manual or automatic rocking of the sample.

STRUCTURAL STUDIES IN IRRADIATED NONMETALS

M. C. Wittels F. A. Sherrill

Comparison of Radiation and Thermal Effects in Quartz

The exposure of single crystals of quartz to fission-spectrum neutrons results in dimensional[30] changes which are strikingly similar to the normal thermal behavior of the unirradiated material. More specifically, the changes observed by irradiation with integrated fluxes in the range 1×10^{19} to 5×10^{19} nvt_f closely parallel (Fig. 45) those observed by heating[31] in the temperature range 0 to 575°C. One simple conclusion to be drawn from these observations is that the lattice distention resulting from displacements is somewhat analagous to the displacement of mean atomic positions due to simple thermal agitation.

[30] M. C. Wittels and F. A. Sherrill, *Phys. Rev.* **93**, 1117 (1954).

[31] R. B. Sosman, *The Properties of Silica*, Chemical Catalogue Co., New York, 1927.

UNCLASSIFIED
PHOTO 16196

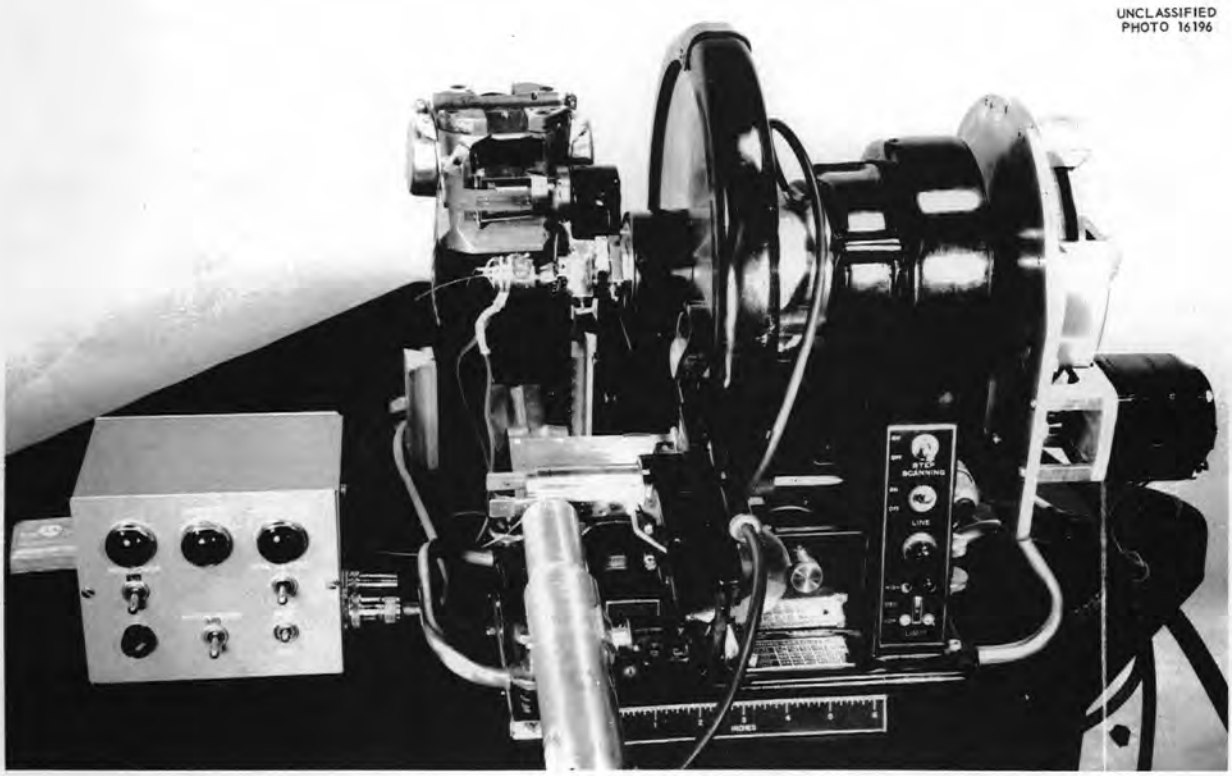

Fig. 44. Rocking-Curve Adapter in Position on Norelco Diffractometer.

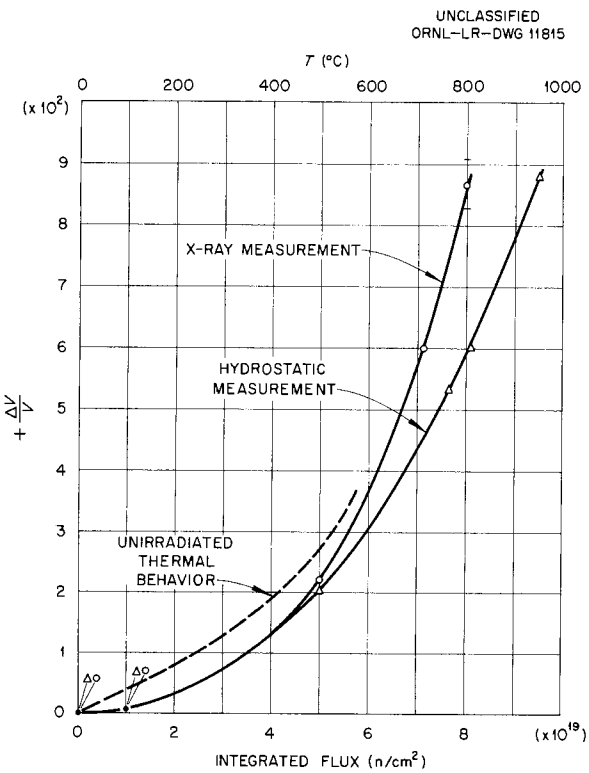

Fig. 45. Volume Changes Induced in Quartz Single Crystals by Irradiation and by Heat.

Irradiation with fluxes in the range described above indicates that Frenkel defects are predominantly formed in this range and that, when the c/a ratio is lowered below 1.094, complex processes are initiated which may be due to the presence of two or more phases within the distended single-crystal lattice. On prolonged bombardment with fluxes between 5×10^{19} to 11×10^{19} nvt_f, the presence of isolated Frenkel defects appears to be greatly diminished, since there is an increasing deviation from the 1:1 ratio expected on comparison of x-ray and normal density data. However, some long-range order is preserved, even in single crystals which have undergone volume increases of more than 10%, as can be seen in coherent x-ray reflections.

It is suggested that in single-crystal insulators such as quartz, in which large numbers of displacements are produced, the attendant lattice distention proceeds in a fairly simple manner to a threshold value beyond which some complex processes of recombination are engendered. Obviously, in the case of quartz this threshold value could well be that point at which the lowest normal value of c/a is reached and beyond which the lattice is unstable even under the extremes of normal thermal behavior.

A Radiation-induced Phase Transition

Possible evidence for the thermal spike has been obtained through the radiation-induced phase transition[32] of monoclinic ZrO_2 to cubic ZrO_2. Observation by G. E. Klein[33] showed that in a "stabilized" sample (cubic ZrO_2 + monoclinic ZrO_2), after an irradiation with 2×10^{20} nvt_f, the monoclinic phase was seen to "disappear." Powder samples of natural, pure monoclinic ZrO_2 were exposed to fission-spectrum neutrons in an integrated fast flux of 9.4×10^{19} nvt_f at an approximate temperature of 100°C. X-ray examination (Fig. 46) of the samples following bombardment revealed that more than 90% of the monoclinic phase had been transformed into the symmetrical high-temperature cubic phase. The polymorphism of ZrO_2 is of interest because it comprises an unusual series in which the higher-temperature forms are more symmetrical, as expected, yet each succeeding high-temperature structure is more dense. Indeed, the low-temperature monoclinic form is a distortion of the cubic fluorite structure, which is stable above 1900°C; and the tetragonal structure, which is stable between approximately 1100 to 1900°C, is similar to the cubic form, and this structure gives the appearance of being in tension in the c direction in its stability field. In pure materials, the cubic phase cannot be quenched-in from high temperature.

It is suggested that the thermal-spike mechanism[34,35] might well account for this radiation-induced phase transition, since the temperatures to be achieved for a rapid quenching-in process are reasonable. The very low values for thermal conductivity and thermal diffusivity in this excellent insulator indicate that rapid temperature fluctuations in excess of 2000°C might ensue in the wake of energetic particles moving within the solid. Indeed, since the tetragonal form is so

[32] M. C. Wittels and F. A. Sherrill, *J. Appl. Phys.* (to be published).

[33] G. E. Klein, *Solid State Semiann. Prog. Rep. Feb. 28, 1955*, ORNL-1852, p 59.

[34] F. Seitz, *Discussions Faraday Soc.* 5, 271 (1949).

[35] H. Brooks, KAPL-360 (August 1950) (Secret).

UNCLASSIFIED
PHOTO 16183

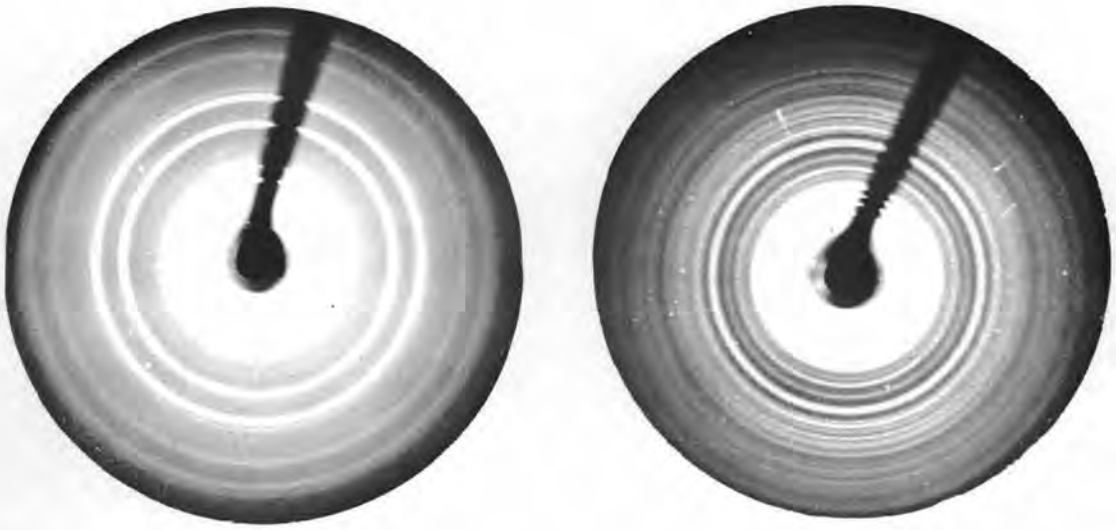

Fig. 46. Debye-Scherrer Powder Photographs of "Stabilized" ZrO_2 Irradiated with 9.4×10^{19} nvt_f at Approximately 100°C.

similar to the cubic phase, perhaps temperatures greater than 1100°C and less than 1900°C might be sufficient for a quenching-in process. The effects of knock-on produced interstitials should not be ruled out, however, since they are very likely present in considerable numbers. H. C. Schweinler has suggested that the transition might well be due to both effects acting together, namely, the high temperatures which make regions thermally capable of transforming and the volume effect. The volume effect would manifest itself as internal stresses about trapped interstitials which might cause the lattice to collapse to the smaller volume and to closer packing. Additional evidence for the thermal spike was obtained in preliminary measurements of particle sizes in the transformed material; the data indicate that regions which have radii of approximately 100 Å and which encompass approximately 10^5 atoms are affected. These particles are smaller, by about a factor of 5, than the original monoclinic particles. These results, too, are in fair agreement with the theory.

Initial annealing studies of the transformed material reveal that the irradiation-induced cubic phase is stable up to approximately 800°C and that above this temperature crystals begin to revert to the low-temperature modification. The subsequent growth of the low-temperature phase is dependent on temperature and time. It should be noted, however, that initiation of the transformation reversal to the low-temperature form begins more than 200°C below the normal low–intermediate transformation point. More fundamental studies are being pursued with single-crystal measurements.

In addition to the irradiation studies on the forms of ZrO_2, progress is also being made on the bombardment effects on its isomorphous counterparts, in an effort to determine the chemical effect of such transitions. Work is also being performed on single crystals of the allotropic forms of TiO_2. Preliminary measurements on these crystals indicate a relatively high degree of stability under irradiations up to 10^{20} nvt_f, with only slight shifts in lattice parameters. Efforts are also being directed toward determining these effects in other allotropic forms, both elemental and complex.

Examples of Radiation-induced Amorphism

Exposure of a large number of silicate and oxide crystals to fission-spectrum neutrons with fluxes up to 4.5×10^{20} nvt_f has resulted in the formation of completely disordered lattices in a number of silicates. The following crystals are so affected:

Quartz, Low tridymite, Low cristobalite	SiO_2 (ref. 30)
Beryl	$Be_3Al_2Si_6O_{18}$
Garnet	$Ca_3Al_2(SiO_4)_3$
Topaz	$Al_2(SiO_4)(OH)_2$
Tourmaline	$Al_5Mg_3CaMg(OH,F)_4(Si_6O_{27}B_3)$

In those cases where single crystals could be employed, it was seen that there are distinct differences in cation-oxygen binding under neutron irradiation. A qualitative view is that those bonds which are more ionic in character are also more stable. Except for the case of tourmaline, which was complicated by the presence of the B^{10} nucleus in its lattice, it was seen that Frenkel defects are produced at early stages (see section: "Comparison of Radiation and Thermal Effects in Quartz") of irradiation and that long-range order persists in single crystals despite large shifts in lattice parameters. It seems probable that in these insulator-type crystals, which are complex both structurally and chemically, the effect of bombardment is to produce a "skeleton" lattice network which contains complex phases having very short-range order and which may be distended only to some reasonable threshold before collapsing.

Fast-Neutron Effects on Single-Crystal X-Ray Reflection

In connection with the x-ray studies of neutron-irradiated nonmetals, two distinct effects were observed on coherent x-ray reflections, which occur singly or together. These observations were made by using the Fox spinner[36] on single crystals of InSb, diamond, and zircon. In the case of InSb (Fig. 47), the formation of mosaic broadening and the absence of any apparent peak shift can be seen. Apparently, bombardment produces highly disoriented crystallites, yet each crystallite appears to retain the normal lattice constant. In the figure, the peak intensity of the irradiated crystal has been greatly exaggerated for descriptive purposes. Actually, the integrated intensity of the irradiated-crystal reflection is highly diminished as a result of bombardment. In single crystals of diamond irradiated as high as 5×10^{20} nvt_f, no apparent line broadening or loss of intensity is observed, but the large shift in peak position (Fig. 48) reveals the pronounced lattice expansion. Finally, in the case of zircon[37] single crystals, the effect of fast neutrons is to produce both these features, namely, mosaic broadening and peak shifting (Fig. 49).

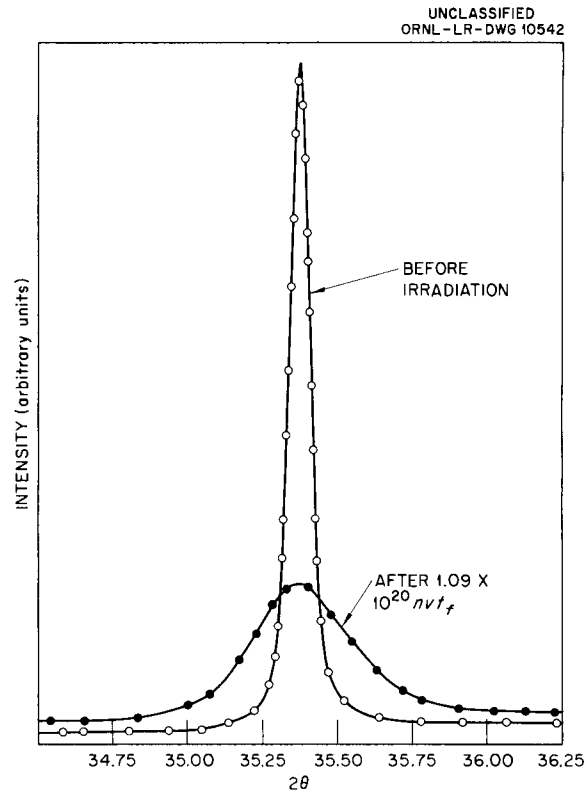

Fig. 47. Fast-Neutron Effect on X-Ray Reflections from Single-Crystal InSb $(220)_\beta$.

[36] R. J. Fox, F. A. Sherrill, and M. C. Wittels, *A Single-Crystal Adapter for the Norelco Wide-Range Diffractometer*, ORNL-1807 (Jan. 1955).

[37] M. C. Wittels and F. A. Sherrill, ORNL-1762 (Aug. 30, 1954) (Confidential).

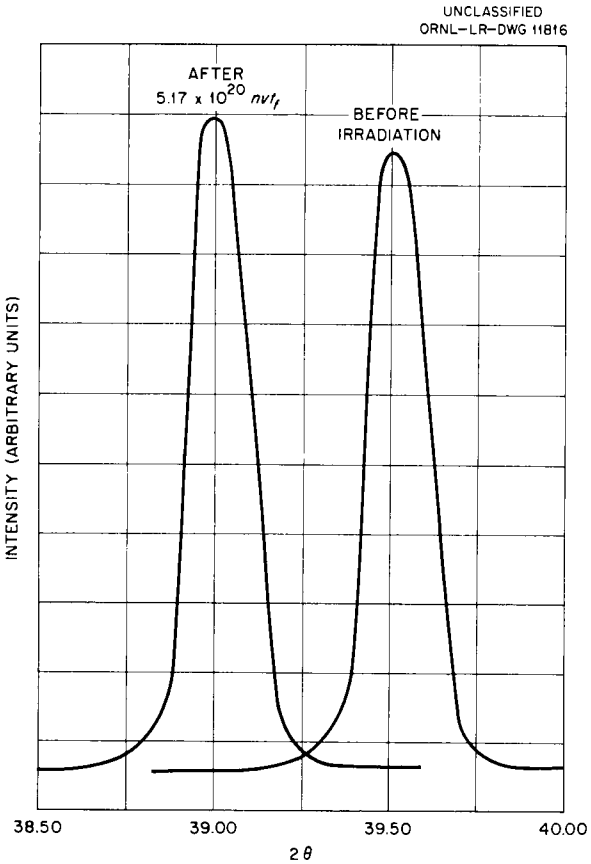

Fig. 48. Fast-Neutron Effect on X-Ray Reflections from Single-Crystal Diamond $(111)_\beta$.

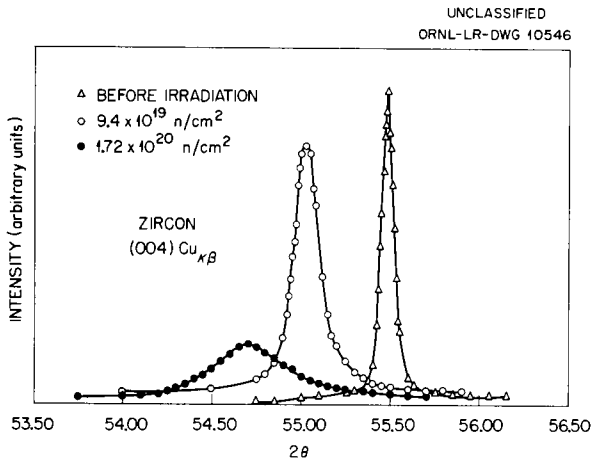

Fig. 49. Fast-Neutron Effect on X-Ray Reflections from Single-Crystal Zircon $(004)_{K\beta}$.

Annealing of Neutron-irradiated Diamond Powder

Preliminary annealing studies of diamond powder irradiated in the range 7×10^{19} to 20×10^{19} nvt_f have been conducted in the temperature range 150 to 1050°C. As was previously reported,[38] the irradiation-induced defects are of the Frenkel type. The back diffusion of carbon atoms is evident at temperatures as low as 150°C and proceeds continuously up to approximately 950°C, where a semiplateau is approached. No discrete activation energies for back diffusion were observed, but tentative indications reveal that two or possibly three rates of recovery take place in this temperature range. It is seen that with increasing radiation dosage both the rate of thermal recovery and the amount of residual damage are higher in the more heavily irradiated samples.

EFFECT OF RADIATION ON ELECTRICAL INSULATION

J. C. Pigg C. C. Robinson[39]

In previous experiments[40] the wire under consideration was placed in the reactor and terminated in the reactor in order to reproduce the conditions that would exist in the case of sample leads. The resistance and photo-emf were then measured between the central conductor and the shield of the wire. Although precautions were taken to make the surface path from the end of the shield to the conductor as long as practicable, the possibility of surface contamination and surface conduction still exists, and experimental data on these two factors must be obtained before it can be said that the results reported previously[40] are bulk effects.

Two Teflon-insulated wires, taken from the same spool of wire, have been installed in hole 5ON of the Graphite Reactor. One wire is terminated inside the reactor as previously; the other wire is twice as long as the first and is bent so that both terminals are outside the reactor. Hence, in the second wire there can be no problem of surface conduction. After two weeks exposure, there is

[38] J. H. Crawford, Jr., and M. C. Wittels, "A Review of Investigations of Radiation Effects in Covalent and Ionic Crystals," A/conf. 8/P/753. Paper presented at International Conference on the Peaceful Uses of Atomic Energy, Geneva, Switzerland, August 13, 1955.

[39] On loan from Wright Air Development Center.

[40] J. C. Pigg and C. C. Robinson, *Solid State Semiann. Prog. Rep. Aug. 30, 1955*, ORNL-1945, p 6.

no essential difference between the two wires that can be detected by this type of measurement.[40]

RADIATION EFFECTS IN BARRIERS

J. C. Pigg C. C. Robinson

A 1N38-A germanium point-contact rectifier was exposed in a 2×10^6 r/hr Co^{60} gamma source, and the forward and reverse currents were measured at a bias of 1 v. The behavior of the current is shown in Fig. 50. These data are in qualitative agreement with the results of R. C. Young at Wright Air Development Center.[41] The increase in reverse current followed by return of the current toward its initial value is a feature not noticed in reactor radiation. The reason for failure to find the effect is due to the low total damage at which the effect occurs. As can be seen from the change in forward current, the effect observed here would have occurred before the sample reached thermal equilibrium in an in-pile experiment. Whether or not the effect does result from neutron irradiation has not yet been determined.

A series of exposures was made in a 5×10^4 r/hr Co^{60} source, and the rectifier voltage-current characteristic was measured after removal from the source. The change in the characteristic curve can be seen in Fig. 51. There is little change in the forward curve, which is in agreement with the data in Fig. 50. The current at 1 v of reverse bias has been normalized to make the preirradiation value coincide with that of the sample

[41] R. C. Young, Wright Air Development Center, WCRT-TN-54-255.

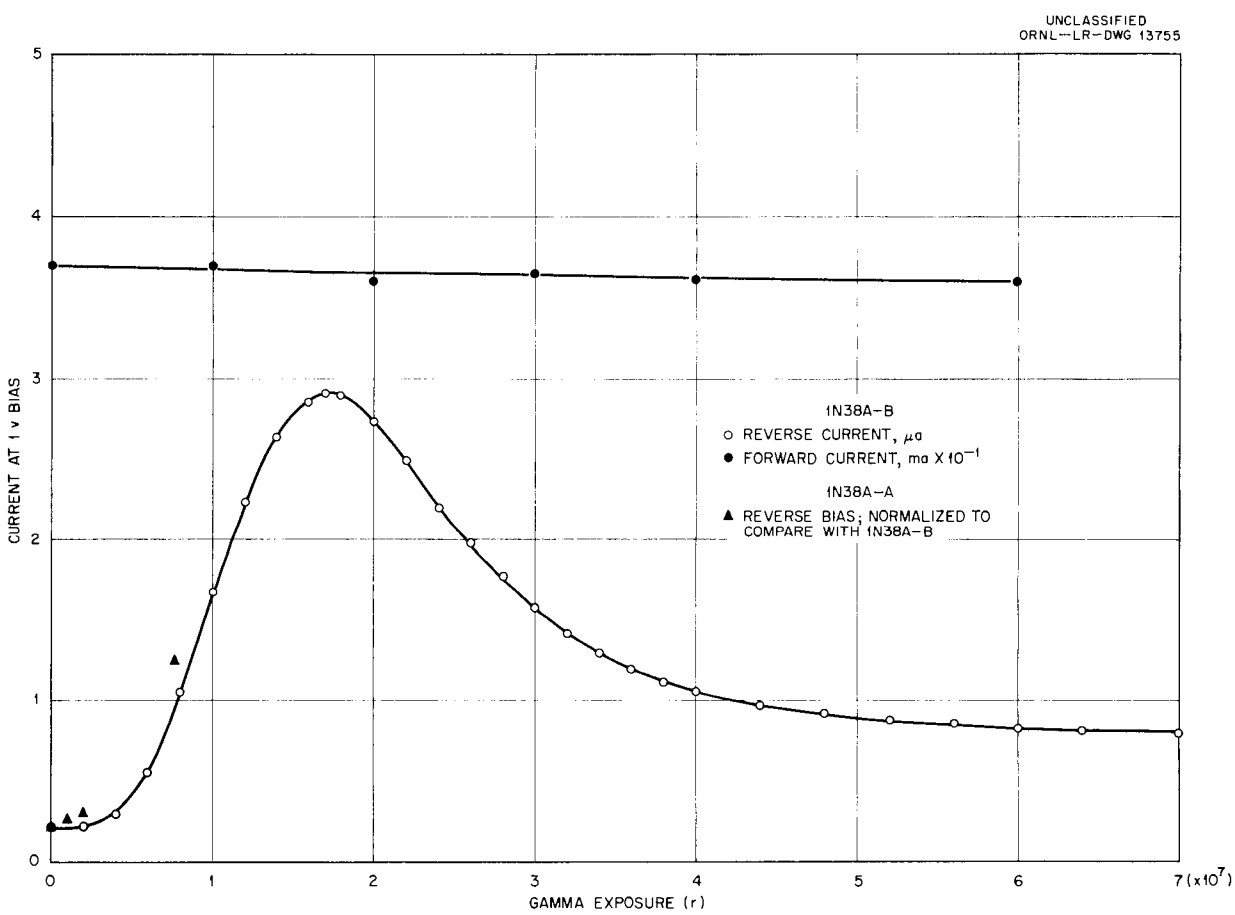

Fig. 50. Effect of Gamma Radiation on Conduction Through a Barrier. Germanium point-contact rectifiers: (*a*) 1N38A-B exposed to 2×10^6 r/hr Co^{60}, (*b*) 1N38A-A exposed to 2.5×10^5 r/hr Co^{60}.

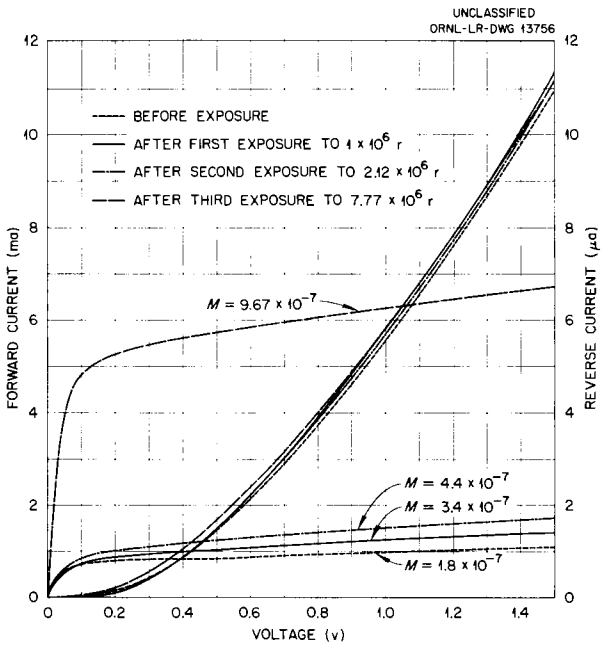

Fig. 51. Effect of Gamma Radiation on Voltage-Current Characteristic of Point-Contact Rectifier 1N38A-A at 20°C. The *M* values are the slopes of the lines.

exposed in the 2×10^6 r/hr source. The normalized data are shown in Fig. 50.

The forward characteristic corresponds to the voltage-current behavior of the emitter of a transistor. The reverse curve corresponds to the collector characteristic of a transistor. It can be seen in Fig. 51 that, although the emitter characteristic is only changed slightly, the collector changes drastically both in magnitude and slope. The magnitude of the current at 1 v of bias changed by about a factor of 6, and the slope changed by a factor of about 5.3. The changes in the characteristics are similar to those observed after exposure to neutron radiation.[42]

A series of transistors has been irradiated, and the circuit shown in Fig. 52 was used to measure the amplification of the unit before, during, and after irradiation.

In each experiment, the series resistances in the emitter and collector circuit are changed to match the unit under consideration. Provision is made for switching from grounded emitter to grounded-base circuitry, so that both types of circuitry can be studied simultaneously with the same unit. Exposures have been made both in Co^{60} gamma sources and in the ORNL Graphite Reactor.

The change in collector current at 2 v of bias and the change in amplification of a Minneapolis-Honeywell H-2 power transistor as a function of gamma irradiation can be seen in Fig. 53. The collector, base, and emitter voltages were adjusted to the original values before each reading; hence, changes in amplification are due to change in characteristic and are not due to change in operating voltages. It can be seen that the collector current and the amplification are essentially the inverse of each other. Whether this change in amplification is due to change in slope of collector characteristic, change in separation of collector curves, or change in impedance matching has not yet been determined.

The change in amplification of two Minneapolis-Honeywell power transistors as a function of irradiation in hole 51N of the ORNL Graphite Reactor is shown in Fig. 54. This curve follows the same type of behavior as that of RCA No. 1241.[43] The temporary increase in amplification observed in RCA No. 1266 was not noted. Again, the flux level was such that this region of the curve would have been traversed before thermal equilibrium was obtained.

THERMAL CONDUCTIVITY OF DIELECTRICS AT LOW TEMPERATURES

A. Foner Cohen L. C. Templeton

In the present investigation, it was felt that if some general conclusions with regard to the nature of radiation-induced lattice defects were to be found from low-temperature thermal-conductivity studies, examination of more than one type of crystal would be worthwhile. To date, only a limited number of experiments of this type have been performed, the most thorough investigation being that of Berman[44] on quartz crystal over the temperature range 2 to 90°K. Lattice defects were later introduced by neutron bombardment, and the thermal resistance due to these defects

[42] J. C. Pigg, ORNL-1606, p 79, esp. p 81 (Aug. 31, 1953) (Secret).

[43] J. C. Pigg and J. W. Cleland, ORNL-1506, p 46–47 (Feb. 10, 1953) (Secret).

[44] R. Berman, *Proc. Roy. Soc. (London)* A 208, 90 (1951).

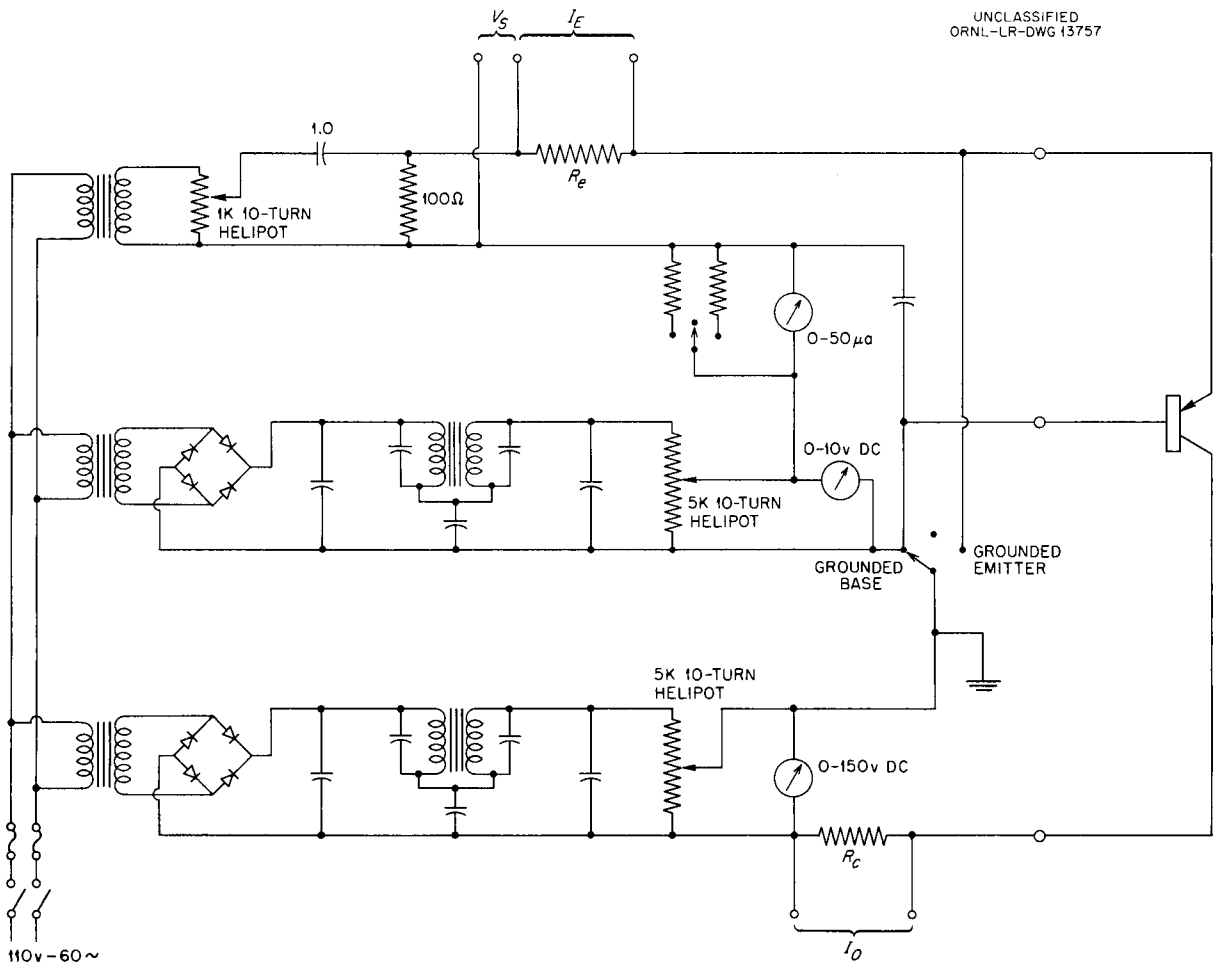

Fig. 52. Transitor Test Circuit.

was measured; Berman found that by giving the crystal a sufficient bombardment the measured low-temperature thermal conductivity approached that of completely disordered quartz glass.

At ORNL somewhat similar experiments with quartz crystal Qu"A" have been carried out. The results of two successive neutron bombardments are shown in Fig. 55 and are in qualitative agreement with the measurements of Berman. The irradiations are, of course, different from Berman's. In addition, a quartz crystal identical with that of Qu"A," which will be referred to as Qu"B1," was measured following a Co^{60} gamma irradiation at room temperature, and the resulting decrease in thermal conductivity is illustrated in Fig. 55. The introduced thermal resistance in the gamma-irradiated quartz seems similar to that due to neutron bombardment. However, experiments are planned in which this crystal will be subjected to further gamma radiation so that a more detailed comparison can be made.

It was of interest to R. L. Sproull of Cornell University to examine the thermal conductivity of a potassium chloride single crystal of high purity and then to directly examine the effect of chemical doping on this property – addition of calcium in various concentrations to the melt and regrowth of the crystals. One of the results indicates that at temperatures above the conductivity maximum, the thermal resistivity increases linearly with temperature, which is as expected for point imperfections according to Klemens[45] theory.

[45] P. G. Klemens, *Proc. Roy. Soc. (London)* **A 208**, 108 (1951).

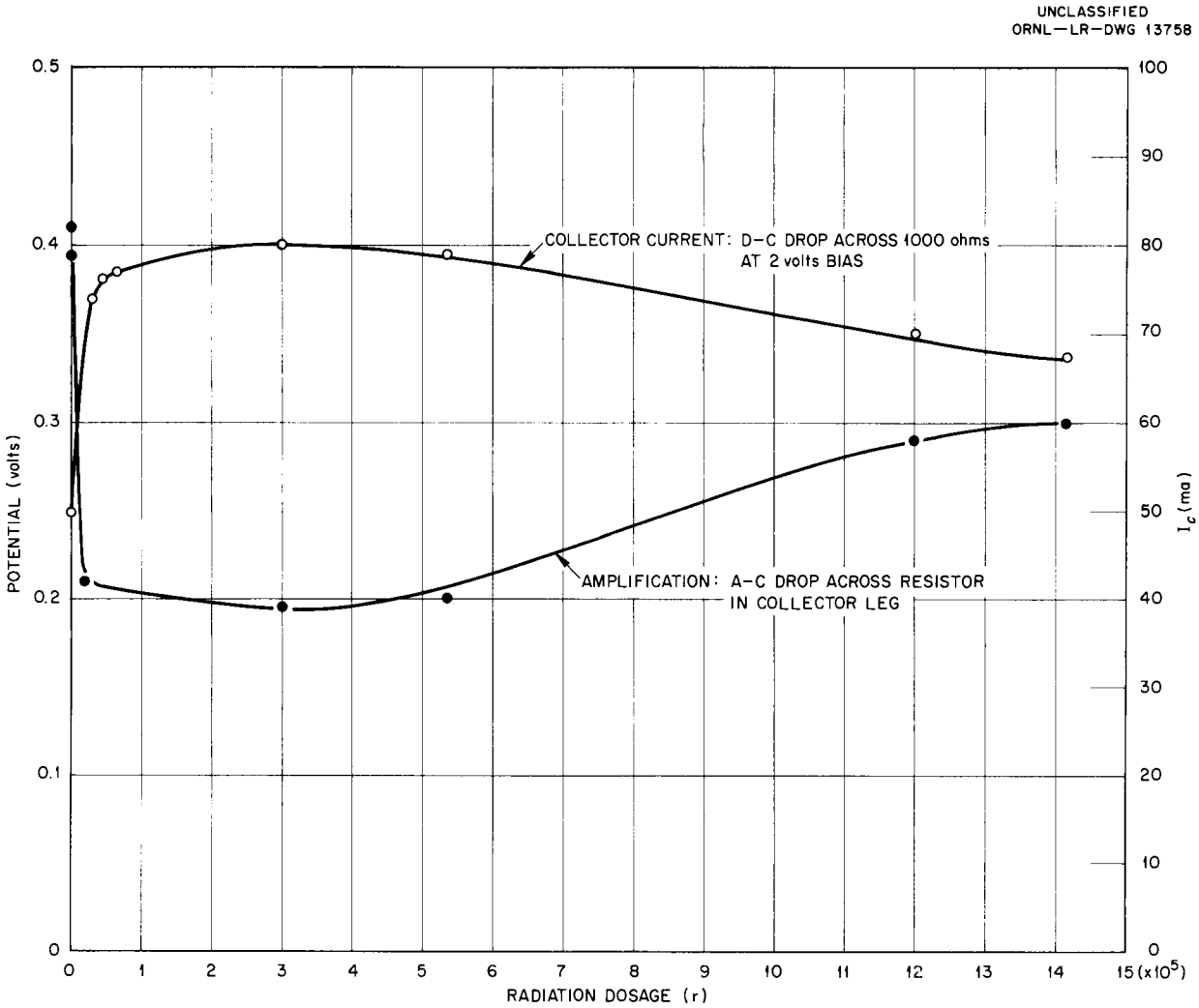

Fig. 53. Effect of Radiation on Collector Current and Amplification of a Minneapolis-Honeywell H-2 Transistor (No. 12) Irradiated in Gamma Source of 2.57 × 10^5 r/hr.

Concurrently, the effect of introducing defects in KCl crystals by Co^{60} gamma bombardment is being investigated at the Laboratory. The first unirradiated KCl crystal, however, had a large chemical-impurity concentration initially. The gamma bombardment caused a decrease in the thermal conductivity, but a detailed comparison with the chemical-doping experiments at Cornell will not be attempted until higher-initial-purity KCl crystals are bombarded. The effect of neutron irradiation on the introduced thermal resistance in KCl is also being studied.

It is of interest that a synthetic sapphire single crystal (Al_2O_3), which is a crystal exhibiting appreciable ionic characteristics, has a thermal resistance above the maximum in the conductivity vs temperature plot which is due mainly to *umklapp* processes (as is the case in quartz crystal), and this behavior is in contrast to that of ionic crystals such as KCl and KBr,[46] in which cases the thermal resistance due to impurities is dominant. Since the thermal-conductivity maximum of Al_2O_3 occurs at approximately 50°K, the boundary resistance is important over a larger range of temperature (0 to 50°K) than it is for quartz (0 to 12°K) and can consequently be studied in greater detail. The

[46] W. J. de Haas and Th. Biermasz, *Physica* 4, 752 (1937).

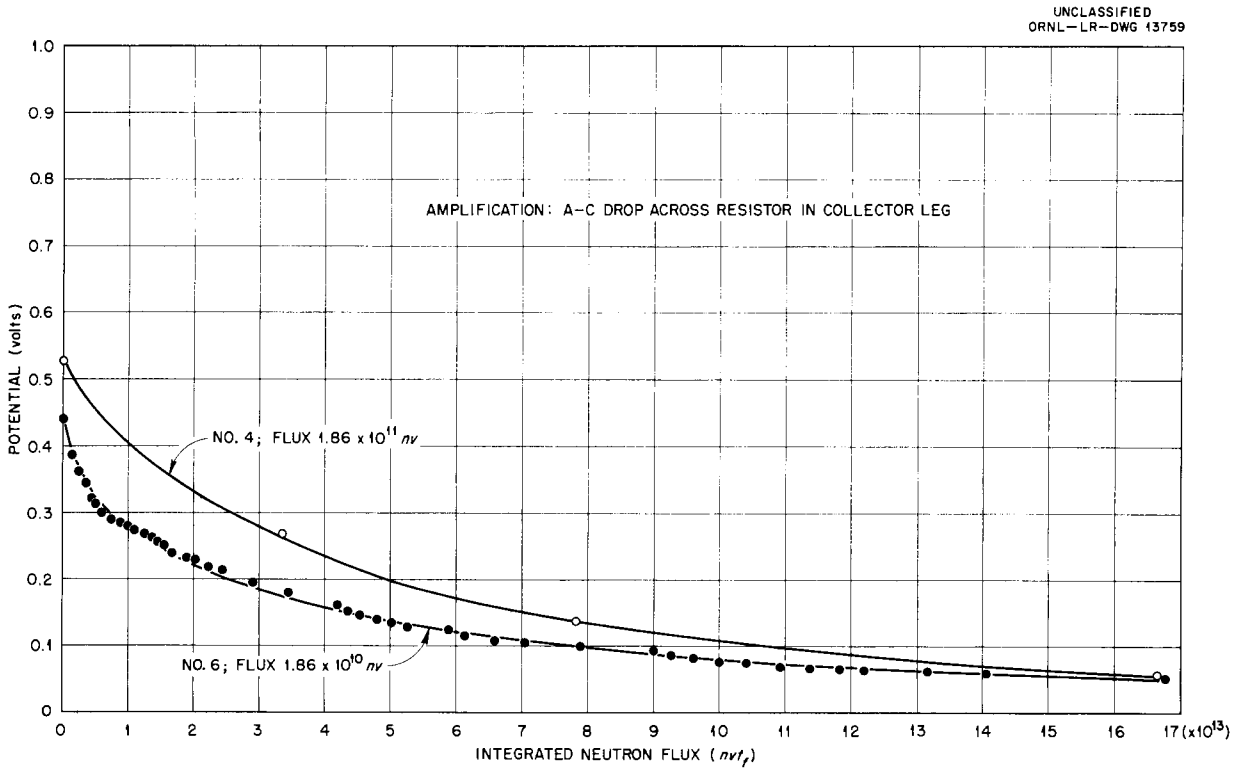

Fig. 54. Change in Amplification of Two Minneapolis-Honeywell H-2 Power Transistors as a Function of Integrated Fast-Neutron Exposure.

effect of neutron bombardment on the thermal conductivity is presently being studied.

Single crystals of MgO and CaF_2 are also being used in a study of lattice defects by means of low-temperature thermal-conductivity measurements. Both crystals exhibit a decrease in thermal conductivity following irradiation. The MgO has been subjected to neutron bombardment, and the CaF_2 has been subjected to gamma bombardment.

At low temperature, very high-purity single crystals of germanium (a semiconductor) behave as insulators. The electrical resistivity at room temperature for the particular specimen reported here was approximately 50 ohm-cm, and the resistivity at 4.18°K was 1.1×10^4 ohm-cm. In such a crystal, as in the five dielectrics already mentioned, it is expected that the conduction of heat at low temperatures is due mainly to lattice and boundary scattering. The introduction of lattice defects by two successive neutron bombardments at room temperature was examined by measurements of the thermal conductivity at low temperatures. The decrease in thermal conductivity following bombardment is shown in Fig. 56. Details concerning the dates and dosages of bombardment are indicated in the figure.

Subsequent measurements following the second bombardment are shown in curve 3. After some further annealing at room temperature, curves 3′ and 3″ were obtained, which indicated annealing of defects in the region near the maximum. Note in curve 2′ that following the first bombardment there is an indication of annealing. However, in the lowest temperature region (2.5 to 6°K), measurements made in February 1956 coincide with the current measurements in this region, shown in curve 3*, where the introduced thermal resistance indicates the possible presence of clustered defects and the absence of any annealing. The temperature dependence of the electrical resistivity of this crystal before and after neutron bombardment was determined but will not be discussed at this time. The germanium crystal will be annealed at a temperature where electrical

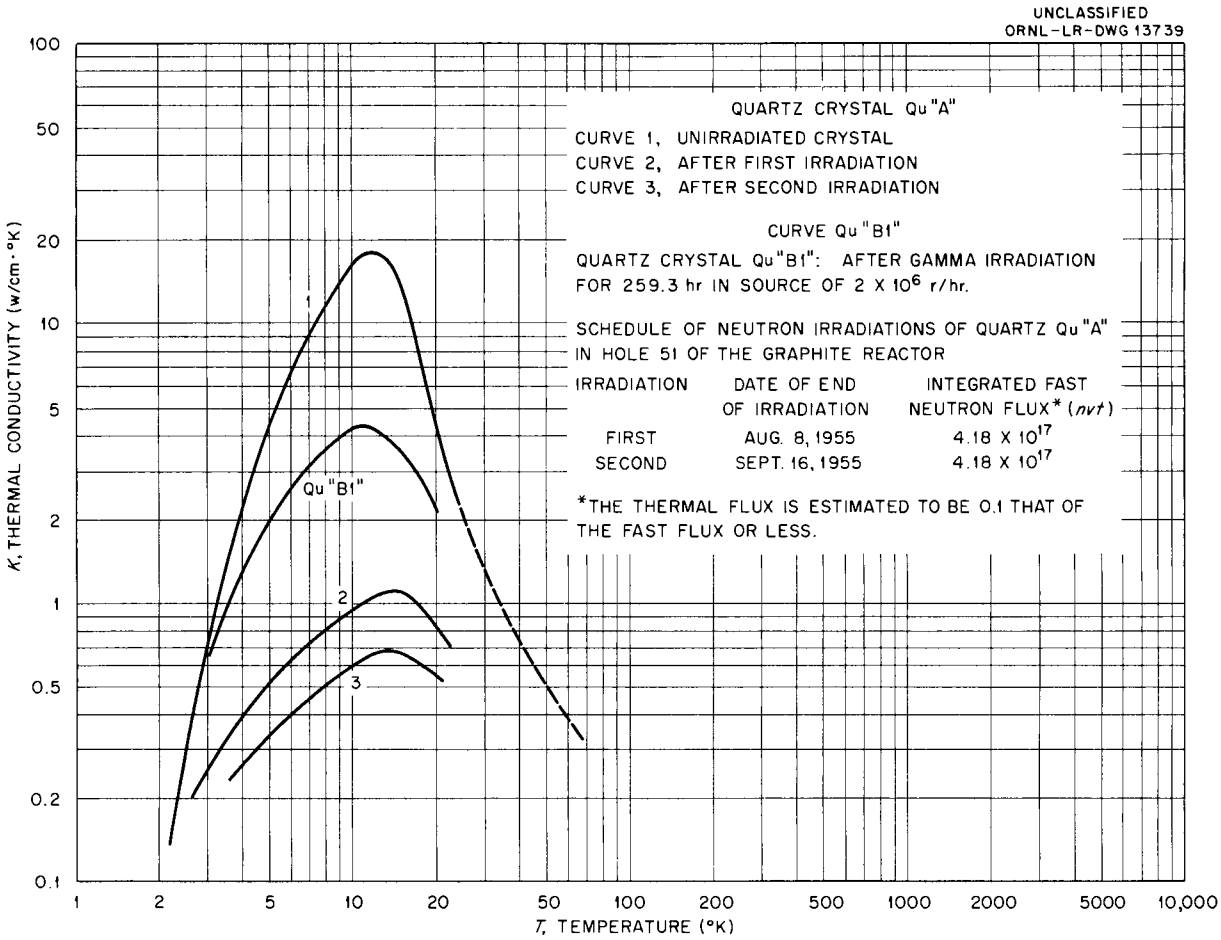

Fig. 55. Thermal Conductivity of Quartz Single Crystals vs Temperature.

properties are generally believed to return to their prebombardment values,[47] after which further low-temperature thermal measurements will be made, and it is anticipated that further information on annealing of the neutron-introduced defects will be afforded.

[47]Private conversations with J. H. Crawford, Jr., J. W. Cleland, and J. C. Pigg, of this Division.

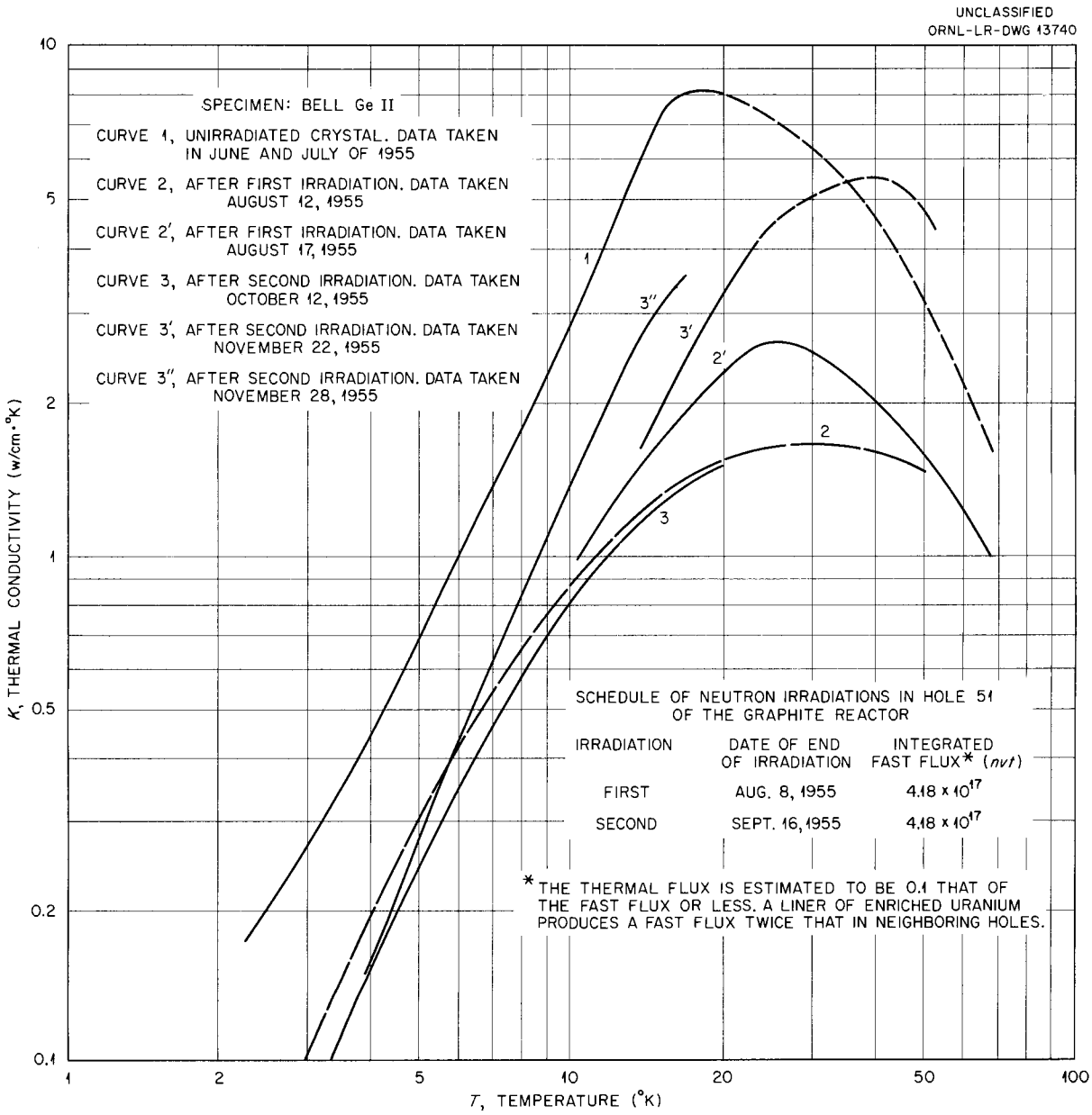

Fig. 56. Thermal Conductivity of Germanium Single Crystal vs Temperature.